NASA Contractor Report 3150

Differences Between Measured and Linearly Interpolated Synoptic Variables Over a 12-h Period During AVE IV

Leonard R. Dupuis and James R. Scoggins

CONTRACT NAS8-31773
JUNE 1979

NASA

NASA Contractor Report 3150

Differences Between Measured and Linearly Interpolated Synoptic Variables Over a 12-h Period During AVE IV

Leonard R. Dupuis and James R. Scoggins
Texas A. & M. University
College Station, Texas

Prepared for
George C. Marshall Space Flight Center
under Contract NAS8-31773

NASA
National Aeronautics
and Space Administration

Scientific and Technical
Information Office

1979

TABLE OF CONTENTS

Page

LIST OF TABLES

LIST OF FIGURES

AUTHORS' ACKNOWLEDGMENTS

The authors express their appreciation to Drs. Dusan Djuric, Edward Gbur, and K. C. Brundidge for reviewing the manuscript, Mr. John Rod for preparing the figures, and Mrs. Janie Leighman for typing the manuscript. The research was conducted under NASA Contract NAS8-31773, which is under the auspices of the Atmospheric Sciences Division, Space Sciences Laboratory, NASA Marshall Space Flight Center, Alabama. The encouragement and support provided by Drs. William W. Vaughan and Robert E. Turner, and Mr. Kelly Hill of NASA are gratefully acknowledged.

1. INTRODUCTION

a. Statement of the Problem

A major problem in many meteorological studies is the lack of sounding data over time intervals less than 12 h. Several studies have shown that the conventional 12-h rawinsonde network does not adequately define large temporal variations in synoptic variables over short time periods that are often related to sub-synoptic systems and severe weather occurrences. Nevertheless, because of the type of data available, several methods are utilized to approximate or estimate values of synoptic variables for times within bracketing rawinsonde observations.

One common method employed by meteorologists is a linear time interpolation of atmospheric variables through a 12-h period. This technique has been used widely in trajectory models and more recently in research to determine the capabilities and limitations of satellite sounding data since simultaneous raob and satellite data were not available (Moyer et al., 1978). In forecast studies, a linear extrapolation of systems in space is often utilized to account for atmospheric structure over a 12-h period beyond a sounding time. While different from a linear interpolation, extrapolation techniques employ the same general principle.

While such methods serve at least as an approximation to atmospheric conditions for times within the regular 12-h sounding observations, they are incapable of resolving rapid temporal changes in synoptic variables that are largely responsible for the development of thunderstorms and severe weather occurrences. Since the life cycles of these sub-synoptic systems are much shorter than 12 h, often they are unresolved using 12-h data. Thus, changes in the structure of the atmosphere not represented by a linear interpolation based upon sounding observations 12 h apart could be very important in the development

and dissipation of convective storms and severe weather. These changes are the subject of this research.

b. Objectives

The main objective of this research is to examine the information content in rawinsonde data taken at 3-h intervals that is not contained in data obtained by assuming synoptic variables to change linearly through a 12-h period.

Specific objectives include:

(1) Examination of differences between variables computed from 3-h measured data and like variables interpolated linearly from 12-h data over 3-, 6-, and 9-h intervals.

(2) Identify systematic patterns in these differences or nonlinear changes, and examine their spatial and temporal continuity.

(3) Establish relationships between these differences or nonlinear changes, synoptic features, and radar-observed convection.

(4) Compare the magnitudes of nonlinear changes in synoptic variables over 3-, 6-, and 9-h intervals with observed changes in like variables over the same time intervals to determine the relative significance of nonlinear changes with respect to observed changes.

c. Previous Studies

Convective systems are of major concern to meteorologists since these systems are largely responsible for many severe weather occurrences (Ninomyia, 1971). A limiting factor in the understanding of these sub-synoptic systems is the 12-h spacing of upper air rawinsonde soundings.

As mentioned above, because of the type of data available, methods are employed by meteorologists to approximate the structure of the

atmosphere for times within the 12-h period between soundings. Horn et al. (1976) used a linear time interpolation between bracketing raobs to compare geostrophic winds derived from satellites to those obtained from radiosonde data. Moyer et al. (1978) found such a technique to be justified since results demonstrated that weighted means of raobs better approximated satellite profiles than did either of the bracketing raob profiles. However, it is obvious that major weather changes take place over short intervals and that such changes often behave in a nonlinear fashion. This study will focus on the information content essentially lost by assuming that synoptic variables change linearly through a 12-h period, and on the nonlinear variability of these variables in relation to synoptic features and weather.

Several studies have shown that the conventional 12-h upper-air network is inadequate to describe convective processes whose life cycles are much shorter than 12 h. House (1960) demonstrated that the 12-h spacing between rawinsonde observations could not detect the processes relevant to the production, propagation, and dissipation of atmospheric phenomena associated with squall lines. Such processes could be more accurately defined through the use of 6-h measurements. Deficiencies in observed data in thunderstorm areas also were pointed out by Fujita and Brown (1960). Fankhauser (1969) identified mesoscale systems moving through the National Severe Storms Laboratory (NSSL) network and concluded that atmospheric structure in areas of thunderstorms could be resolved from rawinsonde data measured over 1.5-h intervals.

Many sub-synoptic systems important in the development of severe weather are related to rapid temporal changes in the observed structure of the atmosphere. Using data collected at 90-min intervals, Kreitzberg and Brown (1970) studied mesoscale circulation in a continental occlusion. They showed that variability in the atmosphere is closely related to mesoscale features within the large-scale system.

Wilson and Scoggins (1976) measured the variability of some basic synoptic variables by computing cumulative frequency distributions of changes in these variables for intervals of 3, 6, 9, and 12 h. They

found that 30 to 60% of a total change observed over a 12-h period occurred within a 3-h interval, and that 3-h data could more accurately identify rapid temporal changes in atmospheric structure. Direct measurement of this variability is lost between 12-h synoptic rawinsonde runs. The magnitudes of some 3-h changes even exceeded those of 12-h changes representing extreme variability of the atmosphere not measured using 12-h data. They also found that many of these changes correlated well in space with radar-observed convection and suggested that the presence of sub-synoptic systems caused variability of the atmosphere over periods less than 12 h.

McCown and Scoggins (1977) computed gradient fields of geopotential height, temperature, wind speed, and mixing ratio, and applied statistical methods to determine changes in gradient patterns associated with cumulus convection. Large variations in these patterns were found to occur over 3-h periods, possibly in relation to subsynoptic scale disturbances. The largest gradients occurred along frontal zones and in areas of convective activity, indicating rapid changes in synoptic variables over short time periods in these regions. Similar results had been reported by Miller (1969). Reap and Alaka (1969) found severe storm activity along lines of maximum dew point gradients.

Large variations in the kinematic structure of the atmosphere are important in describing atmospheric processes which release instability necessary for the development of thunderstorms. Overall and Scoggins (1975) emphasized the importance of 3-h measurements in detecting changes in vertical motions. The rate of change of vertical motion was found to be as large as 8 cm s^{-1} h^{-1} from data taken at 3-h intervals, while 12-h observations displayed a maximum rate of change of only 2 cm s^{-1} h^{-1}. The greatest changes occurred along frontal zones and were related to short wave systems moving through the network. Read and Scoggins (1977) indicated the presence of significant changes in terms of the vorticity equation and in stability parameters over 3-h intervals in response to short wave development. Changes also were observed prior to convective activity. Results indicated that

important development of circulation systems and instability occur on a time scale much less than 12 h, and that kinematic processes are important in the release of instability in the form of thunderstorms. Many of these processes could not be described accurately with the use of 12-h data.

2. DATA

a. Soundings

The data for this research consisted of upper air soundings taken during the fourth Atmospheric Variability Experiment (AVE IV) which was conducted by the National Aeronautics and Space Administration (NASA). Soundings were taken at forty-two upper air stations over the central and eastern portions of the United States (Fig. 1)* at the following nine times: 0000, 0600, 1200, 1500, 1800, and 2100 GMT on 24 April, and 0000, 0600, and 1200 GMT on 25 April.

To supplement the rawinsonde data, surface data were obtained from the National Climatic Center. Locations of the surface stations used within the AVE IV area are shown in Fig. 2.

The data reduction procedure used in processing the AVE IV data was designed to obtain the highest possible accuracy for the rawinsonde soundings. Winds were calculated at 30-s intervals and thermodynamic readings were taken at each pressure contact. Estimates of the RMS errors of the thermodynamic quantities and RMS vector errors in wind speed are presented in Table 1 (Fuelberg, 1974).

All raw data for the AVE IV experiment were keypunched and checked carefully for errors by computer before soundings were calculated. The soundings were then rechecked and corrections made as necessary.

b. Manually Digitized Radar (MDR)

In order to determine accurately the location and intensity of radar-observed convection during AVE IV, Manually Digitized Radar (MDR) data were obtained from the Techniques Development Laboratory of the National Oceanic and Atmospheric Administration (NOAA). The MDR grid network is shown in Fig. 3. Each MDR block is approximately 83 km on a side.

The MDR values, which are coded with a single digit from 1 to 9, represent areal coverage and echo intensity within each block. Three-

*Station names are given in Appendix I.

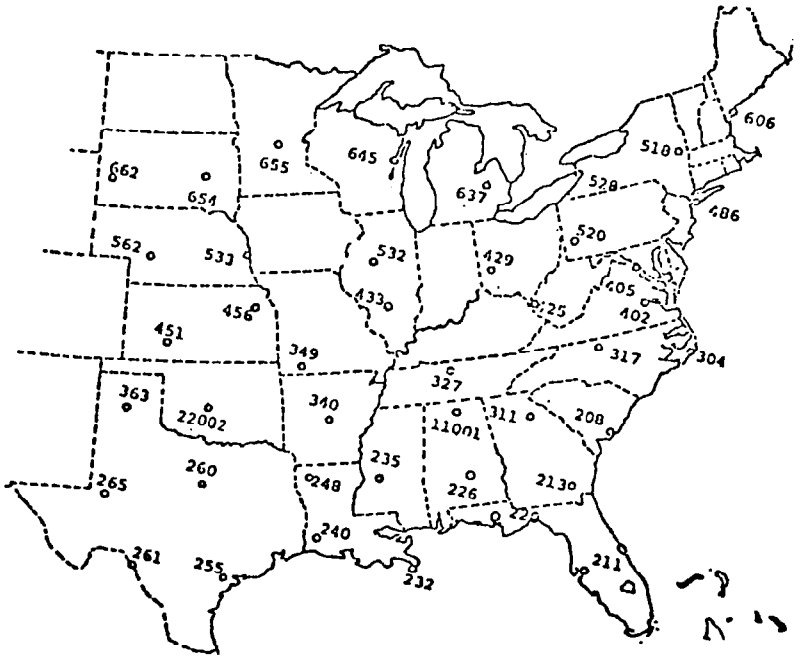

Fig. 1. Location of rawinsonde stations for AVE IV. (after Read and Scoggins, 1977).

Fig. 2. Location of surface stations participating in the AVE IV experiment. (after Read and Scoggins,1977).

Table 1. RMS errors in the rawinsonde data (after Fuelberg, 1974).

a. Thermodynamic

Quantity, variable	Approximate RMS error
Temperature	1°C
Pressure	1.3 mb from surface to 400 mb; 1.1 mb from 400 to 100 mb
Humidity	10 percent
Pressure Altitude	10 gpm at 500 mb; 20 gpm at 300 mb; 50 gpm at 50 mb

b. Wind

Level	Elevation Angle RMS Direction Error		Elevation RMS Speed Error	
	40°	20°	40°	20°
700 mb	1.8°	3.8°	0.5 ms^{-1}	1.0 ms^{-1}
500 mb	2.5°	5.6°	0.8 ms^{-1}	2.0 ms^{-1}
300 mb	3.1°	7.5°	1.0 ms^{-1}	3.8 ms^{-1}
100 mb	6.2°	15.0°	2.0 ms^{-1}	5.7 ms^{-1}

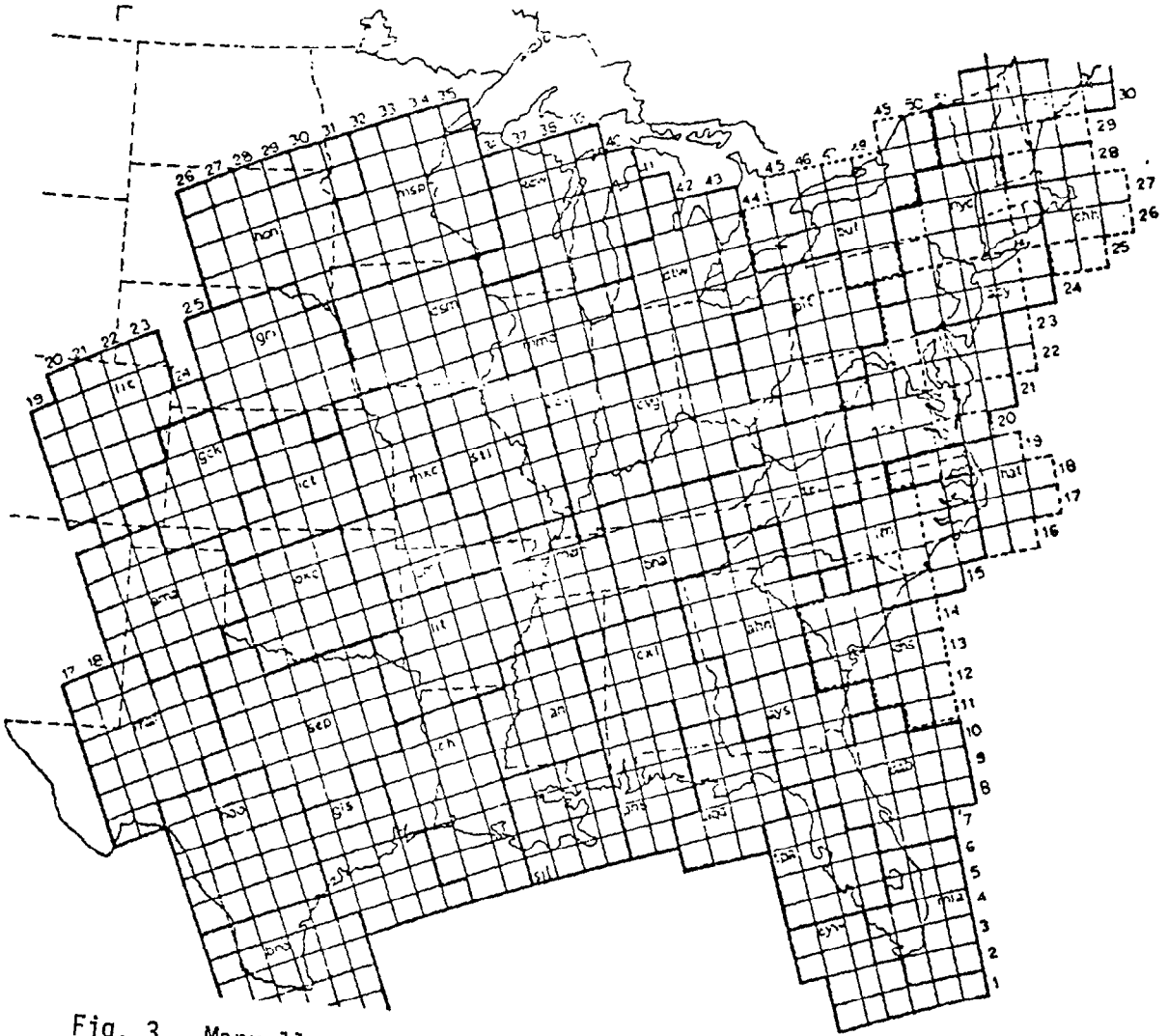

Fig. 3. Manually Digitized Radar (MDR) grid network. (after Scott and Scoggins, 1977).

hour composites of radar data centered on the rawinsonde observation times were prepared. The maximum observed MDR value in each block over the 3-h period was used. Table 2 provides a more detailed description of the MDR codes (Foster and Reap, 1973).

Table 2. Description of Manually Digitized Radar (MDR) Code. (After Foster and Reap, 1973)

Code No.	Maximum Observed VIP[1] Values	Coverage In Box	Maximum Rainfall Rate (in./hr.)	Intensity Category
0	No Echoes			
1	1	Any VIP 1	>.1	Weak
2	2	≤50% of VIP 2	.1- .5	Moderate
3	2	>50% of VIP 2	.5-1.0	Moderate
4	3	≤50% of VIP 3	1.0-2.0	Strong
5	3	>50% of VIP 3	1.0-2.0	Strong
6	4	≤50% of VIP 3 and 4	1.0-2.0	Very Strong
7	4	>50% of VIP 3 and 4	1.0-2.0	Very Strong
8	5 or 6	≤50% of VIP 3,4,5, and 6	>2.0	Intense or Extreme
9	5 or 6	>50% of VIP 3,4,5, and 6	>2.0	Intense or Extreme

[1]Video Integrator Processor

3. SYNOPTIC CONDITIONS

Analysis of the surface, 850-, 700-, 500-, and 300-mb synoptic charts for 1200 GMT on 24 April 1975 through 0000 GMT on April 25 appear in Figs. 4 through 8 inclusive. Frontal positions are presented on the surface charts.

The weather situation in AVE IV was characterized by a mass of cold polar air moving slowly across the northern United States and a large surge of warm moist air flowing over the eastern states from the Gulf of Mexico. The contrasting air masses were separated by a quasi-stationary polar front that extended from a cyclone located over northern Michigan at the beginning of the experiment to a secondary cyclone over Kansas and from there southwestward into Texas. A warm front stretched from the low in Michigan eastward to the mid-Atlantic coast. The primary cyclone moved northeastward to the Gulf of St. Lawrence during the experiment, while the secondary low moved eastward to Kentucky.

The middle and upper tropospheric flow pattern was basically zonal throughout the experiment. Two short waves moved through the zonal flow which generated severe weather in the form of two squall lines.

At 1200 GMT on April 25 moderately strong thunderstorms formed in the Ohio Valley in conjunction with the first short wave and the slight southeastward movement of the cold front. At 1800 GMT, these thunderstorms began to intensify rapidly and by 2100 GMT a strong line with tops to 15 km had formed from central Tennessee to West Virginia. These storms dissipated rapidly within the following 3-h period.

The second area of thunderstorms observed at 0000 GMT on 24 April was associated with the surface cyclone in Kansas and a warm front stretching from the low into northern Missouri. Activity decreased in intensity between 1200 and 1500 GMT due to an upper-level ridge and moved slightly to the southeast. At 2100 GMT the cyclone began intensifying with the eastward movement of another short wave, and a squall line developed by 0000 GMT on 25 April that stretched from central Oklahoma into southwest Missouri with tops over 18 km. This

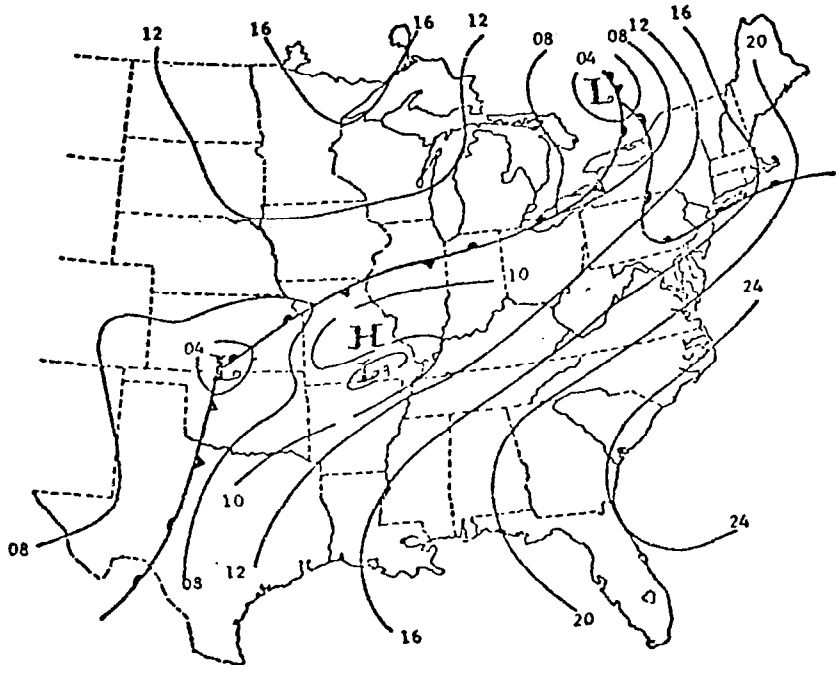

Surface

Fig. 4. Synoptic charts for 1200 GMT, 24 April 1975. (after Fucik and Turner, 1975).

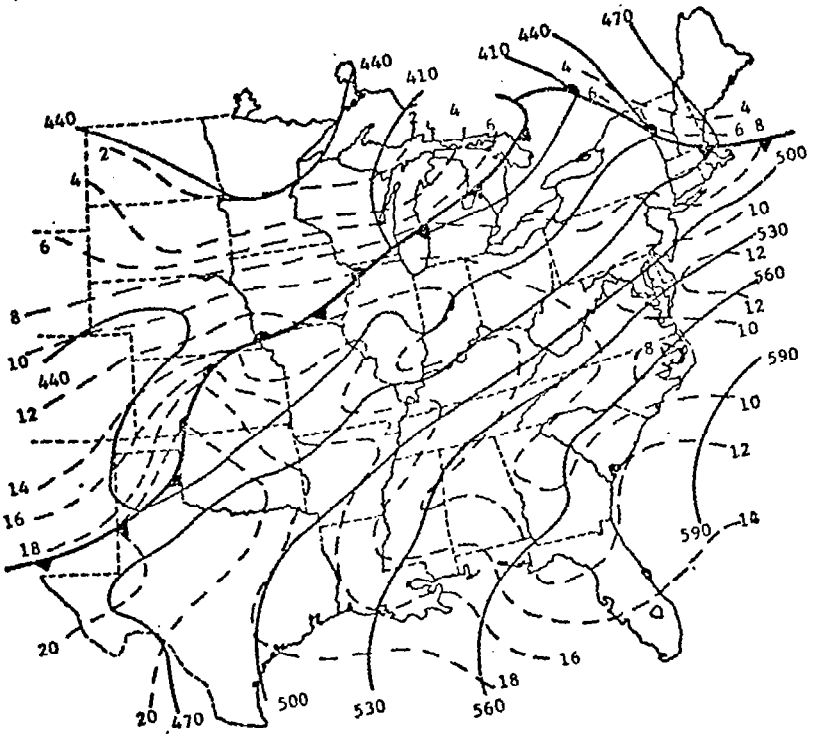

850 mb

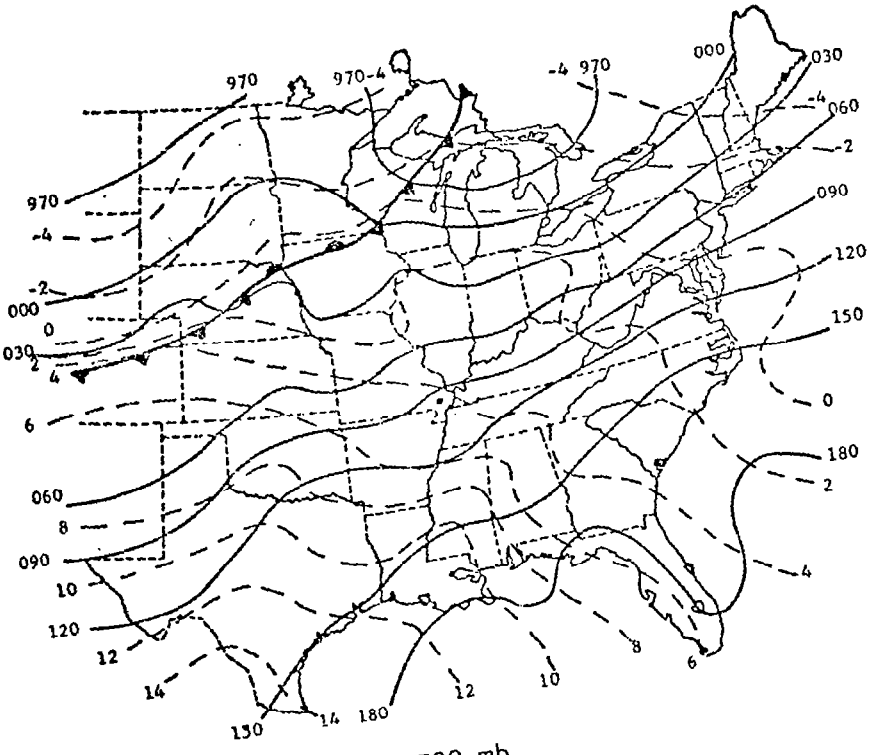

700 mb

Fig. 4. (Continued)

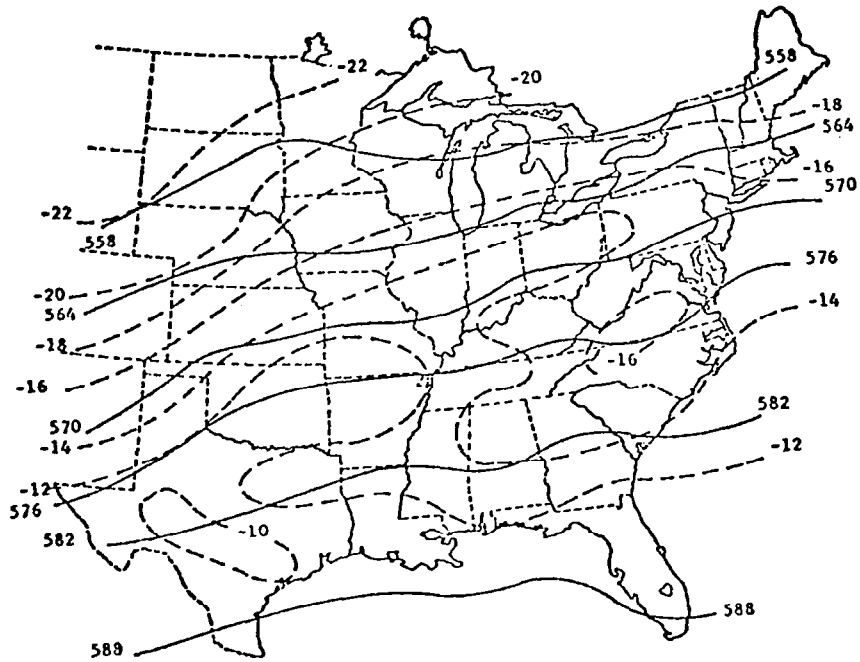

500 mb

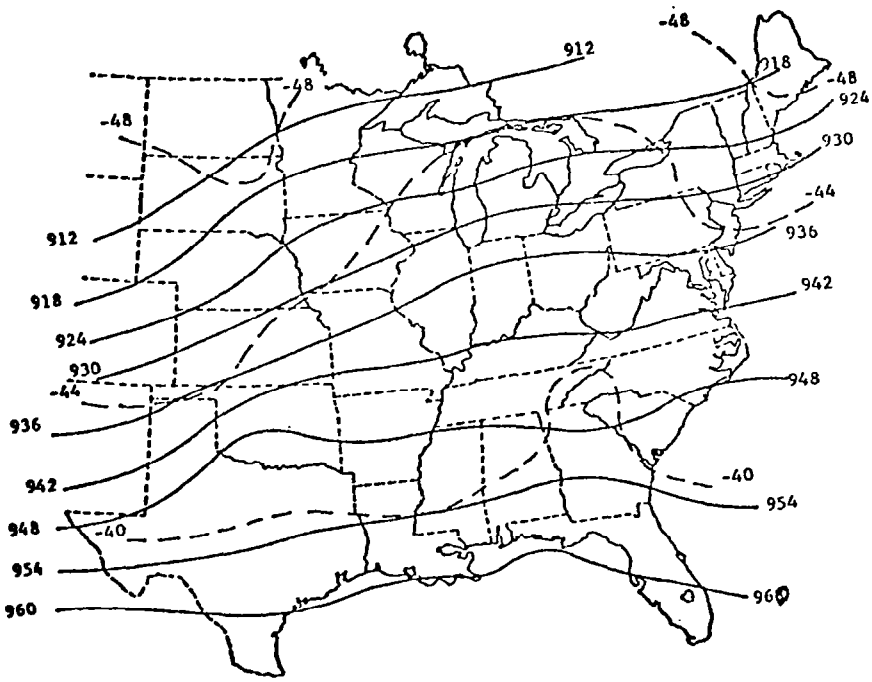

300 mb

Fig. 4. (Continued)

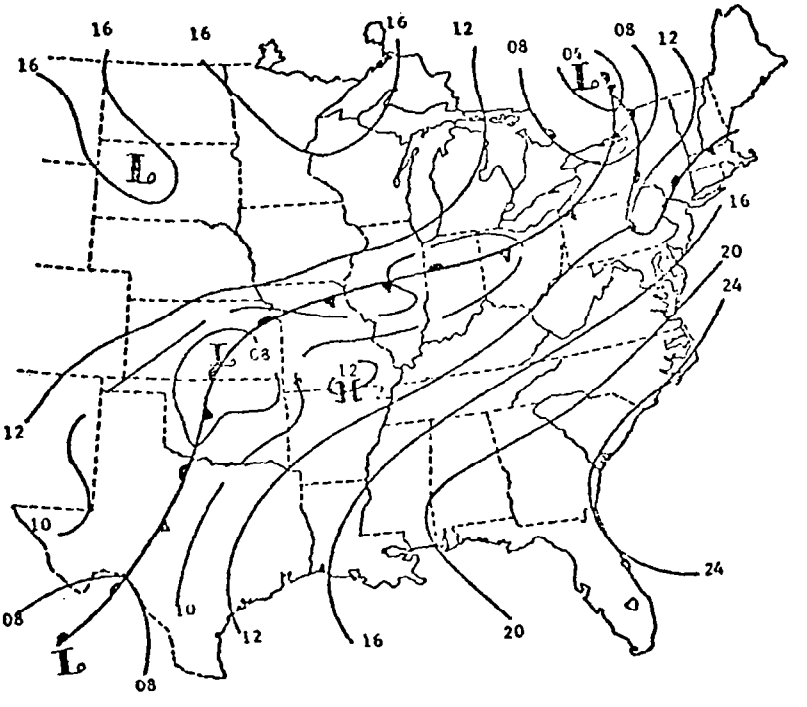

Surface

Fig. 5. Synoptic charts for 1500 GMT, 24 April 1975. (after Fucik and Turner, 1975).

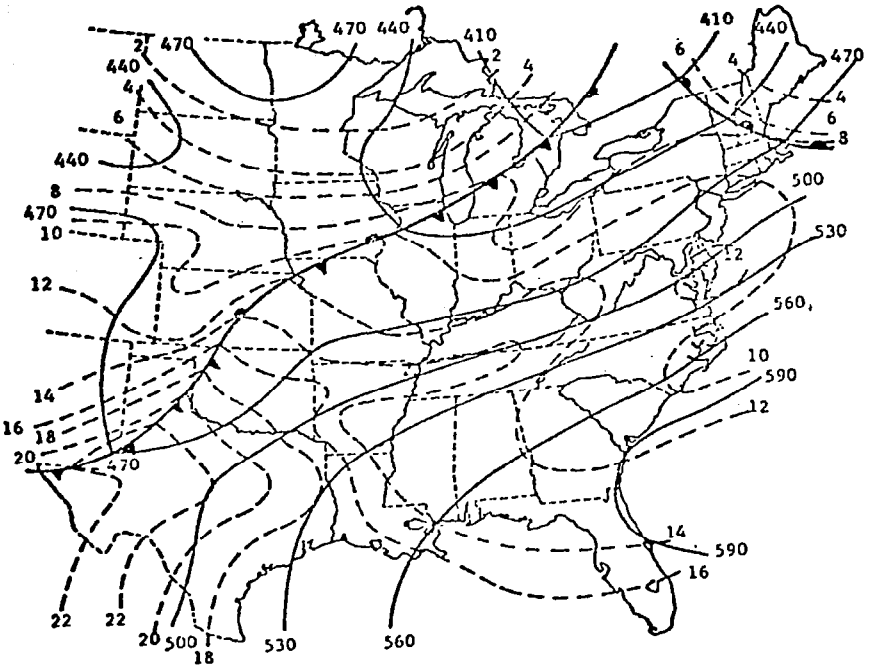

850 mb

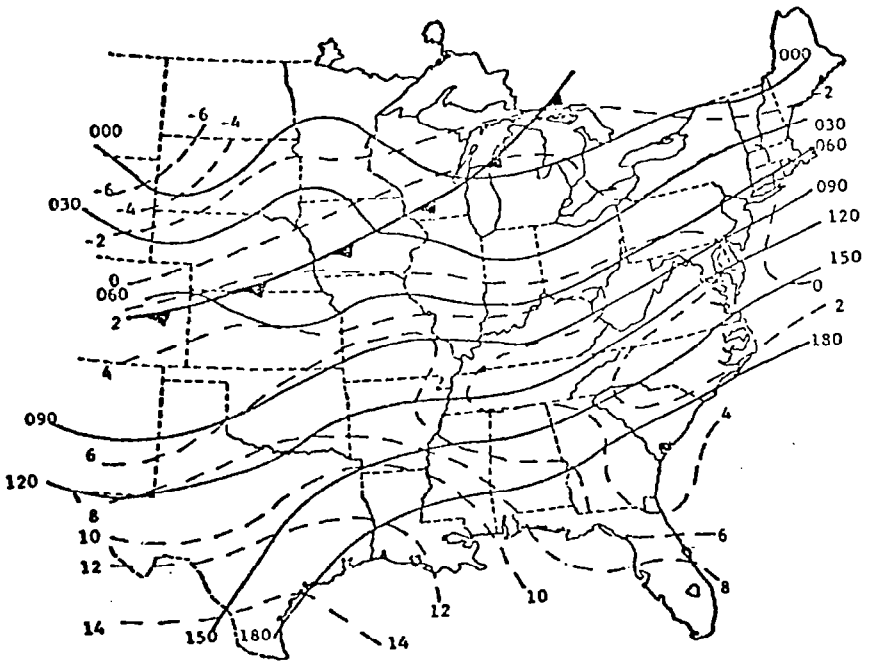

700 mb

Fig. 5. (Continued)

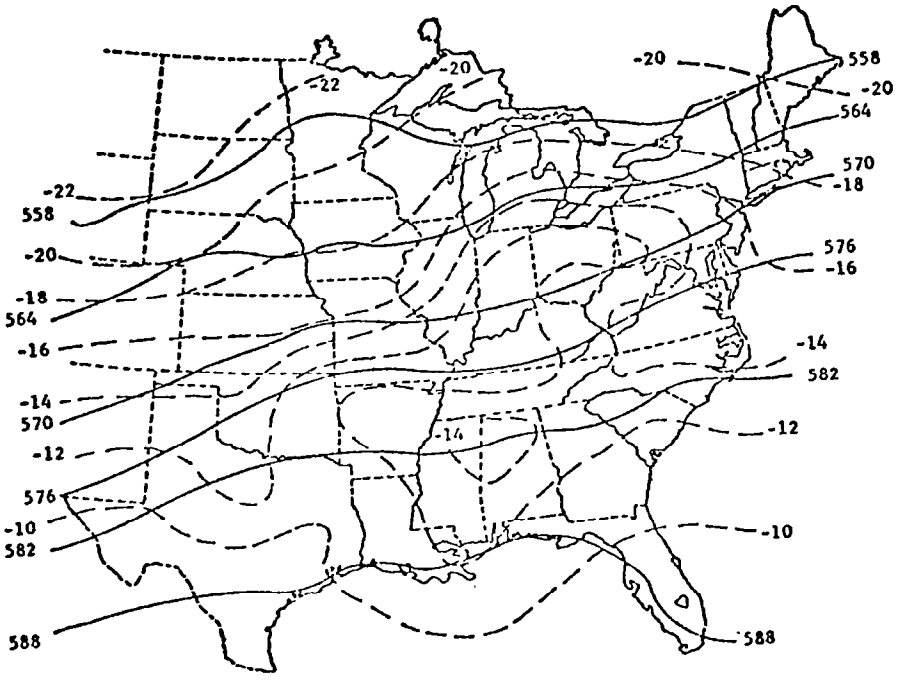

500 mb

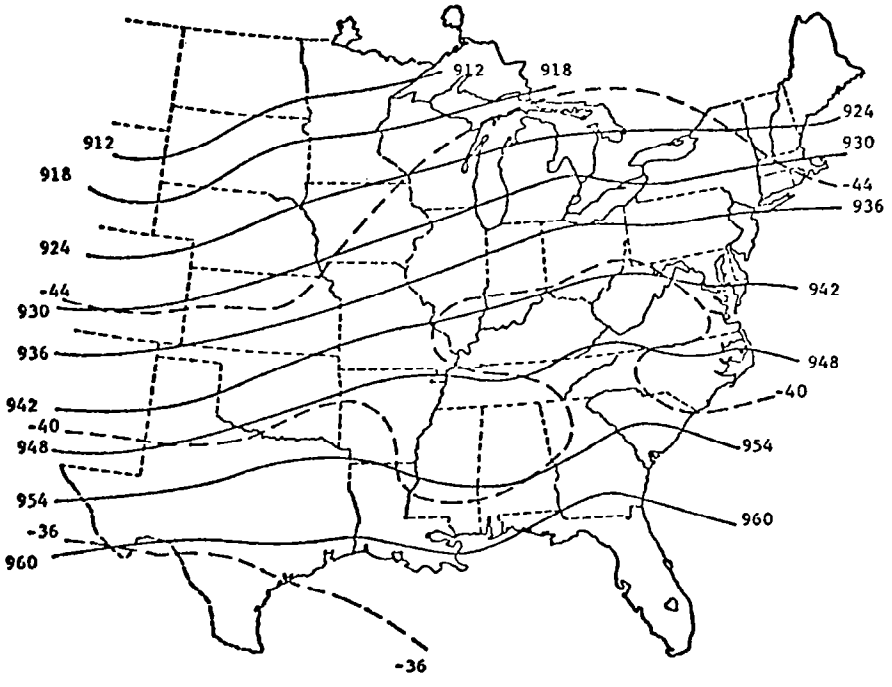

300 mb

Fig. 5. (Continued)

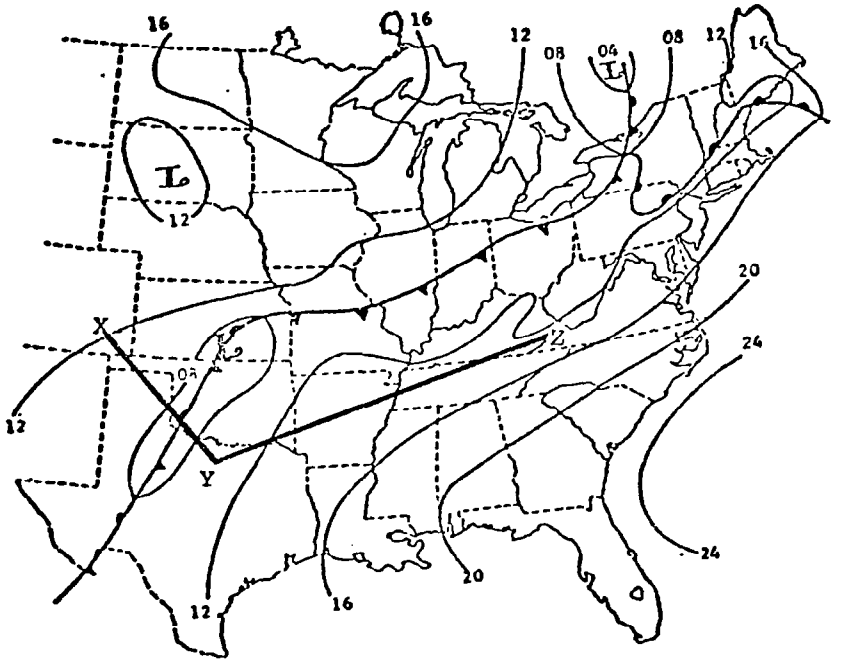

Surface

Fig. 6. Synoptic charts for 1800 GMT, 24 April 1975. (after Fucik and Turner, 1975).

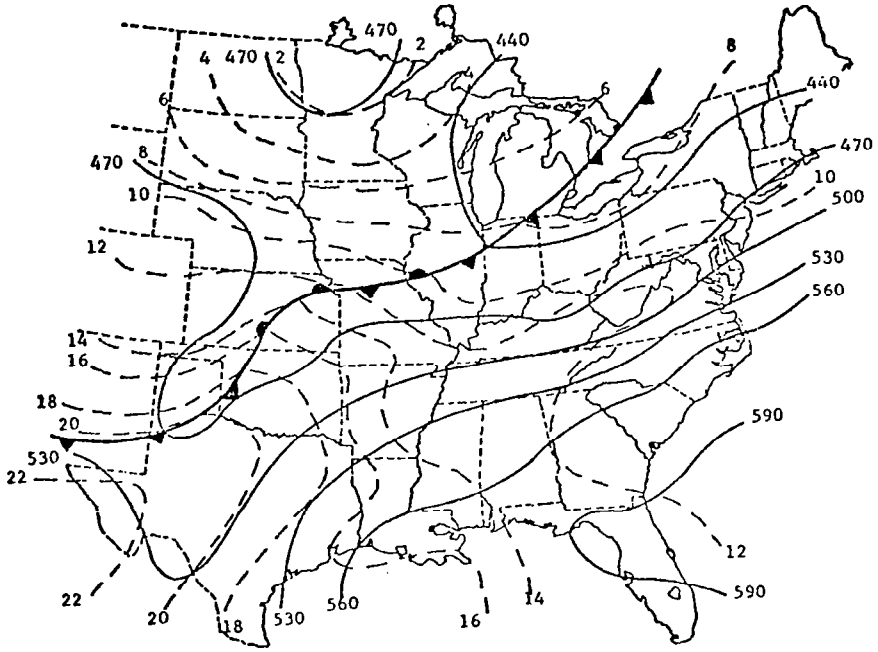

850 mb

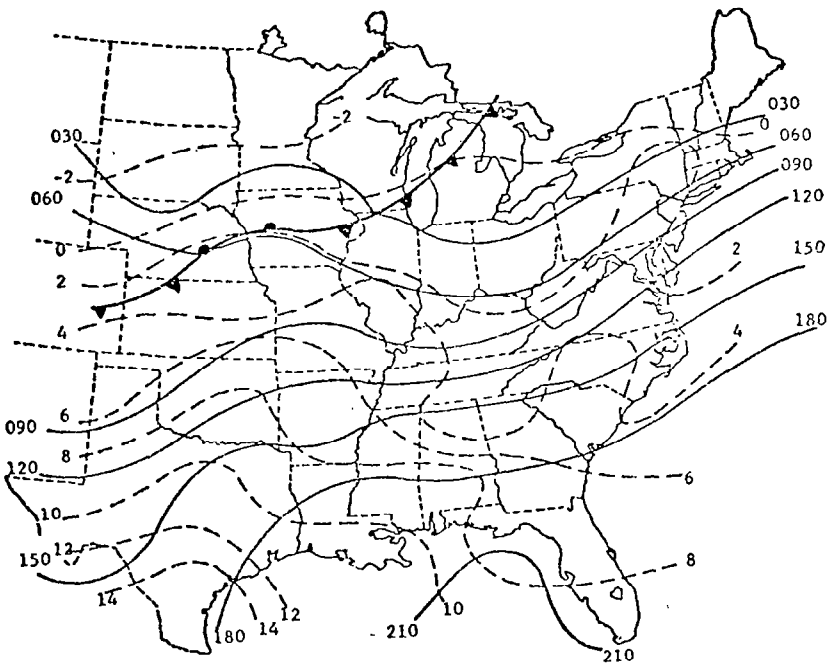

700 mb

Fig. 6. (Continued)

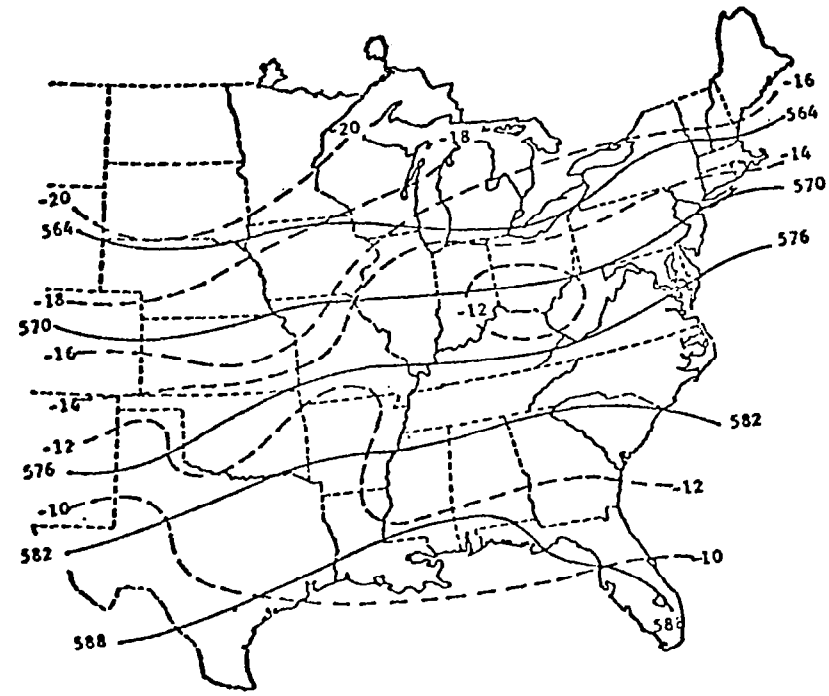

500 mb

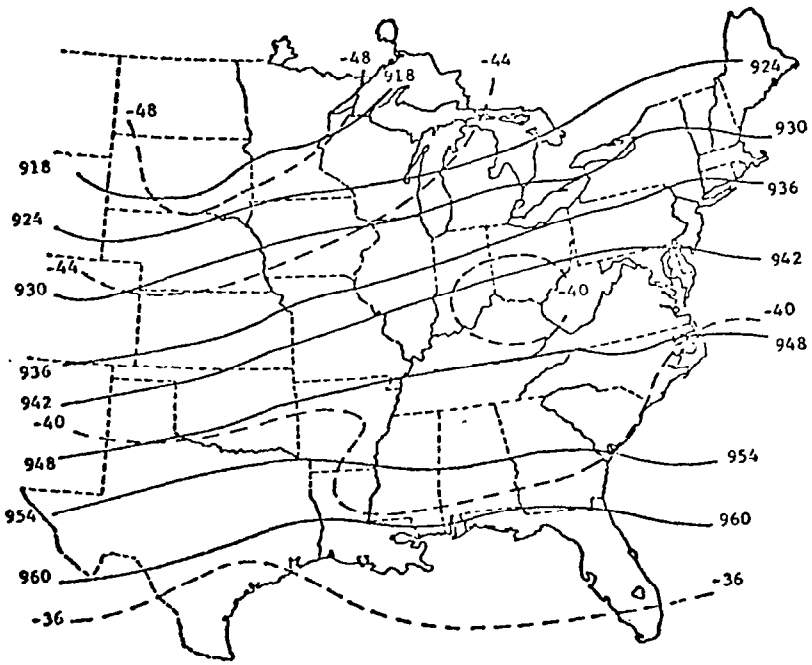

300 mb

Fig. 6. (Continued)

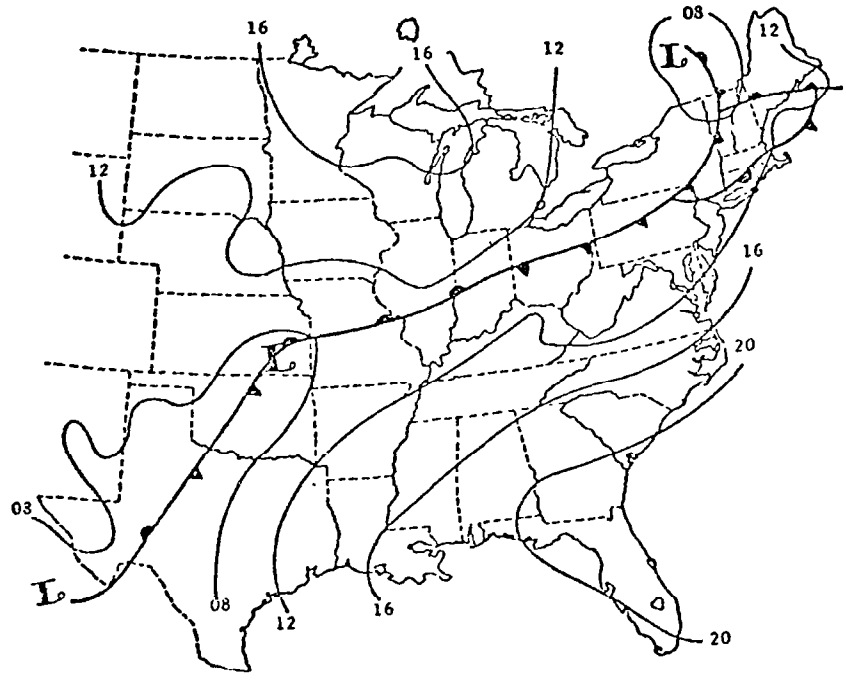

Surface

Fig. 7. Synoptic charts for 2100 GMT, 24 April 1975. (after Fucik and Turner, 1975).

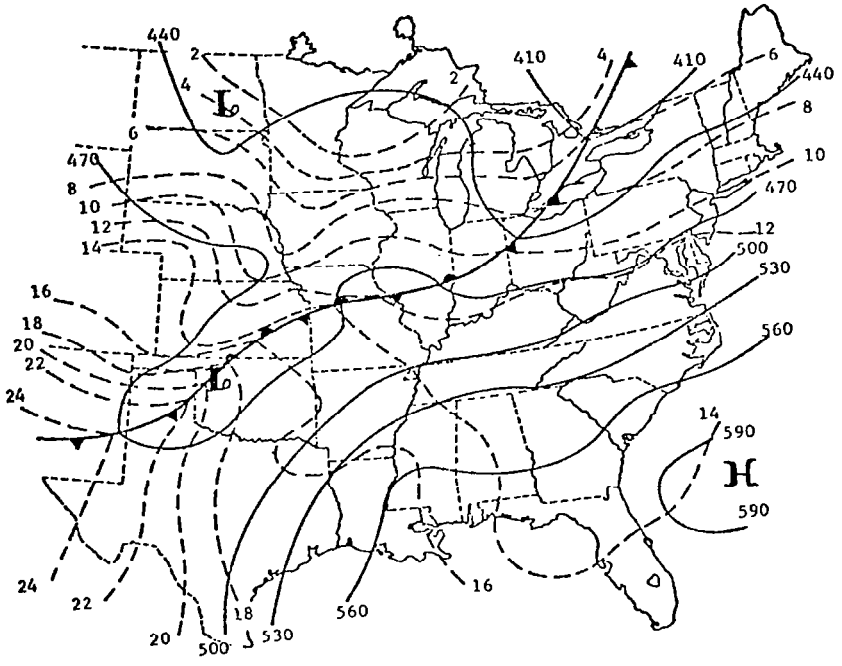

850 mb

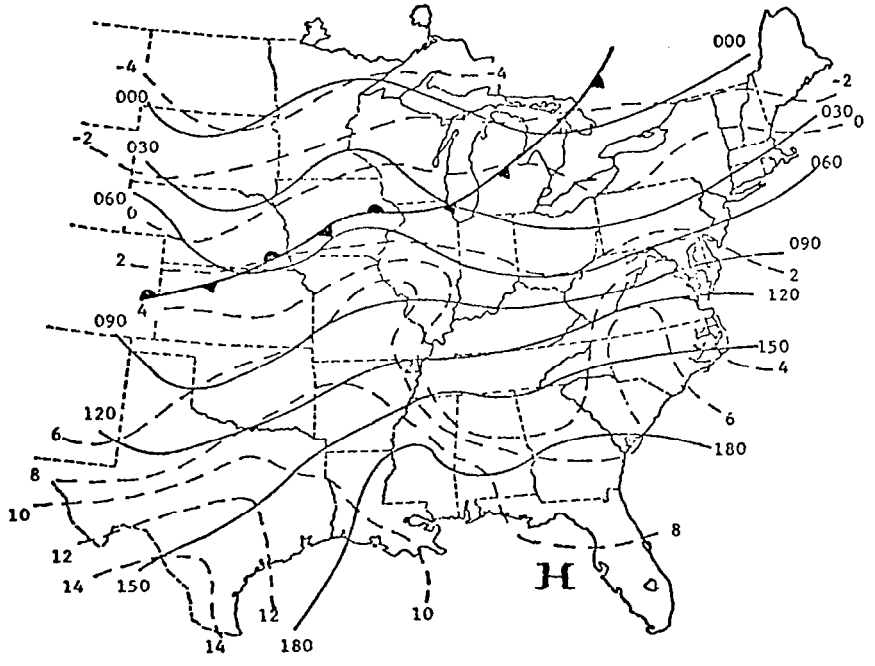

700 mb

Fig. 7. (Continued)

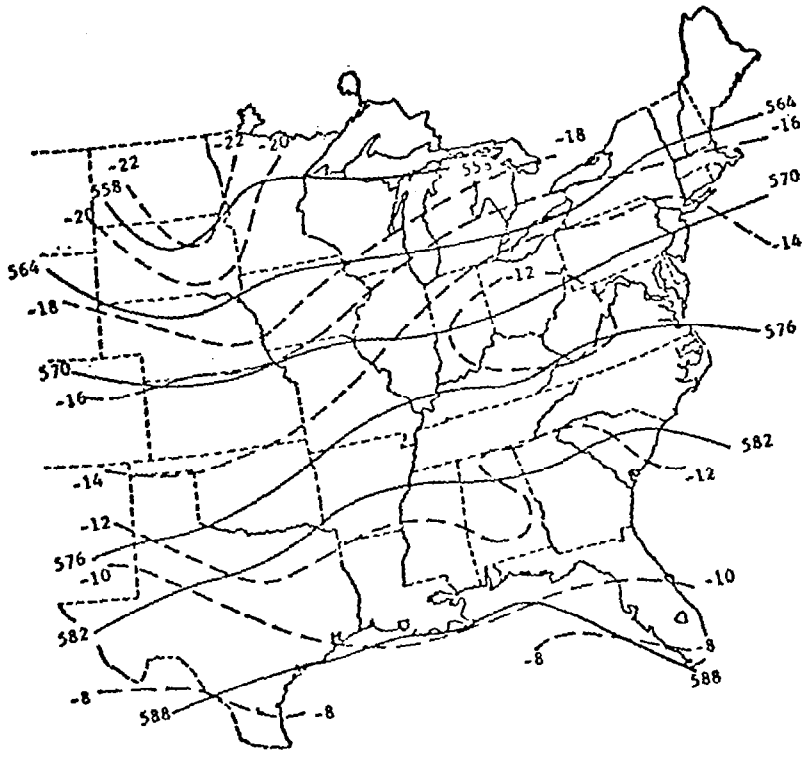

500 mb

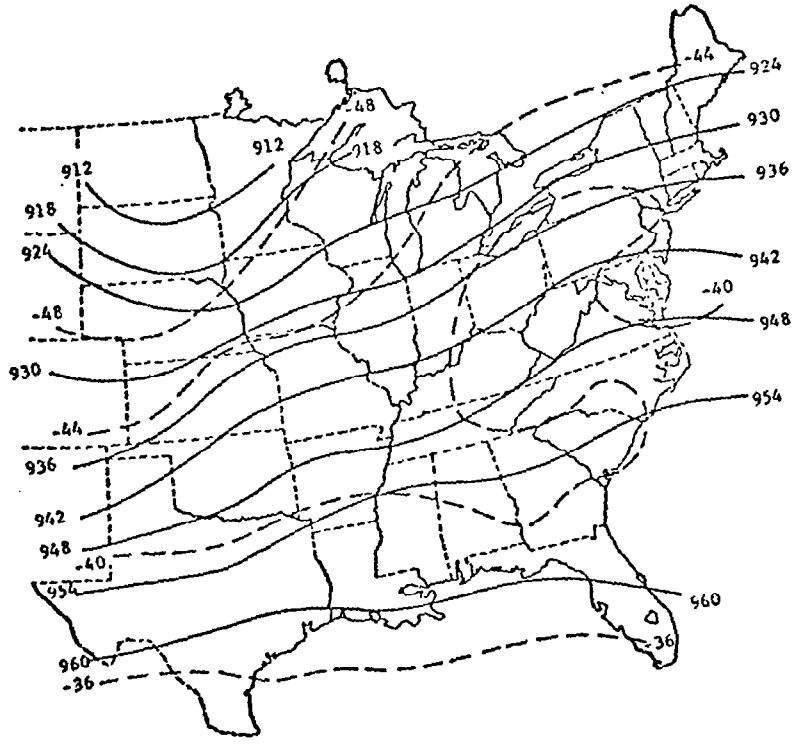

300 mb

Fig. 7. (Continued)

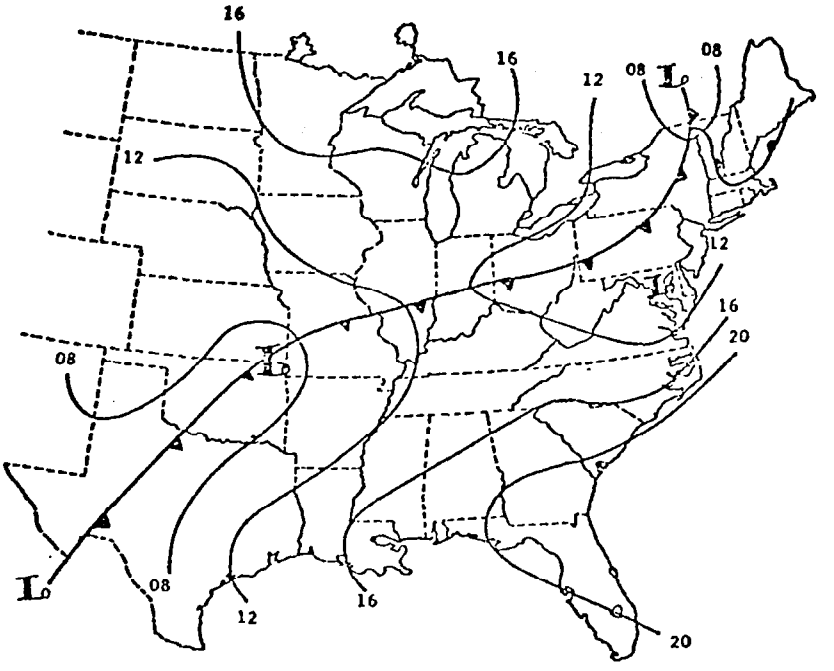

Surface

Fig. 8. Synoptic charts for 0000 GMT, 25 April 1975. (after Fucik and Turner, 1975).

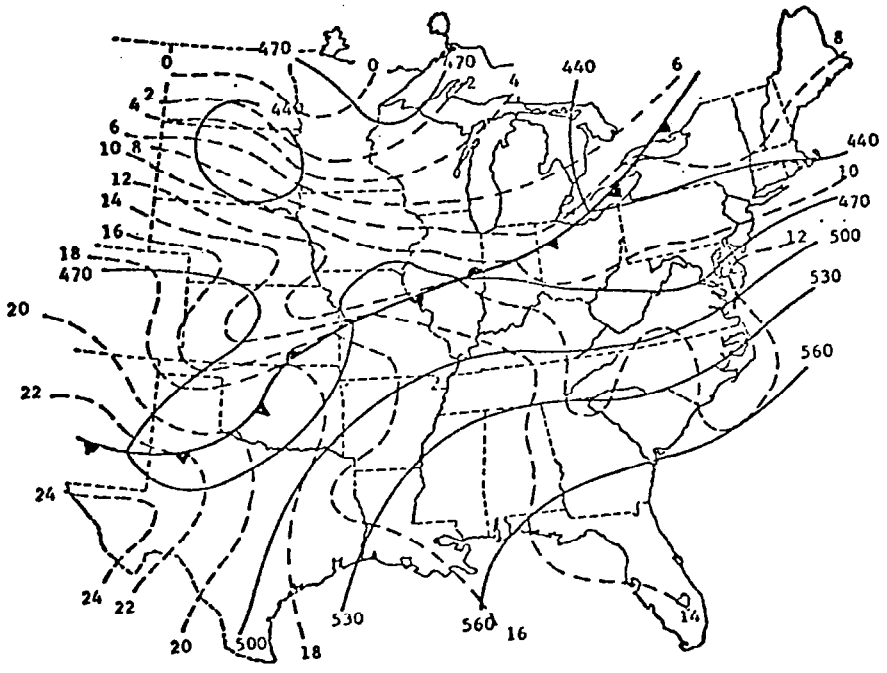

850 mb

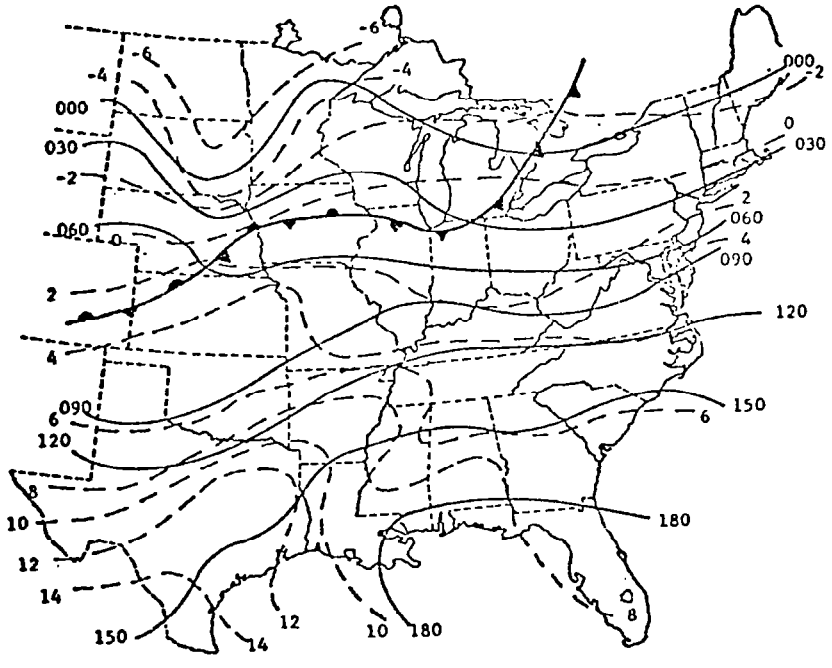

700 mb

Fig. 8. (Continued)

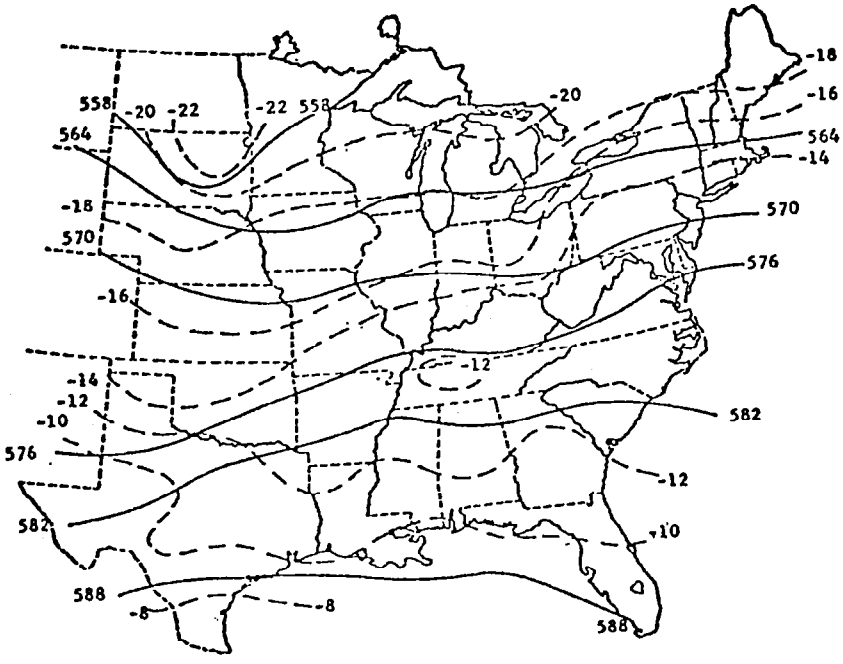

500 mb

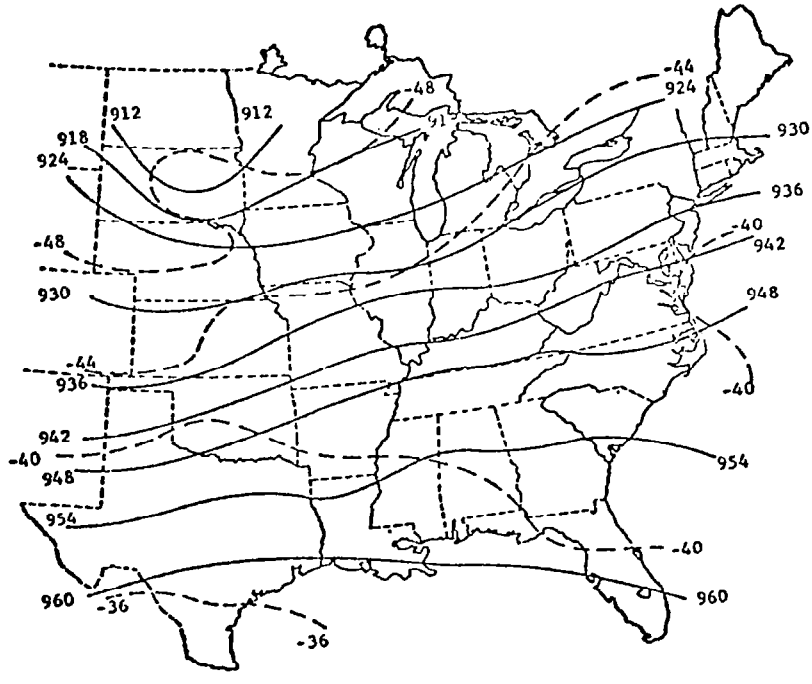

300 mb

Fig. 8. (Continued)

line of thunderstorms intensified rapidly during the next 6-h period and produced severe convective activity in the form of large hail, damaging winds, and tornadoes.

By the end of the AVE IV experiment at 1200 GMT on April 25, this squall line was moving through the southeastern portion of the United States. A trough was developing in the upper-level flow over the northern plains and polar air was replacing the maritime tropical air in the Ohio Valley and southeastern United States.

4. DATA ANALYSIS

a. Gridding of Data

An objective analysis scheme developed by Barnes (1964) was used to interpolate the rawinsonde (every 25 mb) and surface data to an 18x18 grid which is shown in Fig. 9. The Barnes' Technique is based upon the assumption that atmospheric variables may be represented as a sum of an infinite series of waves. Values of a variable are interpolated to grid points forming a first guess field, and successive corrections are then applied to the gridded field on following iterations. A grid spacing of approximately 158 km was used. This spacing is believed to provide the best horizontal resolution possible from randomly spaced rawinsonde stations (Barr et al., 1971).

A radius of influence of three grid distances from each rawinsonde station was employed to ensure adequate data for interpolation to grid points and to include major sub-synoptic features. A scan radius of only two grid distances was used for surface data due to the closer station spacing. Four iterations were performed on the gridded data and the resulting fields were smoothed by a process suggested by Shuman (1957) to further remove unresolvable features from the gridded fields.

b. Definition of Differences and the Nonlinear Coefficient

A 12-h time period from 1200 GMT on 24 April to 0000 GMT on 25 April 1975 was selected within which sounding data were available every 3 h. Values of selected variables were obtained from these sounding data for each grid point at 50-mb intervals from 900 (lowest level not intersecting ground) to 100 mb. The 12-h change for each variable was calculated by a forward time difference. This change was then linearly interpolated over 3-, 6-, and 9-h intervals to obtain interpolated values of the variables at each 3-h interval. Differences between measured and interpolated quantities were then computed by the relation:

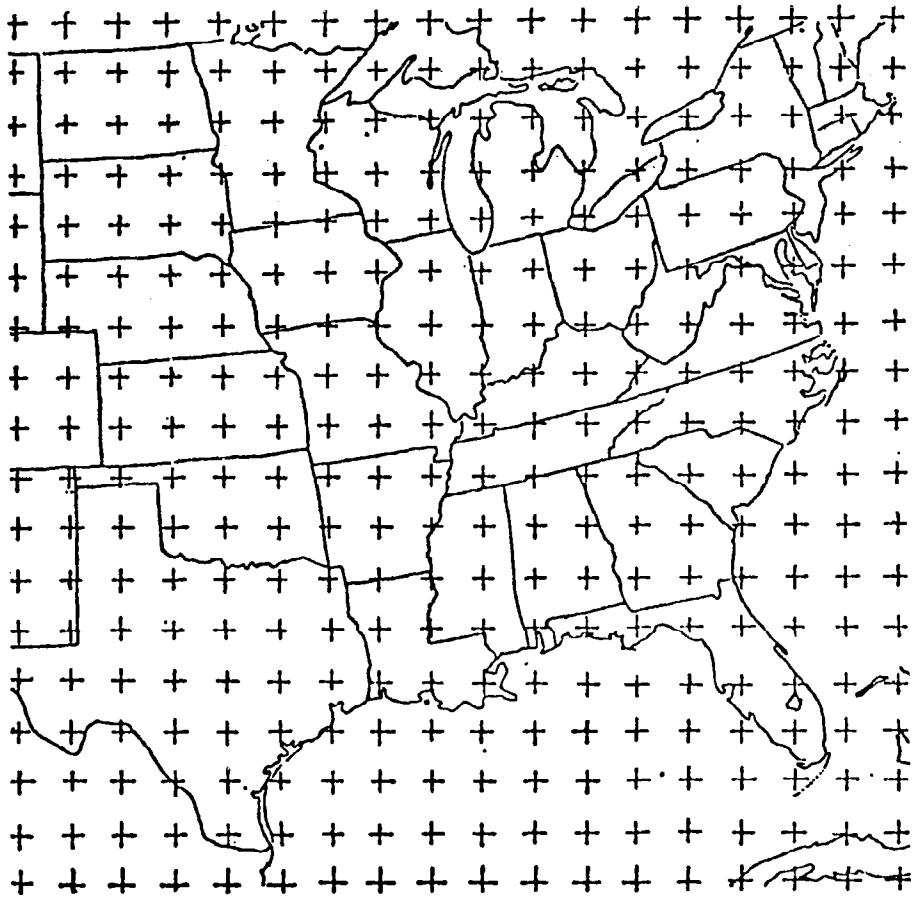

Fig. 9. Grid used for numerical computations.

$$\Delta x' = x_t - \left[\frac{t}{12}\,(x_{12} - x_0) + x_0\right] \qquad (1)$$

where x_t is the measured value of the variable at time t (3, 6, or 9 h), x_{12} is the value of the variable at the end of the 12-h interval, and x_0 is the value at the initial time.

The computed differences between measured and interpolated values represent the amount of change in a variable over a time interval, Δt, that is not accounted for by a linear change. $\Delta x'$, then, can be interpreted as a nonlinear change in the variable, x, over a time interval.

In order to determine the significance of these nonlinear changes over 3-, 6-, and 9-h intervals within the 12-h period between regular synoptic observations, a coefficient of nonlinearity is defined as:

$$C = \frac{\Delta x'}{\Delta x_M} \times 100 \qquad (2)$$

where Δx_M is the measured change in a variable over a time interval of 3, 6, or 9 h, and $\Delta x'$ is the nonlinear change or the difference between the measured change and linear change, Δx_L, over the identical time intervals. All variables are shown graphically in Fig. 10. Substitution of Eq. (1) into Eq. (2) yields:

$$C = \frac{x_t - x_0 - [\frac{t}{12}(x_{12} - x_0)]}{x_t - x_o} \times 100$$

$$= [1 - \frac{\frac{t}{12}(x_{12} - x_0)}{x_t - x_0}] \times 100. \qquad (3)$$

Since the initial and final values at each point are constant throughout the interpolation period, Eq. (3) can be expressed in the form:

$$C = [1 - \frac{t\ K_1}{12(x_t - K_2)}] \times 100 = [1 - \frac{t\ K_3}{x_t - K_2}] \times 100 \qquad (4)$$

where $K_1 = (x_{12} - x_0)$, $K_2 = x_0$, and $K_3 = K_1/12$. The nonlinear coefficient, then, is a function of the time interval (3, 6, or 9 h) and the observed value of the variable at time t. The coefficient of nonlinearity represents the percentage of a change in a variable over a time interval that is not accounted for by a linear interpolation.

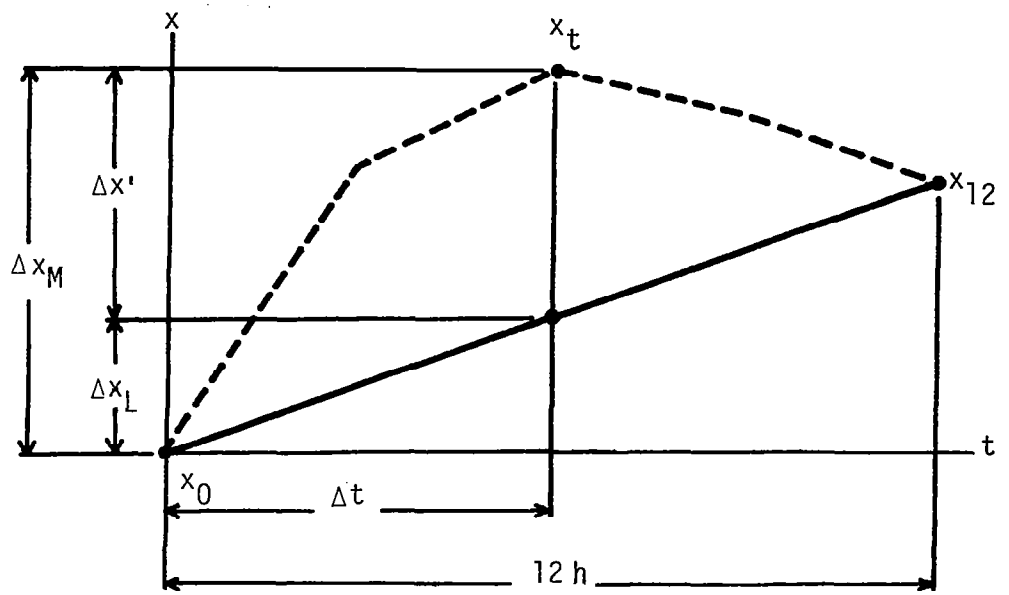

Fig. 10. Schematic diagram showing measured (Δx_M), linear (Δx_L), and nonlinear ($\Delta x'$) changes of a variable over a time interval (Δt) within the 12-h interval between rawinsonde soundings.

c. Variables Considered and Methods of Computation

Both measured and calculated variables are considered in this research. The derived variables are kinematic and stability-related.

1) Basic variables

Basic variables include temperature, mixing ratio, geopotential height, wind speed and direction, and the u and v wind components. Values of these variables were obtained from sounding data.

2) Kinematic variables

Kinematic variables include horizontal wind divergence, vertical motion, relative vorticity, and the advection of vorticity and temperature.

The horizontal wind divergence not accounted for by linear interpolation can be expressed as:

$$(\vec{\nabla}\cdot\vec{V})' = (\vec{\nabla}\cdot\vec{V}_M) - (\vec{\nabla}\cdot\vec{V}_I)$$

$$= \left[\frac{\partial u_M}{\partial x} + \frac{\partial v_M}{\partial y}\right] - \left[\frac{\partial u_I}{\partial x} + \frac{\partial v_I}{\partial y}\right] \qquad (5)$$

where u_M and v_M are the components of the measured vector wind, and u_I and v_I are components of the interpolated wind vector. The fields of divergence were computed at 50-mb intervals from 900 to 100 mb by means of centered finite differences at each grid point. Boundary grid points were not used.

Vertical motion is responsible for transporting moisture upward and releasing instability necessary for convection (Endlich and Mancuso, 1968). It is therefore one of the most important meteorological parameters.

At each sounding time vertical motion was calculated from the average horizontal divergence within each layer by the kinematic method. The equation used was:

$$\omega_k = \omega_0 + \Sigma(\overline{\vec{\nabla}\cdot\vec{V}})_k \, \Delta p \qquad (6)$$

where ω_k is the vertical velocity at the top of the kth layer, ω_0 is the vertical velocity at the bottom of the first layer which includes the terrain-induced vertical motion and a contribution from surface wind divergence, $(\overline{\vec{\nabla}\cdot\vec{V}})_k$ is the average horizontal wind divergence within the kth layer, and Δp = 50 mb.

The vertical motion not accounted for by linear interpolation of the wind field is given by:

$$\omega' = \omega_M - \omega_I$$

$$= \omega_0 + \Sigma(\overline{\vec{\nabla}\cdot\vec{V}_M})_k \, \Delta p - [\omega_0 + \Sigma(\overline{\vec{\nabla}\cdot\vec{V}_I})_k \, \Delta p] \qquad (7)$$

where $\vec{V}_M$ and $\vec{V}_I$ refer to the measured and linearly interpolated velocity vectors, respectively, and ω_0 is the vertical velocity at the bottom of the first layer. Since ω_0 is a function of terrain-induced vertical motion and surface wind divergence, it can be evaluated for any hour desired from available surface reports. Therefore Eq. (7) becomes:

$$\omega' = \Sigma[(\overline{\vec{\nabla}\cdot\vec{V}_M}) - (\overline{\vec{\nabla}\cdot\vec{V}_I})]_K \, \Delta p \qquad (7a)$$

and since $\vec{\nabla}\cdot\vec{V}_M - \vec{\nabla}\cdot\vec{V}_I = (\vec{\nabla}\cdot\vec{V})'$ from Eq. (5)

then $\overline{\vec{\nabla}\cdot\vec{V}_M} - \overline{\vec{\nabla}\cdot\vec{V}_I} = (\overline{\vec{\nabla}\cdot\vec{V}})'$, and Eq. (7a) becomes

$$\omega' = \Sigma(\overline{\vec{\nabla}\cdot\vec{V}})' \, \Delta p \qquad (8)$$

where $(\overline{\vec{\nabla}\cdot\vec{V}})'$ is the average wind divergence through a layer that is not accounted for by linear interpolation.

Since the accuracy of rawinsonde data usually decreases with height (Fuelberg, 1974; see Table 1), the accuracy of divergence also decreases with altitude. In order to reduce the errors which accumulate when vertically integrating horizontal wind divergence, an adjustment technique developed by O'Brien (1970) was applied to the computed vertical motion at all levels. This method involves adjusting vertical motion at 100 mb to zero and applying a correction factor which depends upon the pressure level. The correction factors are given by:

$$\omega_a' = \omega' - (\omega_k' - \omega_{100}') \frac{k(k+1)}{K(K+1)} \qquad (9)$$

where ω_a' is the adjusted vertical velocity for any pressure, ω' is the unadjusted vertical velocity computed from Eq. (8), ω_{100}' is the vertical velocity at 100 mb which was set to zero, ω_k' is the unadjusted value at 100 mb from Eq. (8), k is the pressure level number (k=1, 2, ...K) and K is the total number of pressure levels (K=17).

Vorticity is a measure of the rotation of the wind. Researchers have found that thunderstorms form shortly after the development of cyclonic circulation in the troposphere, and that moderate to strong positive vorticity advection is present during and prior to severe weather outbreaks (Read and Scoggins, 1977).

The relative vorticity that is not accounted for by linear interpolation of the wind field over a 12-h period is given by:

$$\xi' = \frac{\partial v_M}{\partial x} - \frac{\partial u_M}{\partial y} - \left[\frac{\partial v_I}{\partial x} - \frac{\partial u_I}{\partial y}\right] = \xi_M - \xi_I \qquad (10)$$

where u_M and v_M are the components of the measured wind vector, u_I and v_I are the components of the interpolated velocity vector, and ξ_M and ξ_I represent vorticity of the measured and interpolated wind, respectively. The advection of vorticity not accounted for by linear interpolation of the wind field is given by:

$$\begin{aligned}(-\vec{V}\cdot\vec{\nabla}\xi)' &= (-\vec{V}_M\cdot\vec{\nabla}\xi_M) - (-\vec{V}_I\cdot\vec{\nabla}\xi_I) \\ &= -\left(u_M \frac{\partial \xi_M}{\partial x} + v_M \frac{\partial \xi_M}{\partial y}\right) + \left(u_I \frac{\partial \xi_I}{\partial x} + v_I \frac{\partial \xi_I}{\partial y}\right). \qquad (11)\end{aligned}$$

Analogous to Eq. 11, the equation for the advection of temperature is:

$$(-\vec{V}\cdot\vec{\nabla}T)' = -\left(u_M \frac{\partial T_M}{\partial x} + v_M \frac{\partial T_M}{\partial y}\right) + \left(u_I \frac{\partial T_I}{\partial x} + v_I \frac{\partial T_I}{\partial y}\right) \qquad (12)$$

where T_M and T_I are the measured and interpolated temperature,

respectively. All derivatives in Eqs.(10)-(12) were computed by centered finite differences over two grid distances.

3) Stability

Studies have shown that convectively unstable air is required for the development of thunderstorms. In this research, stability was determined for three layers: 900-700 mb; 700-500 mb; and 900-500 mb. The equation used is

$$\sigma_e = -\frac{\partial \theta_E}{\partial p} = -\frac{\Delta \theta_E}{\Delta p} \tag{13}$$

where σ_e refers to convective instability (CI). Gridded fields of equivalent potential temperature, $(\theta_E)_M$, were obtained from measured data by the Rossby formula for pseudo-equivalent potential temperature, namely:

$$\theta_E = \theta_D \exp\left[\frac{Lq}{C_p T_c}\right] \tag{14}$$

where L is the latent heat of condensation, q is the mixing ratio, C_p is the specific heat at constant pressure, and T_c is the temperature at saturation. The partial potential temperature, θ_D, is given by:

$$\theta_D = T\left[\frac{1000}{p-e}\right]^{R/C_p} \tag{15}$$

where R is the gas constant for dry air, p is the pressure, and e is the vapor pressure. Interpolated values of equivalent potential temperature were computed from interpolated quantities of the basic variables.

Measured and interpolated values of CI were evaluated by finite differences from grid point values of $(\theta_E)_M$ and $(\theta_E)_I$, respectively, with Δp equal to the difference between the pressures at the top and bottom of each layer. The convective instability not accounted for by

linear interpolation is given by

$$\sigma'_e = - [(\Delta_E)_M/\Delta p] - [\Delta(\theta_E)_I/\Delta p] \quad . \tag{16}$$

4) Error analysis

The RMS errors of the basic variables obtained from rawinsonde soundings may have a significant effect on computed differences between observed and linearly interpolated values of these variables. If errors in the computed quantities are of the same magnitude or greater than the differences between observed and interpolated variables, then the specification of the differences may not be possible. When the errors are large, the differences may be due entirely to error in the basic data instead of the nonlinearity of synoptic variables.

An error analysis was performed for observed and interpolated variables and their differences to determine the magnitude of the errors. A technique presented by Young (1962) was used and is given as follows. If a quantity, Q, is calculated from observed quantities a and b (Q = f(a,b)), the error in Q resulting from errors in a and b is given by:

$$\sigma_Q = [(\frac{\partial Q}{\partial a} \sigma_a)^2 + (\frac{\partial Q}{\partial b} \sigma_b)^2]^{1/2} \tag{17}$$

where σ_Q, σ_a, and σ_b are the standard deviations of Q, a, and b, respectively.

Errors in wind for an elevation angle of 20°, and errors for temperature, moisture, and pressure were obtained from Fuelberg (1974). The errors in the basic variables were then used in Eq. (17) to compute the errors for derived variables such as kinematic parameters.

Errors for interpolated values of the basic variables and differences between observed and interpolated quantities were computed by applying Eq. (17) to Eq. (1). The terms within brackets in Eq. (1) represent the linearly interpolated quantity of the variables. Therefore,

$$Q_I = \frac{t}{12}(x_{12} - x_0) + x_0 = \frac{t}{12} x_{12} + x_0\left(1 - \frac{t}{12}\right).$$

If we let $a = x_0$ and $b = x_{12}$, then from Eq. (17)

$$\sigma_{Q_I} = \left[\left(\frac{\partial Q_I}{\partial x_0} \sigma_{x_0}\right)^2 + \left(\frac{\partial Q_I}{\partial x_{12}} \sigma_{x_{12}}\right)^2\right]^{1/2}$$

which becomes

$$\sigma_{Q_I} = [(1 - \frac{t}{12})^2 \sigma_{x_0}^2 + (\frac{t}{12})^2 \sigma_{x_{12}}^2]^{1/2}.$$

Since $\sigma_{Q_0} = \sigma_{x_{12}} = \sigma_x$,

we have
$$\sigma_{Q_I} = [(1 - \frac{t}{6} + \frac{t^2}{72}) \sigma_x^2]^{1/2} = \sigma_{x_I}. \qquad (17a)$$

The error in the interpolated parameters resulting from errors in the original data is a function of the time interval within the 12-h period. Substituting for t = 3, 6, and 9 h into Eq. (17a) yields:

$$\sigma_{x_I} = [0.625 \sigma_x^2]^{1/2} \quad \text{for } t = 3 \text{ h}$$

$$\sigma_{x_I} = [0.5 \sigma_x^2]^{1/2} \quad \text{for } t = 6 \text{ h}$$

and
$$\sigma_{x_I} = [0.625 \sigma_x^2]^{1/2} \quad \text{for } t = 9 \text{ h}.$$

Applying the same technique to Eq. (1) yields:

$$\sigma_x' = [1.625 \sigma_x^2]^{1/2} \quad \text{for } t = 3 \text{ h}$$

$$\sigma_x' = [1.5 \sigma_x^2]^{1/2} \quad \text{for } t = 6 \text{ h}$$

and
$$\sigma_x' = [1.625 \sigma_x^2]^{1/2} \quad \text{for } t = 9 \text{ h}.$$

In order to determine errors in differences between parameters computed from observed and interpolated values of the basic variables, Eq. (17) was applied to the equations listed in previous sections using errors for the original data (Fuelberg, 1974), and errors for interpolated quantities of the basic variables that were obtained from Eq. (17a). Results are presented in Table 3.

Table 3 shows that the magnitudes of errors for interpolated quantities and for differences between observed and linearly interpolated quantities were time dependent. The smallest amount of error was introduced at the mid-point of the 12-h interpolation period with larger errors at 3 and 9 h. Errors for linearly interpolated values were less than standard deviations of the original data while errors for the differences were greater than standard deviations of the original data.

Errors in mixing ratio and potential temperature decreased with altitude. This can be expected since moisture content generally decreases with height and is often negligible above 500 mb. Errors in all kinematic parameters increased with altitude since increasing error was introduced in rawinsonde measurements of wind in the upper levels of the atmosphere.

The error analysis performed in this study did not account for smoothing effects of data reduction and the objective analysis method, and therefore the errors presented in Table 3 are approximate errors for the analyzed variables. Little is known about the effects of these techniques in smoothing out or introducing error. However, Vincent and Chang (1975) introduced random errors in rawinsonde data used to compute energy budgets for tropical and extratropical cyclones and found that maximum errors after smoothing by analysis were less than or equal to standard deviations computed in Eq. (17). This implies that smoothing introduced in analysis techniques tends to reduce the effect of errors.

Table 3. Estimated RMS errors for observed, interpolated, and corresponding differences for synoptic variables.

Variable	Pressure (mb)	σ_x	σ_{x_I} 3h	σ_{x_I} 6h	σ_{x_I} 9h	$\sigma_{x'}$ 3h	$\sigma_{x'}$ 6h	$\sigma_{x'}$ 9h
Temperature (°C)		.3	.24	.21	.24	.38	.36	.38
Geopotential Height (gpm)	500	10.0	8.0	7.2	8.0	12.7	12.2	12.7
	300	20.0	15.8	14.1	15.8	25.5	24.5	25.5
Mixing Ratio (g kg^{-1})	850	.69	.55	.49	.55	.88	.84	.88
	700	.40	.32	.28	.32	.51	.49	.51
	500	.15	.12	.11	.12	.19	.18	.19
Wind Speed (m sec^{-1})	850	.8	.62	.56	.62	1.02	.98	1.02
	700	1.5	1.19	1.06	1.19	1.9	1.84	1.9
	500	2.5	2.0	1.8	2.0	3.2	3.1	3.2
	300	4.5	3.6	3.2	3.6	5.7	5.5	5.7
	100	6.0	4.7	4.3	4.7	7.6	7.3	7.6
Divergence (10^{-5} sec^{-1})	850	.5	.4	.35	.4	.63	.60	.63
	700	1.0	.8	.7	.8	1.3	1.2	1.3
	500	1.5	1.2	1.1	1.2	1.9	1.8	1.9
	300	2.2	1.7	1.6	1.7	2.8	2.7	2.8
Vertical Motion (μb sec^{-1})	850	.4	.32	.28	.32	.5	.48	.5
	700	1.5	1.2	1.1	1.2	1.8	1.7	1.8
	500	4.0	3.2	2.8	3.2	4.9	4.7	4.9
	300	7.0	5.5	5.0	5.5	8.8	8.5	8.8
Vorticity (10^{-5} sec^{-1})	850	.5	.4	.35	.4	.63	.60	.63
	700	1.0	.8	.7	.8	1.3	1.2	1.3
	500	1.5	1.2	1.1	1.2	1.9	1.8	1.9
	300	2.2	1.7	1.6	1.7	2.8	2.7	2.8
Advection of Vorticity (10^{-10} sec^{-2})	850	4.0	3.0	2.5	3.0	4.5	4.4	4.5
	700	9.0	7.0	6.5	7.0	11.5	11.0	11.5
	500	16.0	13.0	11.5	13.0	19.0	18.5	19.0
	300	22.0	17.5	15.5	17.5	25.0	24.5	25.0
Advection of Temperature (10^{-5} °C sec^{-1})	850	1.9	1.5	1.3	1.5	2.4	2.3	2.4
	500	4.5	3.6	3.2	4.5	5.7	5.5	5.7
Equivalent Potential Temperature (°C)	850	1.2	1.0	.9	1.0	1.5	1.4	1.5
	700	.7	.6	.5	.6	.9	.8	.9
	500	.5	.4	.3	.4	.6	.6	.6
Convective Instability (10^{-3} °C mb^{-1})	900-700	9.2	7.3	6.5	7.3	11.4	11.0	11.4
	700-500	4.3	3.4	3.0	3.4	5.4	5.2	5.4
	900-500	3.9	3.1	2.8	3.1	4.9	4.8	4.9

d. Statistical Analysis of Differences

Several statistical techniques were employed in analyzing the data. The mean, standard deviation, and extremes for differences computed 3, 6, and 9 h after the initial time of the 12-h interpolation period were calculated for all variables at each pressure level. Mean values were used as measures of central tendency while standard deviations indicated dispersion or variation from the mean. Results were tabulated to determine pressure levels where these statistical parameters were largest and to examine how the parameters changed in time.

A correlation analysis was employed at each time mentioned above to establish relationships between fields of differences at each pressure level with those at 850 mb. This level was chosen as the reference since most centers of differences were well defined at that level. Linear correlation coefficients were computed as follows:

$$r = \frac{COV(x,y)}{\sigma_x \sigma_y} = \left[\sum_{i,j}^{N} (x_{ij} - \bar{x})(y_{ij} - \bar{y})_k \right] / N(\sigma_x \sigma_y) \qquad (18)$$

where x_{ij} refers to grid point values of a variable at 850 mb, $\bar{x}$ is the mean value of the 850-mb field, y_{ij} refers to grid point values at the pressure level, k, $\bar{y}$ is the mean value of the kth pressure-level field, σ_x and σ_y refer to the standard deviations of the 850-mb and kth level difference fields, respectively, and N is the total number of grid points considered. Results were tabulated to determine how r changed with altitude and time. Boundary grid points were not used in computing the correlation coefficients.

e. The Vertical Structure, Temporal, and Spatial Continuity of Differences

Gridded fields of differences between measured and interpolated quantities of the variables were analyzed objectively at 50-mb inter-

vals from 900 to 100 mb for 3-, 6-, and 9-h intervals within the 12-h period between regular rawinsonde observations.

The vertical structure of differences was examined by correlating fields of differences as explained above. Individual centers of systems of differences were also examined to establish vertical and temporal continuity. This was approached by plotting the position of each center at selected pressure levels onto a separate chart. This analysis was employed to determine to what extent the centers sloped with altitude. Plots were constructed at 3-h intervals to determine how the vertical structure of these systems changed with time. The magnitudes of centers at each level and time were tabulated to show levels where differences were largest, to indicate the degree of continuity with height, and to determine time continuity of the centers.

f. Relationships of Differences to Synoptic Features and Weather

Relationships between the computed differences and synoptic conditions were determined by utilizing constant pressure charts and various cross sections. Surface synoptic features, such as cyclones and fronts, as well as areas of intense convection were superimposed upon charts of the nonlinear components of the variables. Selected vertical cross sections were used along with constant pressure charts to show a three-dimensional view of the atmospheric structure. Time cross sections were used to examine changes in magnitude of the differences between measured and interpolated quantities that were associated with changing synoptic conditions.

Direct comparisons of the computed differences to radar-observed convection were determined by use of MDR data. Averages of the differences were calculated at each level, corresponding to each MDR category previously described. Results were presented in vertical profiles for convective verses non-convective areas.

5. RESULTS

a. Relation of Differences to Synoptic Features

Fields of differences between measured values of synoptic variables and values of like variables interpolated linearly over 3-, 6-, and 9-h intervals within the 12-h period between regular rawinsonde observations were computed and analyzed objectively. Negative differences indicated that an interpolated value of a variable was greater than the observed rawinsonde value, while positive differences meant that a value obtained by linear interpolation was less than the observed value. These differences were also an indication of the amount of change in the variable over the time interval that was not accounted for by a linear change. Analysis of the fields of differences or nonlinear changes showed these differences to form centers that were systematic in time and space. Many of the centers correlated well in space with synoptic features, such as frontal zones, areas of low and high pressure, and upper-level troughs and ridges, as well as areas of radar-observed convection.

Differences between measured and linearly interpolated values of temperature computed over 3-, 6-, and 9-h intervals within the 12-h interpolation period for the 850-mb level are shown in Fig. 11. Radar-observed convection (MDR $\geq$ 4) and surface synoptic features are superimposed. Selected centers of differences are labelled for future reference.

Centers of temperature differences (nonlinear changes) were located along and behind the quasi-stationary front and in areas of strong convection. Negative differences were found mainly in the cold air behind the front, while positive differences dominated in the warm air over the eastern United States, which was free of cloudiness. Positive differences were also found behind the stationary front in Texas. Center C, located in the cold air, was negative at all levels, while center D in the warm air was positive up to the tropopause.

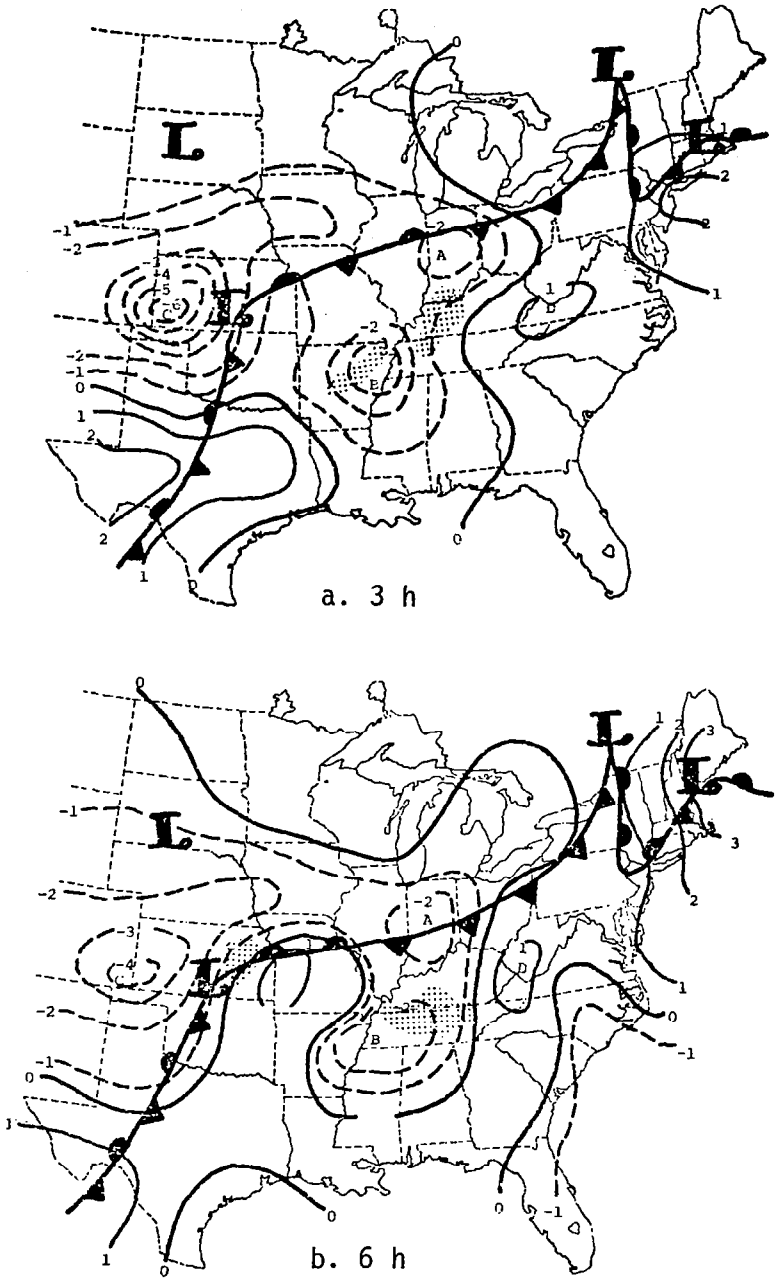

Fig. 11. Differences between measured and linearly interpolated values of temperature (°C) computed over 3-, 6-, and 9-h intervals at 850 mb. Superimposed are surface frontal positions and radar-observed convection. (Letters appearing within each center are used for identification purposes.)

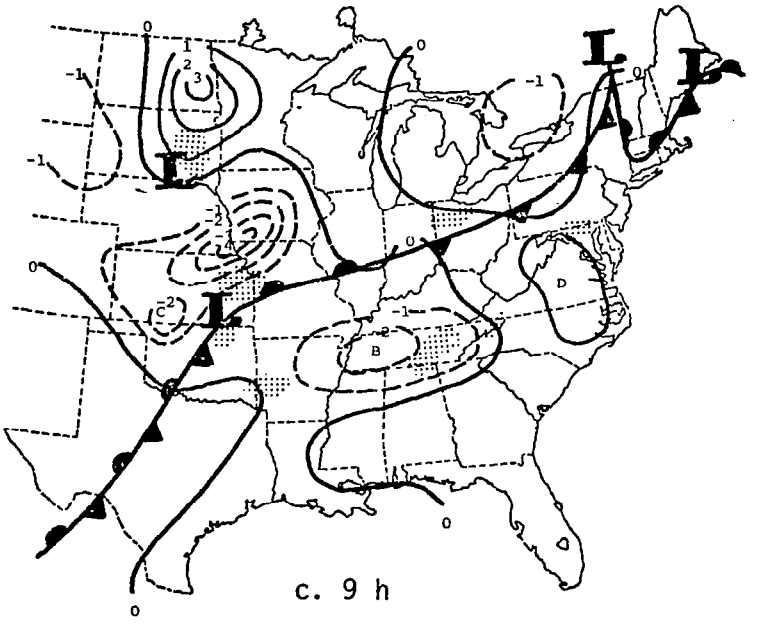

Fig. 11. (Continued)

The negative centers of temperature differences found along and ahead of the front were associated with regions of light showers and strong convection, respectively. Center A (Fig. 11) correlated well in space with a thermal trough located over Indiana and Illinois at the 850- and 700-mb levels throughout most of the interpolation period. In the upper layers, above 500 mb, a "warm pocket" was established

slightly east of this area, and the center changed sign and sloped in that direction (Figs. 5-7). Center B (Fig. 11) was located in an area of strong, but dissipating convective activity 3 h after the initial time of the interpolation period, and moved eastward behind a developing squall line in central Tennessee after 6 h. Negative differences in the lower levels in areas of strong convection may have been the result of sudden temperature decreases from downdrafts of thunderstorms that were not represented by interpolation. Differences behind the areas of convection may have been due to evaporative cooling or loss of insolation due to cloud cover. Above 800 mb, the center sloped westward over a region of subsidence and warm air advection, and changed in sign. Positive differences may be attributed to increases in temperature which were unaccounted for by a linear change, due to adiabatic warming or advection.

Analysis of Fig. 11 shows that these centers of nonlinear changes were continuous in time. Values of differences associated with each center are presented in Table 4 for selected pressure levels. Each center is labelled as it appears in Fig. 11. Table 4 shows that these centers were continuous in the vertical as well as time. Maximum values associated with center C could not be distinguished above 500 mb due to its proximity to the edge of the grid. Vertical structure of these centers are discussed in more detail in Section 5b.

Table 4 also indicates that overall, 3-h nonlinear changes of temperature were greatest in the lower layers of the atmosphere, while

Table 4. Values of temperature differences (°C) for 3-, 6-, and 9-h intervals within the 12-h interpolation period at selected pressure levels for centers in Fig. 11.

Center	Pressure (mb)	3 h	6 h	9 h
A	850	-2.3	-2.1	- .5
	700	-2.2	-1.4	- .6
	500	2.3	3.9	3.5
	300	2.4	2.6	2.0
	100	1.6	3.8	1.5
B	850	-3.3	-2.7	-2.0
	700	1.4	2.6	3.0
	500	.6	1.5	1.3
	300	1.2	1.3	.7
	100	1.2	2.4	1.1
C	850	-6.5	-4.0	-1.8
	700	-1.8	-1.8	-1.2
	500	-1.0	-1.0	- .5
D	850	1.2	1.0	1.5
	700	1.8	1.6	1.5
	500	1.5	1.7	1.3
	300	.7	.8	.6
	100	-1.4	-1.8	- .5

6-h changes were largest in the middle and upper layers. The relative contribution of these nonlinear changes over time intervals of 3, 6, and 9 h to observed changes over the same intervals are discussed in Section 5f.

Differences between measured and interpolated values of mixing ratio for each time interval are presented for the 850-mb surface in Fig. 12. Well-defined centers of maximum differences were located behind and along the polar front, along the Gulf Coast, and in areas of strong convection.

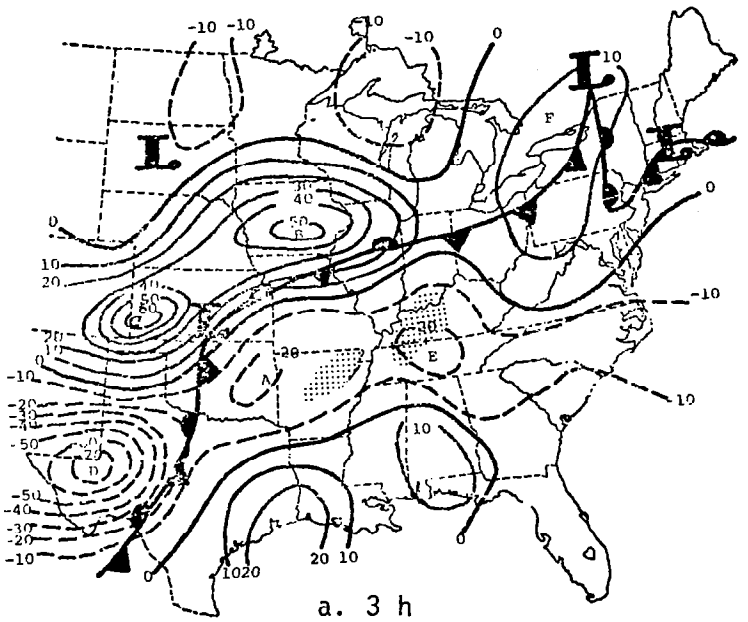

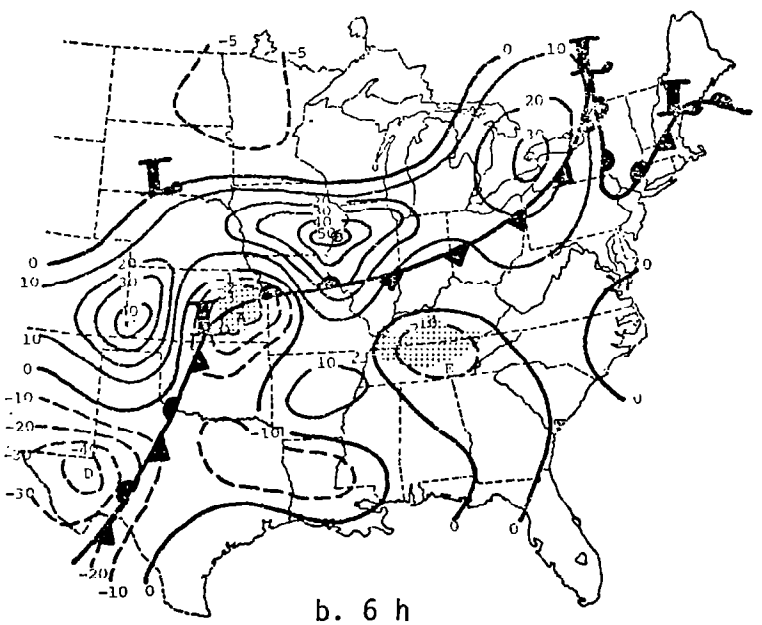

Fig. 12. Differences between measured and linearly interpolated values of mixing ratio (x 10^{-1} g kg^{-1}) computed over 3-, 6-, and 9-h intervals at 850 mb. Superimposed are surface frontal positions and radar-observed convection.

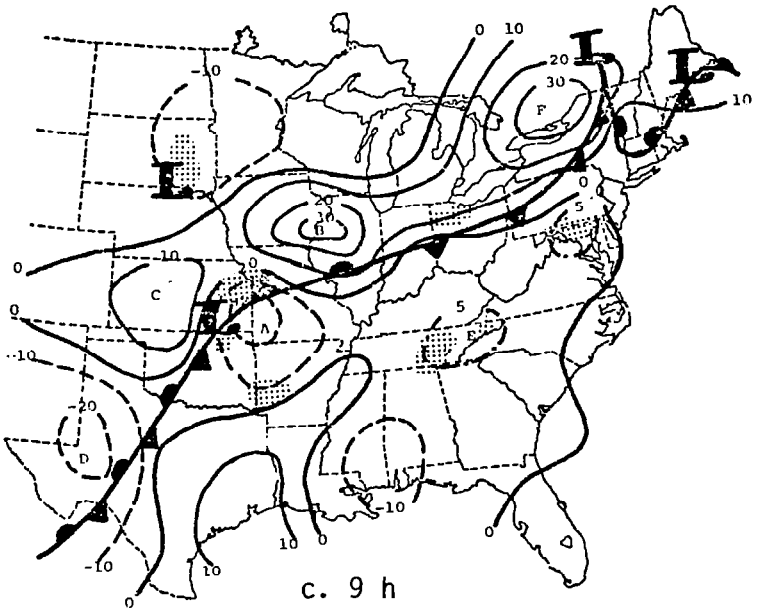

Fig. 12. (Continued)

Largest differences were found in regions behind the front. Positive values associated with centers B and C indicated that the air behind the front contained more moisture than indicated by linear interpolation, while the large negative center in Texas (D) suggested the air behind the stationary front to be much drier than indicated by interpolation. In areas of strong convection, differences were negative in the lower layers of the atmosphere and positive above 700 mb. This may have been the result of strong low-level convergence and upward motion transporting moisture aloft in these areas, causing losses of moisture in lower layers and increases aloft. Since these processes can occur over time scales much less than 12 h, these rapid changes in moisture content could not be identified by linear interpolation over a 12-h period.

Values of differences associated with each center in Fig. 12 are presented in Table 5. Overall, centers are best defined at the 850-mb level and decrease in magnitude with altitude. Three-hour nonlinear changes were largest for most centers at the 850-mb level. Changes were more variable with time at most other levels. However, centers were continuous both temporally and vertically as shown by Fig. 12 and Table 5.

Table 5. Values of mixing ratio differences (g kg^{-1}) for 3-, 6-, and 9-h intervals within the 12-h interpolation period at selected pressure levels for centers in Fig. 12.

Center	Pressure (mb)	3 h	6 h	9 h
A	850	-2.3	-3.1	-2.1
	700	-2.6	-4.1	-4.6
	500	1.0	- .8	- .6
B	850	5.8	5.4	3.3
	700	.8	2.5	2.4
	500	- .7	- .7	- .9
C	850	6.7	4.9	1.8
	700	- .8	- .7	- .8
D	850	-7.3	-4.2	-2.2
	700	-1.3	-1.6	-1.0
E	850	-2.4	-1.1	- .6
	700	-1.3	-1.2	-4.6
	500	.7	1.9	1.7
F	850	1.8	3.2	3.5
	700	1.3	1.5	1.7
	500	1.2	1.2	.9

Differences between measured and linearly interpolated values of geopotential height 6 h after the initial time of the 12-h interpolation period at 500 mb are shown in Fig. 13. Negative differences (center A) correlated well in space with an upper-level trough which was established over Indiana, Kentucky, and Tennessee (Figs. 5-7). This indicated a decrease in geopotential height in association with the passage of the trough that was not accounted for by interpolation. Negative differences were also located on the western edge of the grid network where another trough was located. The large area of positive differences in the central portions of the United States were associated with a weak upper-level ridge.

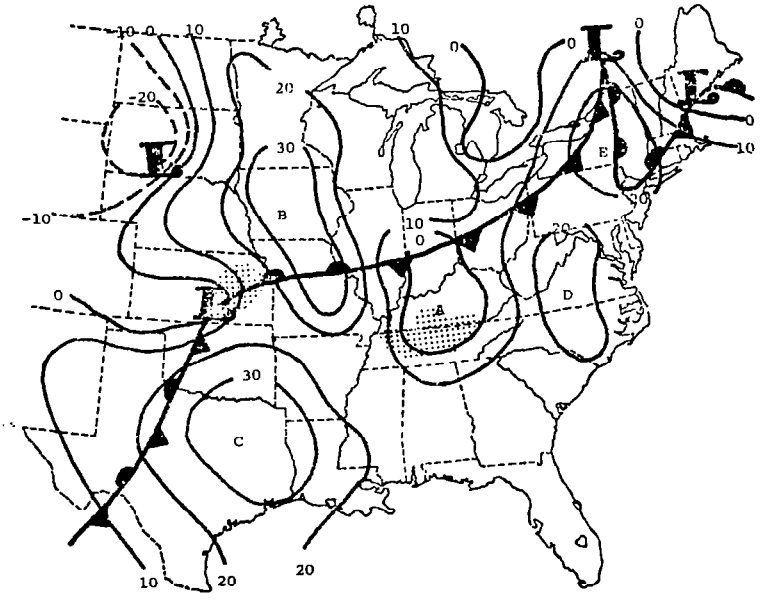

Fig. 13. Differences between observed and linearly interpolated values of geopotential height (gpm) at 500 mb computed 6 h after the initial time of the 12-h interpolation period. Superimposed are surface frontal positions and radar-observed convection.

Centers of geopotential height differences moved only slightly eastward throughout the period. This can be attributed to the slow movement of systems during the AVE IV experiment. Table 6 gives the values of geopotential height centers at various levels and shows that variations in the intensity of these centers were systematic in time. Overall, 6-h differences were largest, except for an area along the mid-Atlantic coast (center D) where 3-h differences were largest.

Table 6 also shows that positive geopotential height differences increased with altitude and negative differences became less negative above 700 mb. Since geopotential height is a function of the vertical integral of temperature, this vertical increase of the differences can be expected, since temperature differences were either positive through the troposphere or became less negative and changed sign with increasing altitude.

Differences between measured and interpolated values of wind speed computed 6 h after the initial time of the interpolation period at the 850- and 300-mb levels are presented in Fig. 14. The largest differences at 850 mb were found along the frontal zone and along the zone of maximum observed winds denoted by the dark arrow. Positive centers were found directly over areas of strong convective activity in central Tennessee and east of a surface low in Kansas. At 300 mb, largest differences were likewise associated with the zone of maximum observed wind speeds. Similarities were found for all levels at all time periods suggesting that these centers of maximum difference sloped with altitude following the zone of maximum wind, and that the magnitudes of differences between measured and interpolated wind speed may be a function of observed wind speeds.

A cross section of measured and interpolated values of the wind field, and the corresponding differences in wind speed along line XYZ of Fig. 6 are shown in Fig. 15. The largest differences were found in the upper levels, corresponding to the jet core near the tropopause. Centers of maximum differences also were found ahead of the frontal zone and in regions of strong convection denoted along the bottom axis. Figure 15 indicates that linear interpolation could

Table 6. Values of geopotential height differences (gpm) for 3-, 6-, and 9-h intervals at selected pressure levels for centers in Fig. 13.

Center	Pressure (mb)	3 h	6 h	9 h
A	850	- 4	- 9	- 6
	700	-17	-14	- 8
	500	-12	- 8	- 7
B	850	16	23	17
	700	18	23	19
	500	25	35	32
	300	32	46	42
	100	56	97	52
C	850	20	31	18
	700	26	35	17
	500	33	23	23
	300	49	47	38
	100	68	88	68
D	850	12	12	7
	700	14	14	10
	500	28	24	22
	300	56	54	53
	100	82	81	45
E	850	5	9	4
	700	16	15	8
	500	17	25	12
	300	20	44	29
	100	32	77	59

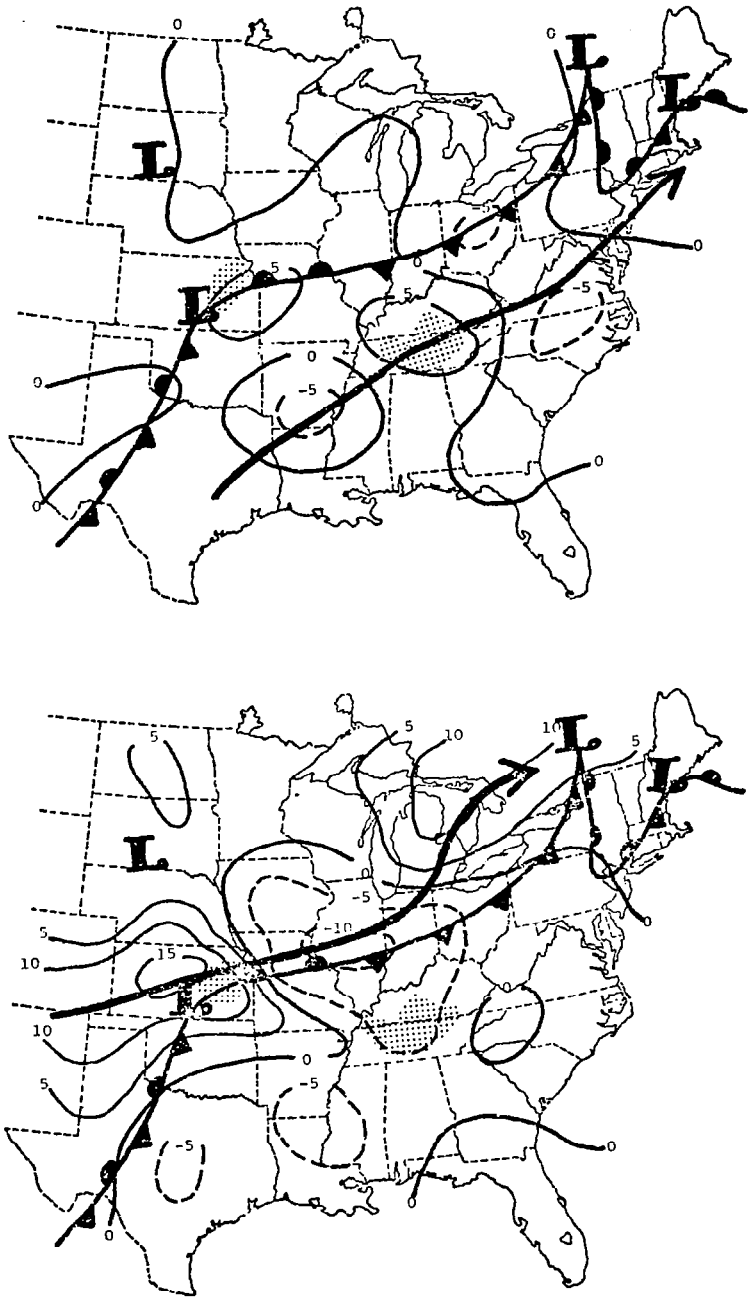

Fig. 14. Differences between observed and linearly interpolated values of wind speed computed 6 h after the initial time of the interpolation period at the 850- and 300-mb layers. Superimposed are surface frontal positions and radar-observed convection. Arrow indicates zone of maximum wind speed for each pressure level. Units are m s^{-1}.

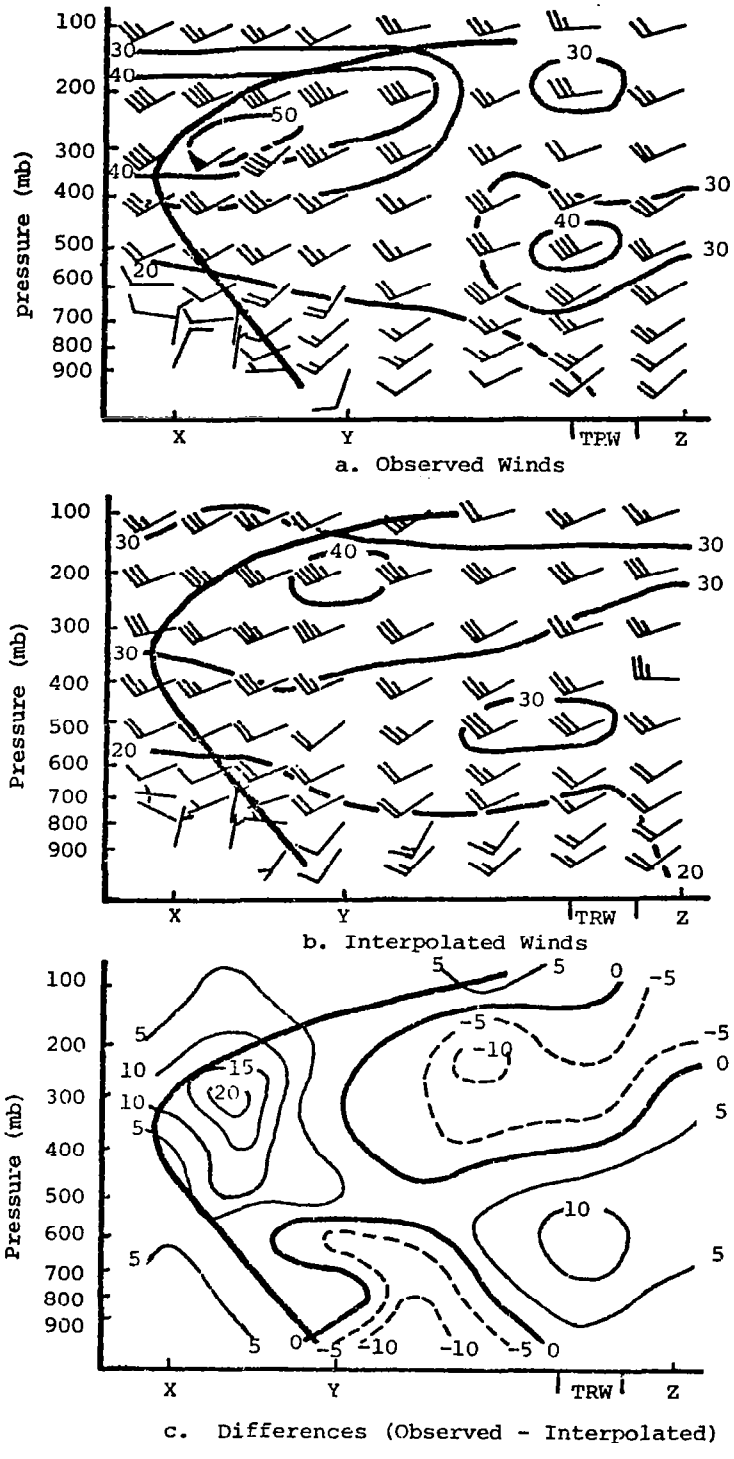

Fig. 15. Vertical cross sections of observed and interpolated winds, and corresponding differences (m s^{-1}) along line XYZ of Fig. 6 at 1800 GMT, 24 April 1975.

define the direction of the upper-level air flow with reasonable accuracy. Largest differences in wind direction were found in the lower levels just ahead of the front. However, interpolation was able to denote the wind shift behind the front.

As discussed in Section 4c, the wind field obtained by linear interpolation was used to compute various meteorological variables. Differences between the values computed from observed winds and those derived from interpolated winds represent the kinematic structure of the atmosphere that is not measured by assuming a linear change in the winds over a 12-h period.

Fields of differences for the horizontal wind divergence over 3, 6, and 9 h are shown in Figs. 16-18 for the 850- and 300-mb pressure levels. Negative differences were found in areas of developing and intensifying convective activity which indicated that the wind field was becoming more convergent in the lower layers of the atmosphere than shown by interpolation. Center E, for example, correlated well in space with the squall line which intensified rapidly over Kentucky and Tennessee between 1800 and 2100 GMT. The positive differences over these areas after the first 3 h of the interpolation period (Fig. 16a) and the negative differences over the area after 6 h (Fig. 17a) suggests large increases in the convergence of the wind 3 h prior to convective activity that were not accounted for by linear changes in the wind field. Negative centers were also located along the polar front in Indiana and Illinois, but were associated with only light rain showers.

In AVE IV, convection also occurred in areas where the wind field was divergent in the lower layers of the atmosphere, such as in Arkansas at 1500 GMT, 24 April. Activity, however, diminished rapidly within the following 3 h. The intense positive center (B) over Arkansas after the first 3 h of the interpolation period (Fig. 16a) indicated increasing divergence in the low-level wind field over the 3-h period that was not indicated by interpolation. The center moved eastward throughout the interpolation interval and was positioned

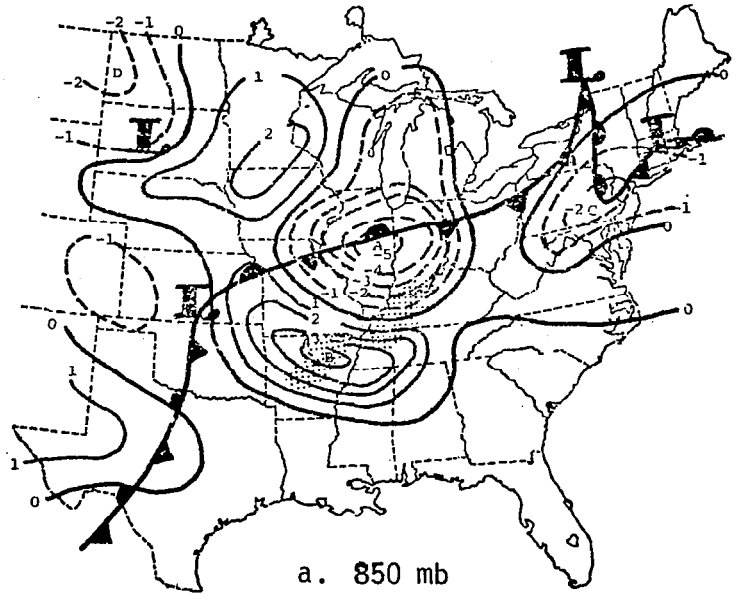

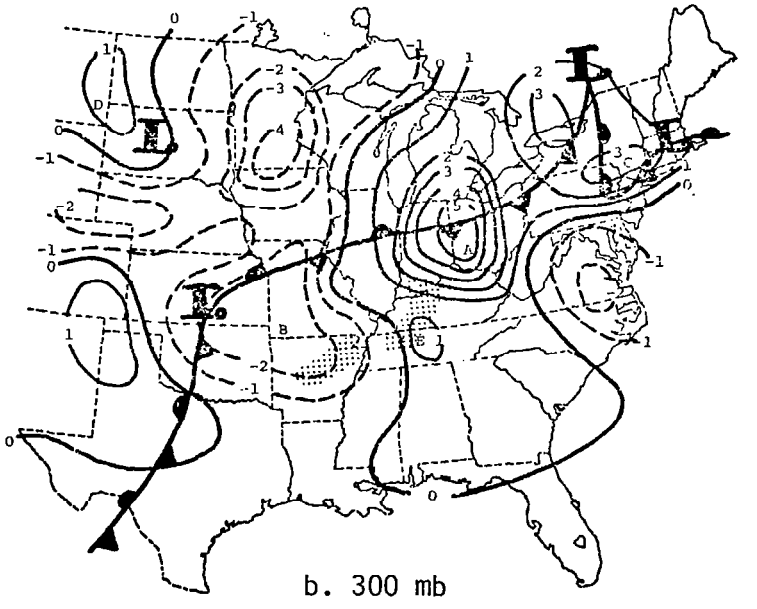

Fig. 16. Differences between values of horizontal wind divergence (x 10^{-5} s^{-1}) computed from observed and interpolated winds 3 h after the initial time at 850 and 300 mb. Superimposed are surface frontal positions and radar-observed convection.

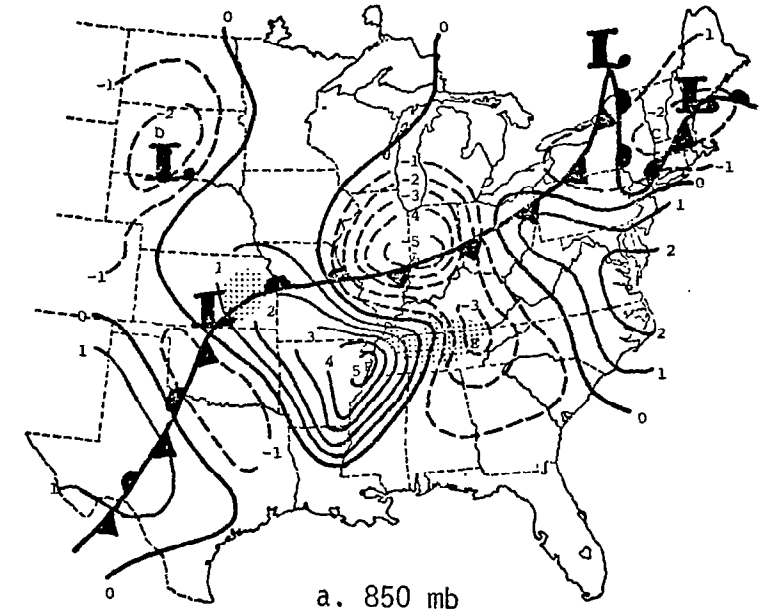

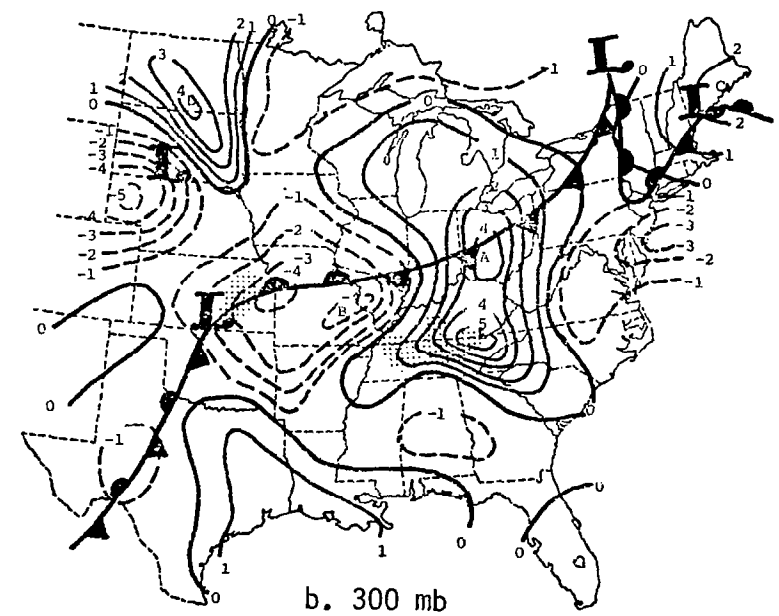

Fig. 17. Differences between values of horizontal wind divergence (x 10^{-5} s^{-1}) computed from observed and interpolated winds 6 h after the initial time at 850 and 300 mb. Superimposed are surface frontal positions and radar-observed convection.

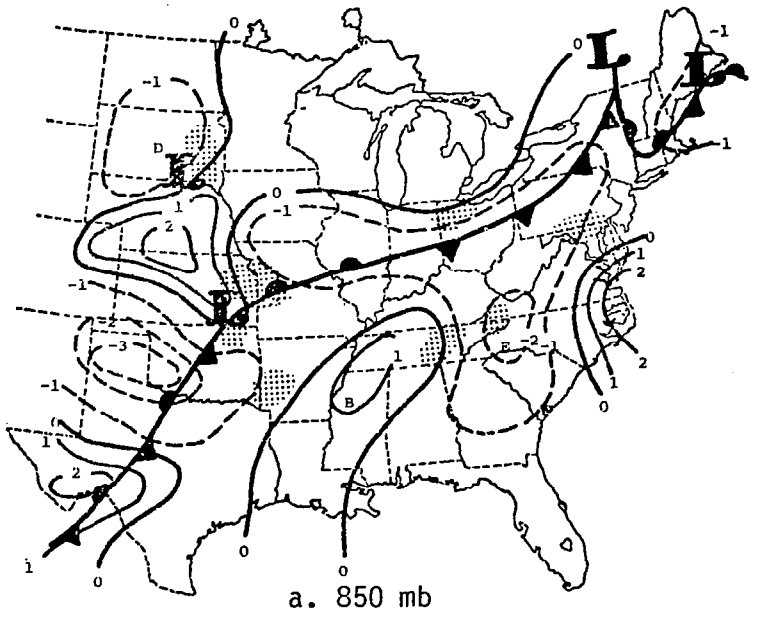

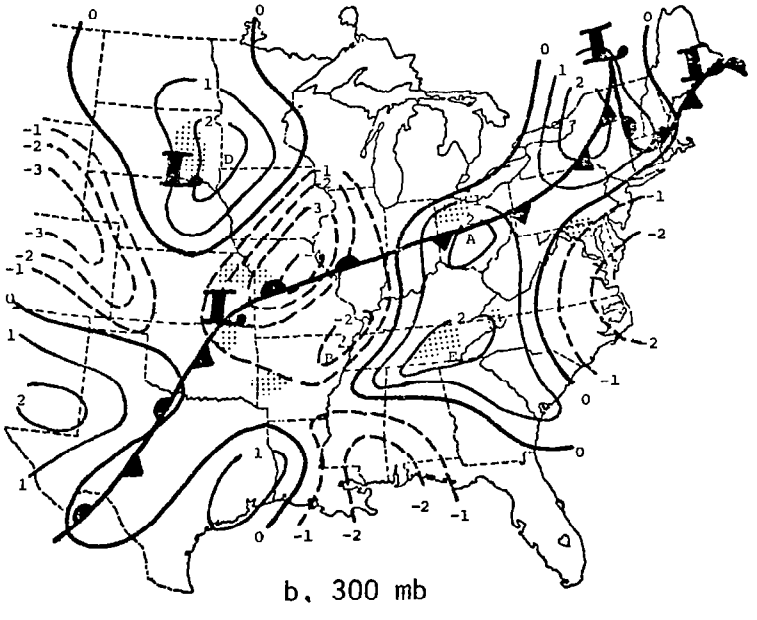

Fig. 18. Differences between values of horizontal wind divergence ($\times 10^{-5}$ s^{-1}) computed from observed and interpolated winds 9 h after the initial time at 850 and 300 mb. Superimposed are surface frontal positions and radar-observed convection.

behind the squall line in western Tennessee by 1800 and 2100 GMT (Figs. 17a and 18a).

Analysis of the wind divergence differences at the 300-mb level shows that large positive centers were generally over areas of convection which indicated more divergence in the upper levels of the atmosphere over areas of convection than was accounted for by interpolation. Well-defined positive centers existed along the polar front, over the squall line in Kentucky and Tennessee, and over the area of convection east of the surface low in South Dakota.

Values of maximum differences associated with centers in Figs. 16-18 are presented for selected pressure levels in Table 7. Vertical and temporal continuity of these centers is again established. The change in sign and decrease in center intensities near the 500-mb level was an indication of the level of non-divergence. Overall, centers were best defined at 3 and 6 h after the initial time of the interpolation period.

Fields of vertical motion differences, calculated using Eq. 8, are shown in Fig. 19 for the 850-mb level. Negative centers were found along the polar front and in areas where convective activity was generally increasing in intensity, such as central Tennessee and South Dakota, which indicated more upward motion in these areas over the time period than was measured by interpolation. The positive differences in these areas 3 h after the initial time and negative differences established after 6 h suggest rapid increases in upward motion in the boundary layer 3 h prior to convection that were unaccounted for by interpolation of the wind field.

An intense positive center was found after the first 3 h in northeastern Arkansas where a squall line was located. The intensity of convection, however, was decreasing and all activity dissipated within the following 3-h period. Rapid decreases in the amount of upward motion in this area over the first 3 h and a change to downward motion during the following 3 h was not accounted for by assuming linear changes in the wind field over a 12-h period, which suggests that the nonlinear changes in the kinematic structure of the atmosphere were im-

Table 7. Values of divergence differences (10^{-5} s^{-1}) for 3-, 6-, and 9-h intervals at selected pressure levels for centers in Figs. 16-18.

Center	Pressure	3 h	6 h	9 h
A	850	-5.5	-5.3	-1.8
	700	-3.1	-2.9	-3.4
	500	-2.5	-3.4	- .9
	300	5.4	4.5	2.0
B	850	4.0	5.4	1.1
	700	4.8	4.3	4.1
	500	2.3	2.2	2.1
	300	-2.5	-4.5	-2.0
C	850	-2.7	-2.3	*
	700	-1.3	-1.0	*
	500	-2.8	-1.3	*
	300	2.5	2.2	*
D	850	-2.7	-2.3	-1.4
	700	-2.4	-4.8	-4.4
	500	-1.3	-3.8	-3.4
	300	1.6	4.9	2.3
E	850	-	-3.3	-2.4
	700	-1.0	-1.3	-2.0
	500	.5	-1.9	- .6
	300	1.6	5.3	2.4

*Center could not be distinguished due to proximity to edge of grid.
-Centers not defined at this level and time.

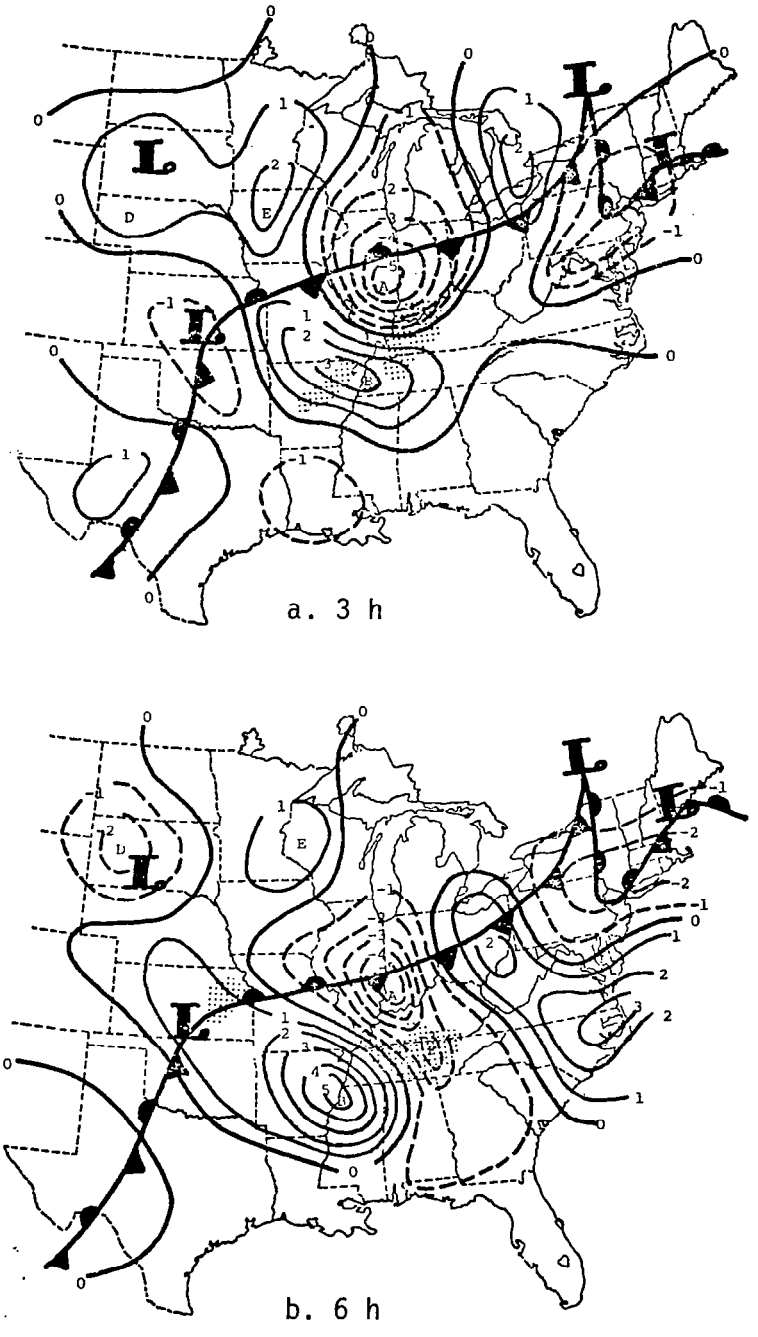

Fig. 19. Differences between values of vertical motions ($\mu b\ s^{-1}$) computed from observed and interpolated winds over 3-, 6-, and 9-h intervals at 850 mb. Superimposed are surface frontal positions and radar-observed convection.

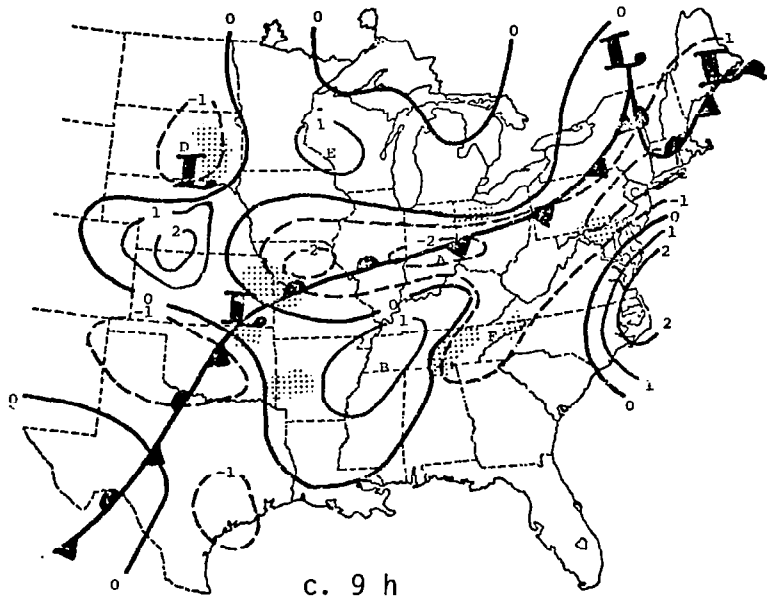

Fig. 19. (Continued)

important in the dissipation of convection. This also shows that upward motion in the boundary layer of the atmosphere is an essential condition for the maintenance of convection (Endlich and Mancuso, 1968). Positive centers were also located behind the polar front in the northern plains, and behind the stationary front in Texas.

A cross section of observed and interpolated vertical motion, and the corresponding differences after 6 h along line XYZ of Fig. 6 are shown in Fig. 20. Frontal structures and observed convection (MDR ≥ 4) are also shown.

The observed vertical motion field (Fig. 20a) shows good correlation with areas of strong convection. Upward motion occurred just ahead of and in the area of strong thunderstorms, as well as near the frontal zone. Upward motion was also found behind the front; however, the system did not produce convective showers. Upward motion in the boundary layer was much weaker in the areas along and

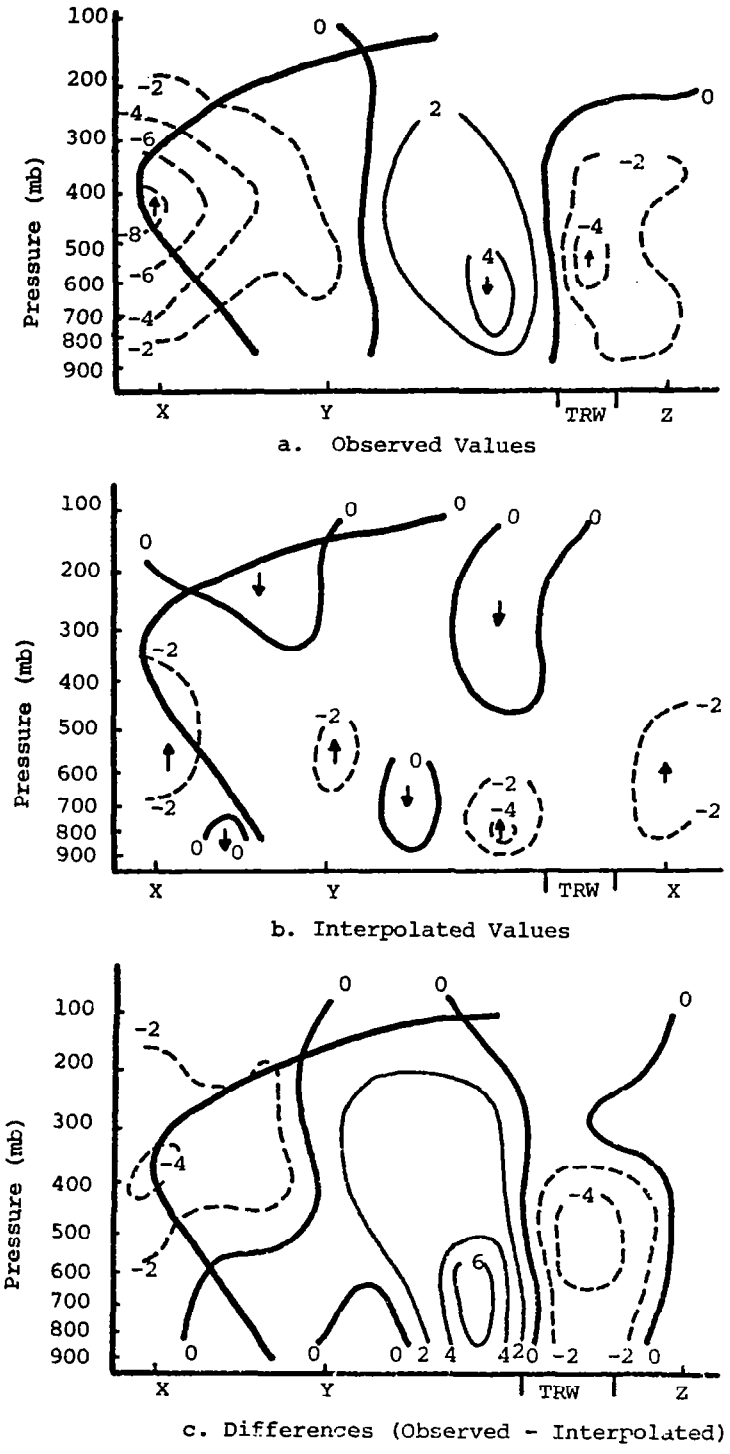

Fig. 20. Vertical cross section of vertical motions computed from observed and interpolated winds, and corresponding differences ($\mu b\ s^{-1}$) along line XYZ in Fig. 6 at 1800 GMT, 24 April 1975.

behind the front than in the areas of strong convection, which again establishes the necessity of upward vertical motion in the lower layers for the production and maintenance of convection. In regions of strong subsidence, no convection was observed.

Although interpolation, on the whole, could determine regions of upward and downward motion with some accuracy, this method proved grossly inadequate in areas of strong upward and downward motions in the observed wind field. Figures 20b and c show that interpolation could not define the kinematic structure of the atmosphere in the area of strong thunderstorms and in the region behind the squall line. Differences equal or greater in magnitude than observed values were found in these areas, which means errors greater than 100 percent are possible by assuming linear changes in synoptic variables. This further shows that large and rapid changes in the observed vertical motion field over the time period could not be accurately defined by linear interpolation over a 12-h period, and further suggests the importance of nonlinear changes in the development of convective activity.

Values of maximum difference for vertical motion centers in Fig. 19 are given for selected pressure levels in Table 8. Centers exhibit both vertical and temporal continuity. Differences computed after 6 h were generally largest, and 3- and 6-h differences were much larger than 9-h differences. Maximum values for most centers occurred at the 500-mb level near the level of non-divergence.

The error analysis presented in Table 3 indicated that vertical motion differences were subject to considerable error above 500 mb. Table 8 shows that magnitudes of the centers of differences for vertical motions were less than the estimated errors at and above 500 mb. Caution therefore must be exercised when referring to values of the differences at these levels.

Fields of vorticity differences calculated using Eq. 10 are shown in Fig. 21 for the 500-mb surface for each time interval. Centers of vorticity differences clearly depict the existence of short waves. Intense positive centers, indicating increased circulation over the time interval that was not represented by interpolation, correlated

Table 8. Values of vertical motion differences ($\mu b\ s^{-1}$) for 3-, 6-, and 9-h intervals at selected pressure levels for centers in Fig. 19.

Center	Pressure (mb)	3 h	6 h	9 h
A	850	-5.7	-5.2	-2.2
	700	-8.2	-8.5	-5.2
	500	-2.4	-7.4	-4.2
	300	-2.3	-7.0	-3.8
B	850	3.8	5.2	1.3
	700	6.4	8.7	3.5
	500	3.7	3.8	3.0
	300	1.9	3.4	3.0
C	850	-2.6	-2.6	-2.2
	700	-3.2	-2.9	-2.5
	500	-3.4	-3.2	-2.0
	300	-2.5	-1.1	-2.5
D	850	-1.5	-2.6	-1.6
	700	-2.3	-3.7	-1.5
	500	-4.9	-4.0	-3.0
E	850	2.1	1.6	1.1
	700	3.6	3.1	2.1
	500	1.7	1.9	-
	300	.7	3.7	-
F	850	-	-3.1	-1.1
	700	-	-3.8	-4.6
	500	-	-2.1	-5.6
	300	-	-2.4	-5.4

- Centers not defined at this level and time.

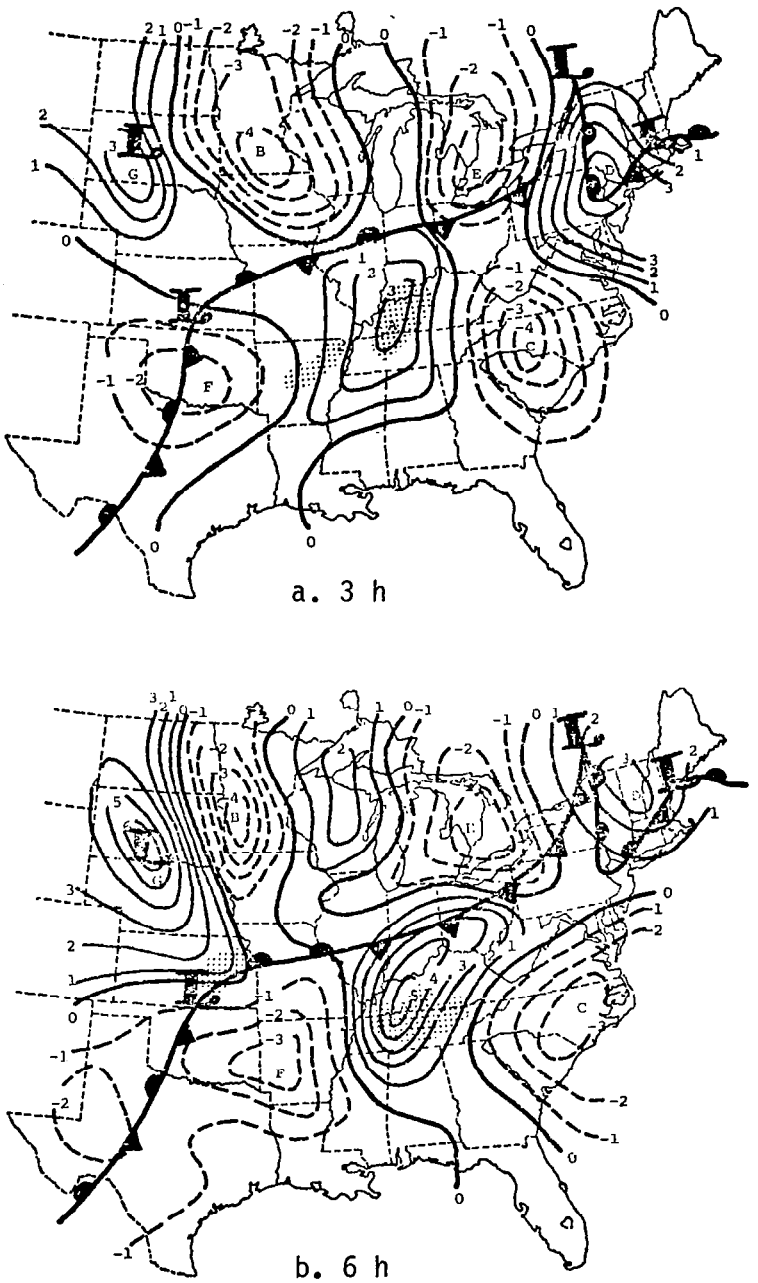

Fig. 21. Differences between values of vorticity (x 10^{-5} s^{-1}) computed from observed and interpolated winds over 3-, 6-, and 9-h intervals at 500 mb. Superimposed are surface frontal positions and radar-observed convection.

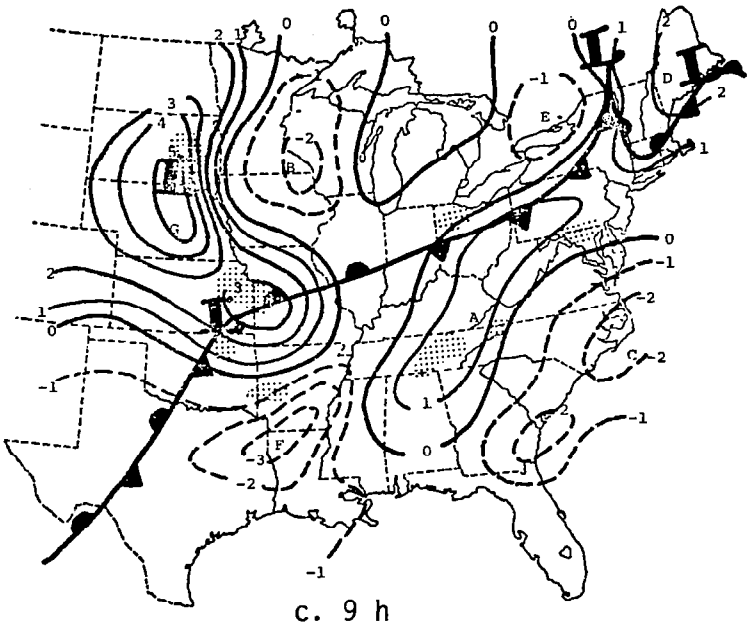

c. 9 h

Fig. 21. (Continued)

well in space with troughs, such as over Indiana, Kentucky, and Tennessee, as well as with developing surface lows, such as in New England and South Dakota. Negative centers were found in bands between positive centers, mainly behind the polar front and in regions where ridges were established such as Missouri and Arkansas.

Centers were found to fit the synoptic situation in the lower layers of the atmosphere as well. Table 9, which lists values of differences associated with various centers for selected pressure levels, indicates that the centers were well established in the vertical. Overall, differences were largest aloft except for Center A, where 700-mb differences were most pronounced after 3 and 9 h. Synoptic charts show the short wave over this area to be best defined at the 700-mb level (Figs. 5-7). Differences were largest in the upper levels in this region after 6 h when the squall line was developing

Table 9. Values of vorticity differences (10^{-5} s^{-1}) for 3-, 6-, and 9-h intervals at selected pressure levels for centers in Fig. 21.

Center	Pressure (mb)	3 h	6 h	9 h
A	850	2.4	2.0	3.1
	700	6.8	4.1	4.5
	500	3.2	5.5	1.7
	300	4.5	5.7	2.5
B	850	-2.7	-3.8	-1.9
	700	-2.4	-4.3	-1.7
	500	-4.9	-4.9	-2.4
	300	-5.3	-8.9	-6.8
C	850	-3.9	-3.5	-3.0
	700	-2.8	-2.5	-2.1
	500	-4.0	-3.5	-2.0
	300	-1.0	-2.7	-3.9
D	850	3.9	2.5	1.2
	700	2.8	3.2	2.0
	500	4.8	3.8	2.1
E	850	-	-	-
	700	-2.4	-1.9	-1.7
	500	-3.7	-3.8	-1.3
	300	-5.3	-5.7	-3.5
F	850	2.0	-2.3	-2.2
	700	-2.4	-1.3	-1.8
	500	-2.2	-3.2	-3.5
	300	-1.0	-1.6	-2.5
G	850	1.5	3.9	.8
	700	3.5	6.9	4.3
	500	3.1	6.9	5.7
	300	2.2	9.0	7.5

- Centers not defined at this level and time.

which suggests a possible correlation between large changes in the vorticity field in the upper levels prior to convection.

Table 9 also shows temporal continuity in these centers. For most centers, 6-h differences were largest, especially for centers in the western portion of the network where surface lows over South Dakota and Kansas began intensifying in conjunction with the development of the second short wave. Values associated with these centers were sometimes larger in magnitude than values of vorticity computed from observed wind at the same time, indicating errors greater than 100% were possible in calculating vorticity from interpolated winds. Figure 21 shows that most of the centers moved slightly eastward through the interpolation period with the movement of these short waves.

Differences between values of vorticity advection computed from observed and interpolated winds are shown for the 500-mb level in Fig. 22. Differences over all time intervals fit the synoptic situation very well, with positive centers, which indicate greater amounts of positive vorticity advection than measured by interpolation, occurring ahead of vorticity difference centers and negative differences located upwind of vorticity difference centers. This pattern depicts the existence of short waves in the wind field. Similar results were found in fields of vorticity advection computed from observed winds in AVE IV. Areas of strong positive advection (PVA) existed ahead of vorticity centers with negative advection upstream from the centers.

Fig. 22 suggests a possible lag relationship between positive vorticity advection differences in the upper levels of the atmosphere and radar-observed convection. Positive centers were located ahead of areas of strong convection and studies have indicated that the development of PVA at the mid and upper levels is required, along with favorable conditions in the lower levels, to initiate or maintain thunderstorms (Read and Scoggins, 1977). Since most of these centers of vorticity advection differences move eastward in time and maintain their position ahead of areas of strong thunderstorms, it is apparent that significant development of PVA 3 h prior to convective activity

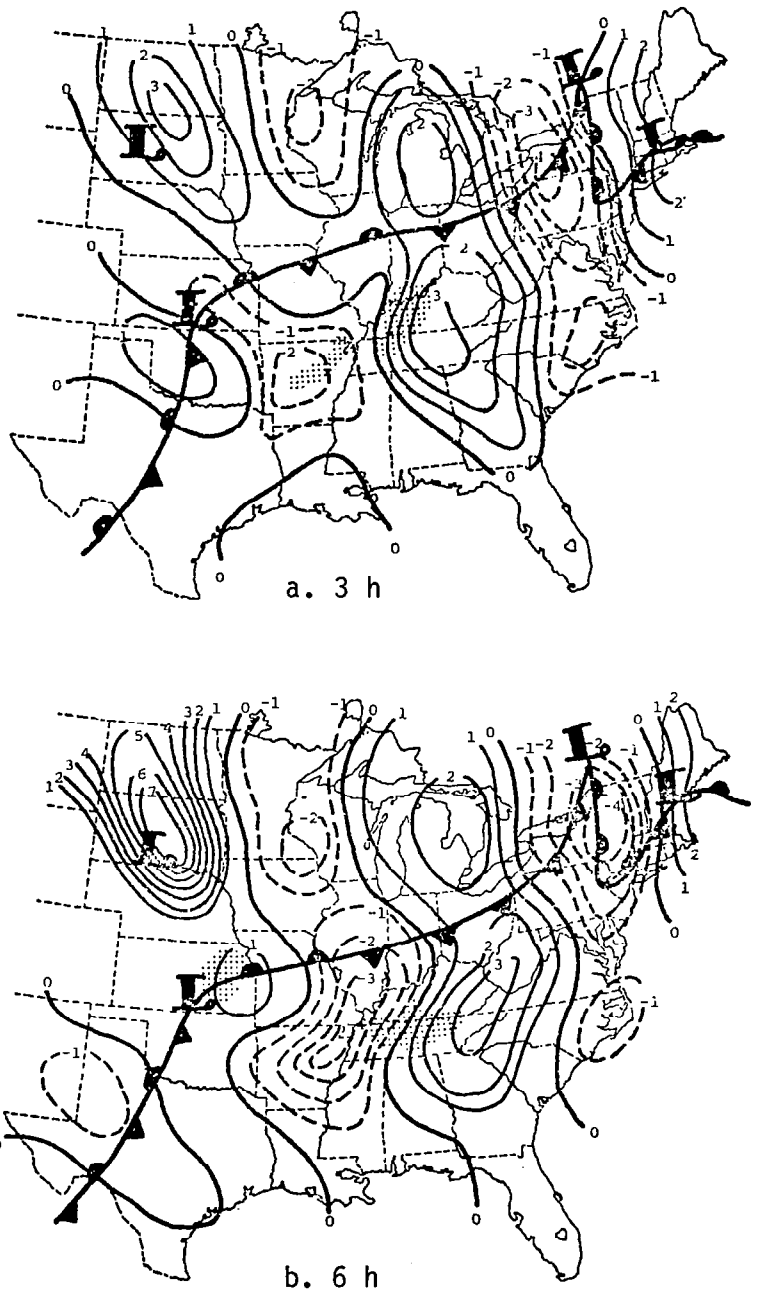

Fig. 22. Differences between values of vorticity advection (x 10^{-9} s^{-2}) computed from observed and interpolated winds over 3-, 6-, and 9-h intervals at 500 mb. Superimposed are surface frontal positions and radar-observed convection.

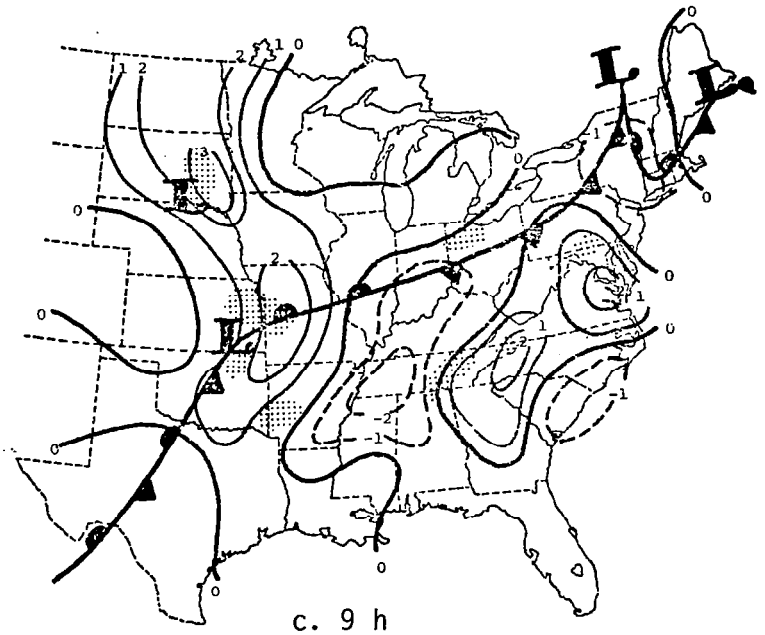

Fig. 22. (Continued)

is not accounted for by linear interpolation of the wind field. This result also depicts the possibility that cyclonic development in the mid to upper troposphere may be important in the initiation and maintenance of convective storms. Values of several of the centers were nearly equivalent to and, in some cases, greater in magnitude than centers of vorticity advection computed from 3-h rawinsonde values. Thus, errors of nearly 100% or greater were possible by assuming linear changes in winds over a 12-h period.

Patterns of vorticity advection differences in the lower levels also correlated well in space with synoptic features. Narrow bands of positive and negative centers were found in areas where upper-level short waves were established. Relationships to convective activity, however, were not well defined at lower levels.

Fig. 23 shows differences between temperature advection computed from observed and interpolated winds and temperatures at the mid point

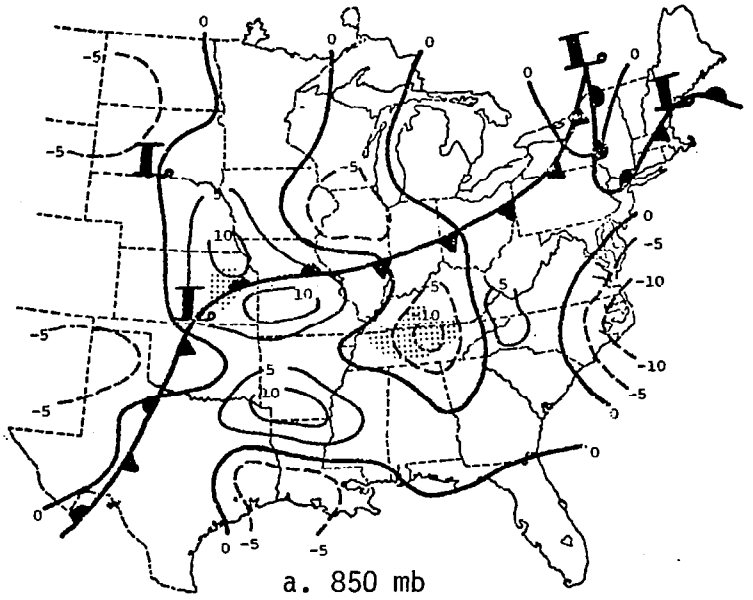

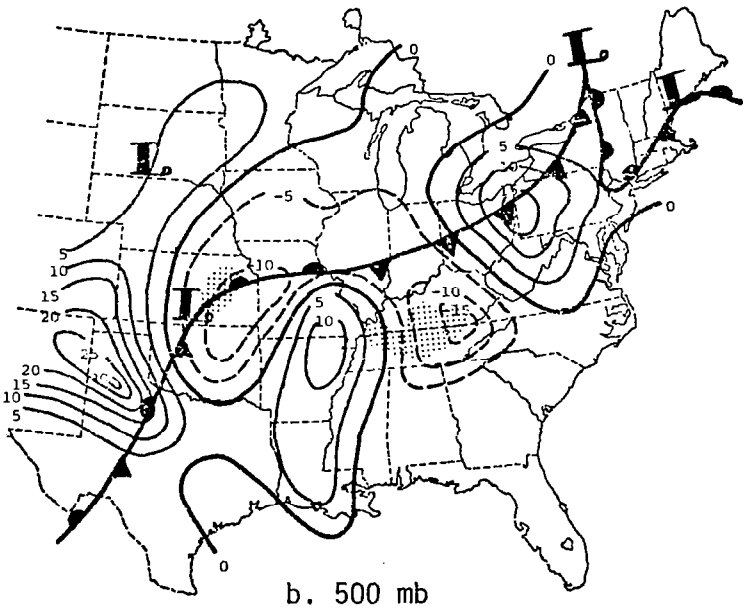

Fig. 23. Differences between values of temperature advection (x 10^{-5} °C s^{-1}) computed from observed and interpolated winds and temperatures 6 h into the interpolation period at 850 and 500 mb. Superimposed are surface frontal positions and radar-observed convection.

of the 12-h interpolation period for the 850- and 500-mb levels. Bands of negative differences at 850 mb were found mainly along and behind the polar front and in the area of strong thunderstorms in central Tennessee. Negative values of differences indicate colder temperatures being advected into these regions than was indicated by linear interpolation. Positive differences were found in a band east of the surface lows in South Dakota and Kansas, and in the warmer air along the Gulf Coast and Eastern States. Warmer air was being advected into these regions than was measured by interpolation.

At 500 mb, negative centers were located in and ahead of areas of strong convection, with positive differences over the northeastern, southern, and western portions of the network. Warm air advection is generally found in lower layers in areas of strong convection with less warm air or even cold air advection aloft (Petterssen, 1956). In eastern Kansas, increases in warm air advection in the lower layers and cold air advection aloft, that were not represented by linear interpolation, were found prior to and during thunderstorm development. Although decreases in warm air advection in the lower layers were associated with the squall line over central Tennessee, even larger decreases were found aloft. Thus, in all areas of convection, temperature advection patterns supported decreasing stability through a deep layer of the atmosphere that was unaccounted for by assuming linearity in synoptic variables over a 12-h period.

Fields of convective instability not represented by linear interpolation are shown for three layers of the atmosphere (900-500 mb, 900-700 mb, and 700-500 mb) 6 h into the interpolation period in Fig. 24. Negative differences, indicating nonlinear decreases in stability through a deep layer (Fig. 24a), were found to correlate well in space with unstable areas depicted by temperature advection (Fig. 23). Although the field indicated convection in unstable air, differences were small for this deep layer and the field was too smooth to pinpoint strong relationships between stability and convection.

Values of σ_e' for the 900-700-mb layer show that nonlinear decreases in stability (negative differences) existed in most areas of

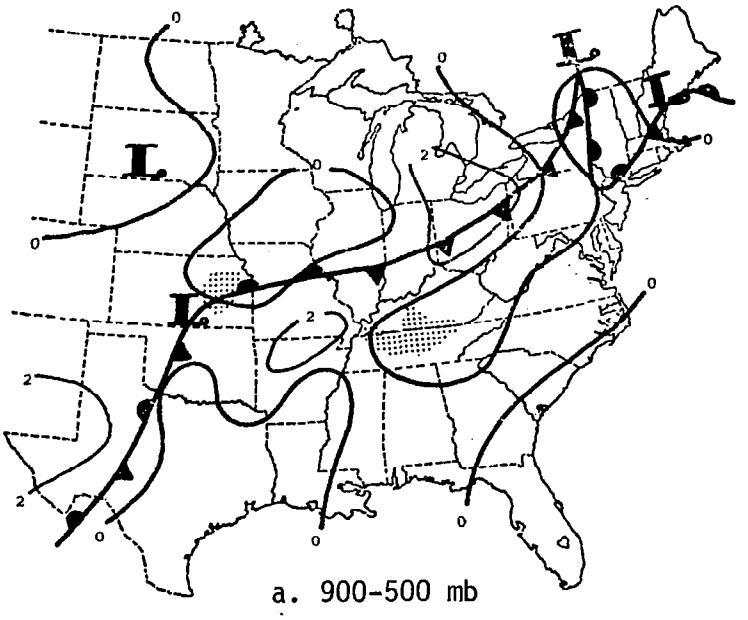

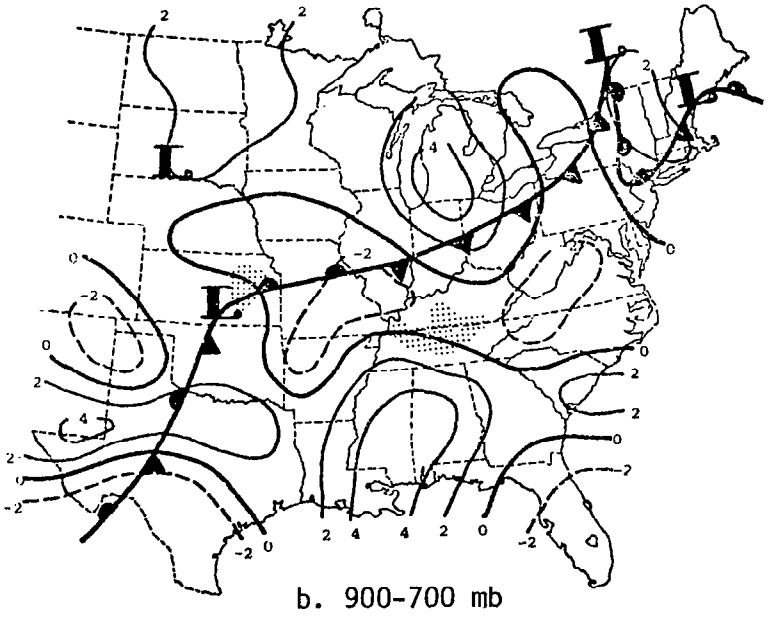

Fig. 24. Differences between measured and linearly interpolated values of the convective instability index (x 10^{-2} °C mb^{-1}) computed 6 h into the interpolation period for various levels of the atmosphere. Superimposed are surface frontal positions and radar-observed convection.

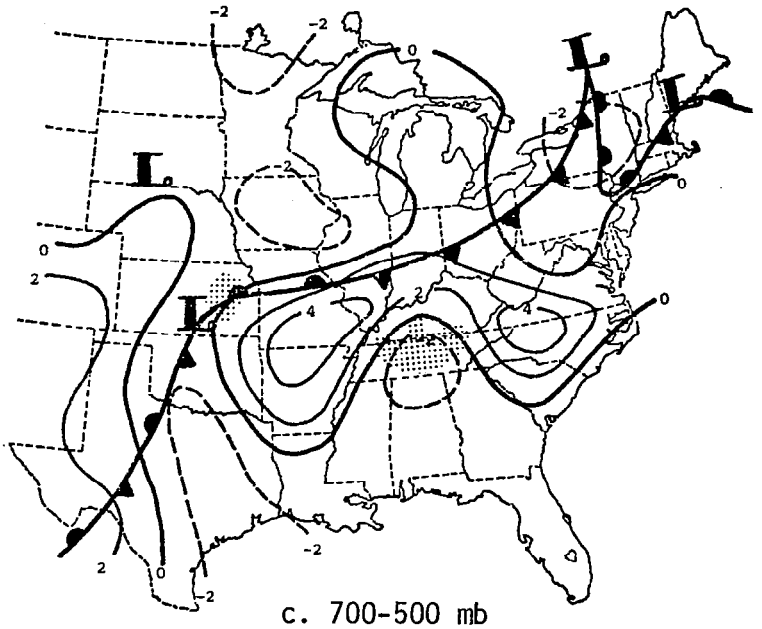

c. 700-500 mb

Fig. 24. (Continued)

strong thunderstorms. Larger decreases, however, were often found in regions free of thunderstorms. The fact that areas of strong convection were more stable than some areas free of convection indicates the possible effect of thunderstorms interacting with their environment to stabilize the lower layers of the atmosphere.

In the 700-500-mb layer, greater nonlinear decreases of stability occurred than in the lower layer (900-700-mb) in areas of thunderstorms. Instability in the middle troposphere may have been important in the maintenance of thunderstorm activity.

Several studies have indicated that a convectively unstable layer of air is necessary for the development of thunderstorms (Miller, 1967; Wilson and Scoggins, 1976). Nonlinear decreases of stability were found at least in one layer in all areas of convection in this study. Large decreases in areas free of thunderstorms, however, suggest that other factors must be important in the release of this instability and the development of thunderstorms.

b. Vertical Structure

The vertical structure of centers of differences between measured and linearly interpolated values of variables, or the nonlinear changes in the variables over 3-, 6-, and 9-h intervals, was examined with regard to vertical extent and slope of these centers. If these centers were established only in the lower layers of the atmosphere, then the nonlinear changes may be due mostly to diurnal effects, since the 12-h interpolation period over the grid network runs from 6:00 a.m. CST to 6:00 p.m. CST. Centers that extend vertically to the upper layers of the atmosphere are more likely due to synoptic features such as frontal zones, short waves, or sub-synoptic systems.

The vertical structure of these differences was first examined by determining relationships between fields of differences at various levels and a selected reference level. The 850-mb level was chosen since many of the centers of maximum difference were first well-defined at this level. A correlation analysis was employed to determine such vertical relationships. Correlation coefficients for each variable were calculated using Eq. 18 and results are shown in Table 10.

All coefficients in Table 10 were statistically significant at the five percent level with the exception of values between -0.13 and +0.13 (Wine, 1964). A coefficient of 1.00 indicates a perfect correlation or perfect linear relation between the two fields of differences and, therefore, a high coefficient indicates a strong relationship. Negative correlation suggests the two fields of differences had an out of phase relationship.

Table 10 shows that relationships between fields of temperature differences at various pressure levels and the 850-mb field were largest in the lower layers. Correlations changed sign around the 600-mb level and again at the tropopause which suggests that, overall, differences changed sign in the mid troposphere and above the tropopause. Relationships were fairly well established up to 400 mb where temperature difference centers were not well defined, and increased again near the tropopause. Correlation decreased with time in the

Table 10. Correlation coefficients for temperature, mixing ratio, and geopotential height differences computed for 3-, 6-, and 9-h intervals within the 12-h interpolation period.

a. Temperature

Pressure Intervals	3h	6h	9h
850-800 mb	.43	.44	.38
850-700	.32	.19	.14
850-600	-.29	-.27	.17
850-500	-.30	-.25	-.42
850-400	-.03	-.02	-.14
850-300	-.14	-.37	-.06
850-200	-.26	-.15	-.16
850-100	.13	.11	.09

b. Mixing Ratio

Pressure Intervals	3h	6h	9h
850-800	.34	.42	.50
850-700	.04	.27	.40
850-600	.06	-.14	.02
850-500	-.04	-.04	-.20
850-400	-.22	-.03	-.30

c. Geopotential Height

Pressure Intervals	3h	6h	9h
850-800	.95	.98	.97
850-700	.79	.91	.78
850-600	.72	.86	.65
850-500	.53	.67	.49
850-400	.33	.29	.20
850-300	.24	.11	.11
850-200	.20	.10	.15
850-100	.26	.02	.09

Table 10. (Continued)

d. Divergence

Pressure Intervals	3h	6h	9h
850-800	.80	.73	.53
850-700	.42	.22	.32
850-600	.37	.28	.21
850-500	-.20	-.12	-.05
850-400	-.14	-.05	-.23
850-300	-.13	-.16	-.11
850-200	-.14	-.17	-.48
850-100	-.10	-.11	-.10

e. Vertical Motion

Pressure Intervals	3h	6h	9h
850-800	.96	.95	.82
850-700	.78	.67	.49
850-600	.47	.39	.20
850-500	.25	.25	.16
850-400	.17	.20	.12
850-300	.05	.13	.17
850-200	.37	.12	.16
850-100	.12	.05	.11

f. Vorticity

Pressure Intervals	3h	6h	9h
850-800	.72	.77	.67
850-700	.23	.26	.24
850-600	.21	.24	.20
850-500	.21	.22	.26
850-400	.10	.21	.13
850-300	-.14	-.06	-.11
850-200	-.25	-.15	-.09
850-100	-.22	-.11	-.05

lower layers, except at 800 mb and above the tropopause, while correlations were more variable in time in the mid troposphere.

Relationships for fields of mixing ratio were established only in the lower layers of the atmosphere and coefficients changed sign above 600 mb. Differences changed sign in the mid troposphere, particularly in areas of strong convection where losses of moisture in lower layers due to convergence and lifting and subsequent increases in moisture content aloft, were not represented by assuming a linear change in mixing ratio over a 12-h period. Coefficients increased in magnitude with time at most levels and were largest for 9-h differences. Areal coverage of strong convective activity also increased with time within the 12-h interpolation period which suggests that the vertical structure of mixing ratio differences were largely influenced by convection.

Vertical relationships between the 850-mb field of geopotential height differences and fields at other levels were very well established at all levels of the atmosphere, particularly to the 400-mb level. This suggests good vertical continuity for geopotential height differences, and centers were found to be nearly vertically stacked in the atmosphere with only slight slopes above 400 mb. The good vertical extent of these centers also indicates that nonlinear changes in geopotential heights were related to disturbances in the large-scale flow, such as short waves or troughs. Coefficients were largest for 6-h differences in the lower layers, and for 3-h differences in the mid and upper troposphere.

Correlations between differences in divergence, vertical motion, and vorticity were well-established in the vertical. Vertical motion relationships were especially good, as centers of vertical motion were nearly vertically stacked in the atmosphere. Relationships for fields of divergence differences changed sign above the level of non-divergence which was above 500 mb for AVE IV, although differences themselves changed sign at or above 500 mb. Overall, correlations for divergence and vertical motion were best established for 3-h differences up to 400 mb and were more variable with time above that

level. Vorticity correlations showed a marked decrease from the lower to mid troposphere and remained nearly constant with height to the upper levels of the atmosphere where differences were negatively correlated with those at 850 mb. The decrease in correlations from lower to mid layers may be due to large increases in differences with altitude from 850 to 700 mb in areas associated with short waves and strong convective activity (centers A and G of Table 9). In these areas, large changes in the vorticity field which were not measured by linear interpolation were occurring in the mid to upper troposphere, which may also explain the small change in the coefficient with altitude for these upper layers. These results also suggest that grid points associated with the passage of short waves and thunderstorms may have been a dominating influence on the calculation of the correlation coefficient.

The fact that vertical correlations for some of the variables were not as strong as for other variables does not imply that centers of differences were not continuous with altitude. Individual centers for each variable were examined, and Tables 4 through 9 clearly indicate that centers were well-established at most levels of the atmosphere. Analysis of individual centers also indicate that centers of variables for which correlations were poor sloped with height, while centers for which correlations were good stacked nearly vertically in the atmosphere.

Position plots of selected centers of temperature, vertical motion, and vorticity differences at various pressure levels are shown in Figs. 25 through 27. Numbers designate selected pressure levels while letters refer to centers identified on constant pressure charts. Fig. 25 shows that temperature difference centers sloped in the vertical. Most centers sloped toward the west and northwest, particularly those in the colder air. Center C, for example, which was located behind the polar front and the surface low in Kansas (Fig. 11), sloped with the frontal zone in the vertical. Center A, located over Indiana (Fig. 11), was the only center which sloped eastward. This center correlated well in space with a thermal trough in the lower

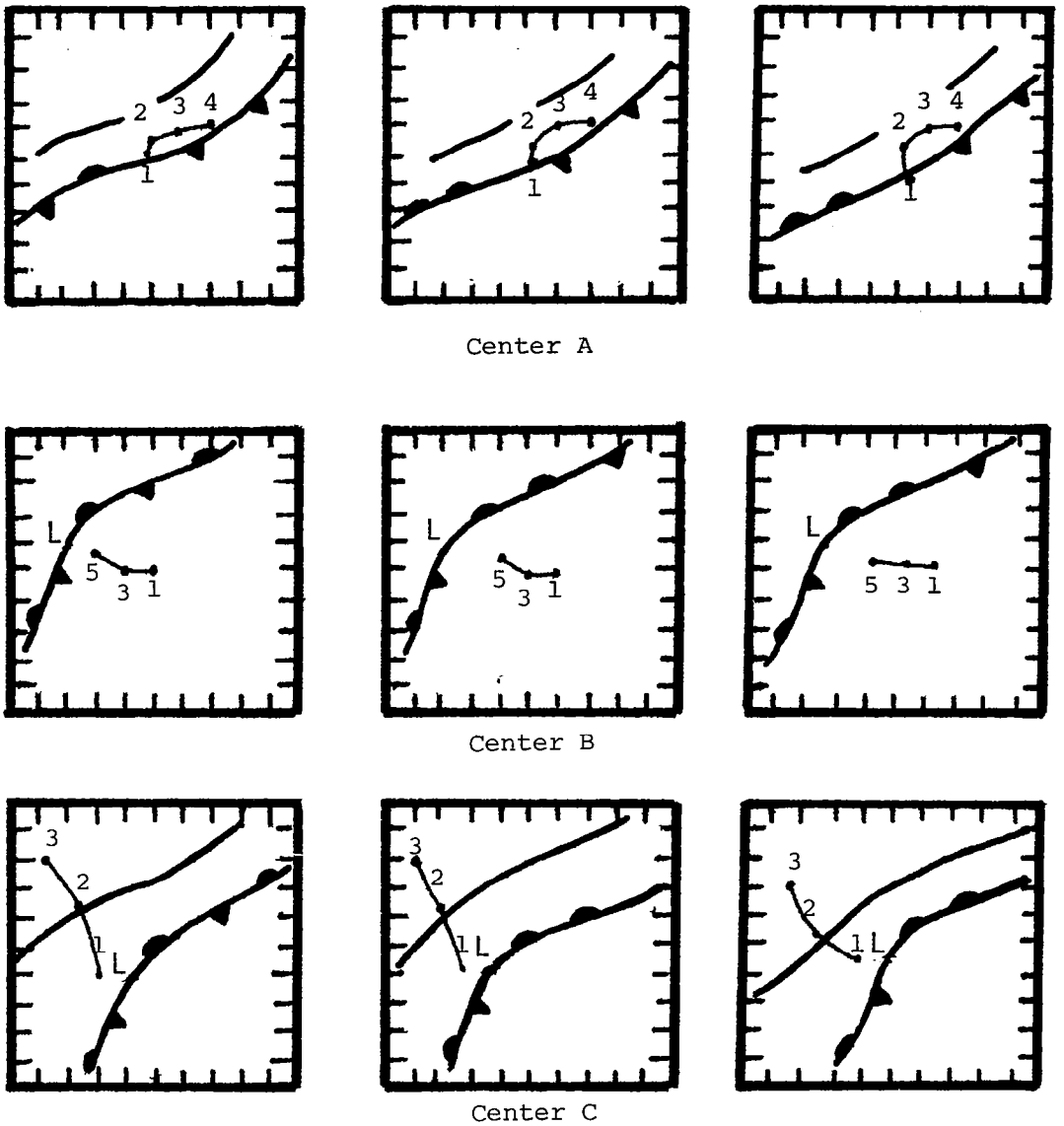

Fig. 25. Position plots of centers of temperature differences (Fig. 11) at various pressure levels. Surface and 700-mb fronts superimposed.

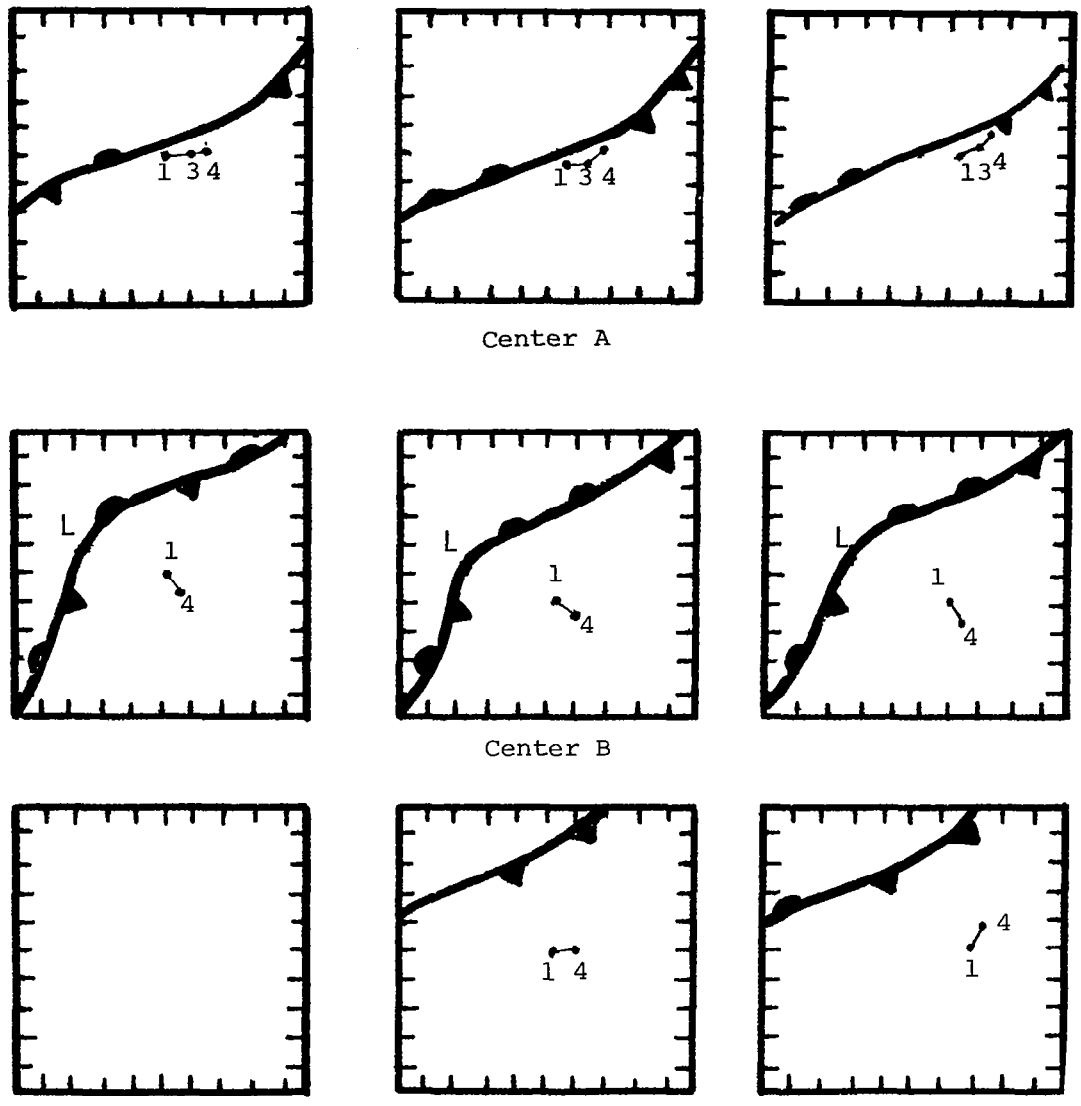

Fig. 26. Position plots of centers of vertical motion differences (Fig. 19) at various pressure levels.

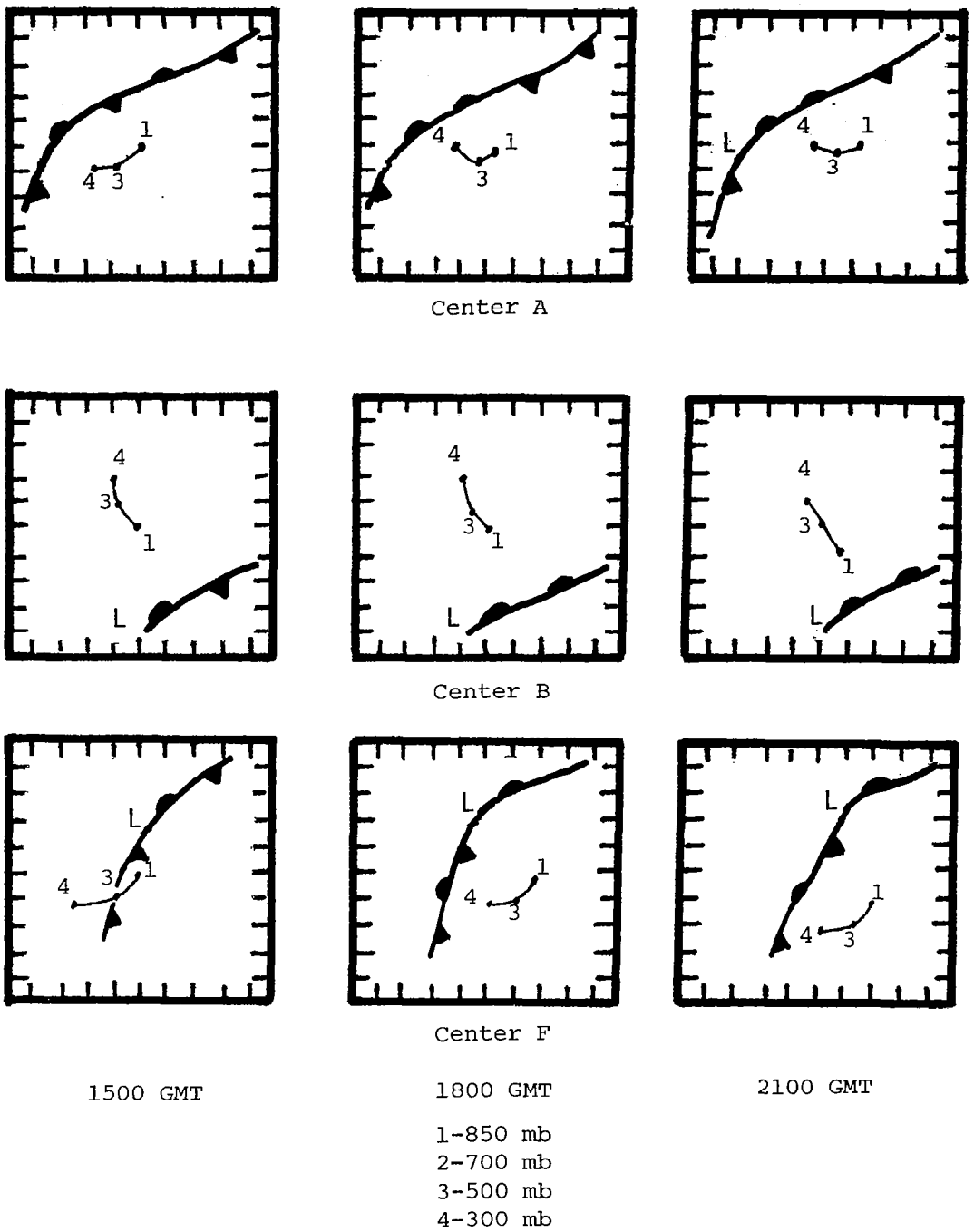

Fig. 27. Position plots of centers of vorticity differences (Fig. 21) at various pressure levels.

layers, but changed sign and sloped eastward in the mid to upper troposphere where a warm thermal pocket was established. Slopes for temperature difference centers in the warmer air (center B) were not as pronounced as those for centers in the colder air or along fronts. However, the slopes of temperature centers in the vertical could explain why correlations between fields of differences at the 850-mb level and fields at levels above decreased rapidly with height and changed sign in the mid troposphere.

Slopes of vertical motion differences,shown in Fig. 26, were much less pronounced than were those for temperature. The centers stacked nearly straight up in the vertical, especially to 500 mb which explains the good correlations between fields of differences through most levels of the atmosphere and the 850-mb field. Although plots in Fig. 26 show centers sloped mostly eastward and southward, other centers sloped randomly. Vorticity centers stacked nearly vertical with altitude up to around the 400-mb level, and sloped very slightly westward (Fig. 27). Slopes for most centers increased above 400 mb with a distinct westward or northwestward shift in the centers at 300 mb. This change in slope may be due to the fact that the short wave in the Ohio Valley stacked nearly vertical from 700 to 400 mb, and shifted westward at 300 mb. Center G (Fig. 21) was vertically stacked at all levels in conjunction with the second short wave which moved into the grid network 6 h into the interpolation period and was vertically stacked to the upper layers of the atmosphere. These results further suggest a strong relationship between nonlinear changes in synoptic variables over time intervals shorter than 12 h and synoptic features,and further document results obtained from analysis of constant pressure charts.

c. Statistical Analysis of Differences

The average, standard deviation, and extreme values of the differences between measured and interpolated data at 3, 6, and 9 h after the initial time of the 12-h interpolation period were calcu-

lated for each variable and pressure level. The average difference at each pressure level represents a bias in the interpolated data relative to the measured data. If vertical variations of the biases over 3, 6, and 9 h are similar, their effect could be removed by applying a correction factor that would be pressure dependent. On the other hand, if variations of the biases in time were similar at each pressure level, a time-dependent factor might be applied to remove the biases.

The standard deviations represent the variation or dispersion of magnitudes of differences at a pressure level. If the mean of a field of differences is close to zero, the standard deviation is a good approximation to the RMS difference between measured and linearly interpolated data. Large values of the standard deviation imply large variations in the magnitude of the differences, and are interpreted as errors in the interpolated data. Extreme values provide an indication of the variability of each data set or the range of values of the data set.

Statistical parameters for differences between measured and interpolated values computed 3, 6, and 9 h after the initial time of the 12-h interpolation period are presented in Table 11. Meteorological variables and selected pressure levels are listed on the left, and statistical parameters and time intervals are listed along the top.

Mean values for most variables were not very large and in some cases close to zero. In fact, means for most fields of differences for derived parameters were an order of magnitude smaller than observed or actual values measured in the atmosphere. This does not indicate that interpolation was an accurate estimation of the actual kinematic structure of the atmosphere since standard deviations of the differences were quite large. Mean values for some variables were systematic in time and in the vertical, while mean values for other variables did not display systematic tendencies. Averages for temperature differences were largest at 6 h for most levels of the atmosphere above 850 mb, and changed sign from negative in the lower layers to positive in the mid to upper troposphere. Mean values of geopotential

Table 11. Statistics for differences between observed and linearly interpolated values of synoptic variables.

		3 h				6 h				9 h			
Variable	p (mb)	Mean	St. Dev.	Max	Min	Mean	St. Dev.	Max	Min	Mean	St. Dev.	Max	Min
Temperature (°C)	850	-.2	1.4	3.1	-6.5	-.3	1.3	3.4	-4.0	.1	1.0	3.0	-4.5
	700	.3	1.0	2.9	-3.2	.5	.8	3.8	-1.4	.2	.8	3.0	-1.9
	500	.2	1.0	2.3	-2.2	.6	.9	3.7	-1.5	.5	.8	4.1	-1.6
	300	.5	.7	2.5	-1.5	.5	.8	2.6	-2.2	.3	.9	2.6	-2.7
	100	.2	.9	2.0	-2.5	.5	1.5	4.2	-3.8	.5	.9	2.8	-1.8
Mixing Ratio ($g\ kg^{-1}$)	850	-.1	2.0	6.7	-7.3	.4	1.6	5.4	-4.3	.1	1.2	3.9	-6.8
	700	.1	1.1	3.9	-3.1	-.1	1.3	2.5	-4.2	-.2	1.4	4.8	-4.6
	500	0	.5	1.6	-1.8	-.2	.7	1.7	-2.0	0	.6	1.9	-1.5
Geopotential Height (gpm)	850	9.2	5.4	20.4	-16.5	11.8	9.0	30.9	-13.9	6.7	6.1	23.2	-6.2
	700	9.8	7.4	26.5	-16.6	12.3	7.9	35.2	-14.2	7.0	5.2	19.3	-7.6
	500	11.5	10.5	32.9	-24.1	15.9	8.0	35.3	-7.7	9.4	7.1	33.5	-11.2
	300	16.7	17.6	56.4	-39.2	22.3	13.1	54.2	-20.5	14.9	12.2	52.6	-27.1
	100	31.5	23.0	82.9	-41.0	36.0	23.2	97.1	-26.0	27.3	20.0	68.2	-24.8
Wind Speed ($m\ s^{-1}$)	850	.3	2.2	7.0	-9.9	-.1	2.9	7.5	-10.9	.1	2.1	5.9	-10.7
	700	-1.2	2.7	7.2	-7.3	-.2	3.3	10.6	-9.8	.8	2.5	8.1	-4.6
	500	.2	2.4	9.1	-6.6	.4	2.9	10.7	-7.6	1.2	2.0	6.9	-4.6
	300	-.1	3.7	11.9	-9.7	.1	4.2	14.8	-12.3	-.1	3.2	8.3	-13.0
	100	-.2	6.0	24.0	-13.7	-1.2	5.2	16.3	-15.3	-.1	3.9	10.6	-8.5
Wind Direction (Degrees)	850	.7	29.2	161	-122	-2.7	41.4	174	-176	-6.6	29.7	148	-149
	700	-1.7	25.0	80	-112	-9.7	28.9	107	-132	.6	20.1	121	-49
	500	-1.7	23.4	167	-171	-8.1	18.3	30	-117	-7.0	11.9	35	-42
	300	-.3	7.7	29	-23	-1.4	11.5	42	-28	-2.8	10.1	36	-43
	100	.5	6.9	17	-18	-2.1	7.3	16	-31	-3.8	6.9	25	-18
u component ($m\ s^{-1}$)	850	.1	2.1	8.6	-4.8	-.2	3.1	15.7	-7.6	.7	2.7	16.6	-6.1
	700	-1.1	2.5	5.7	-7.5	-1.1	3.2	7.8	-11.3	.3	2.9	8.5	-7.3
	500	-.4	2.7	9.1	-6.2	-.4	2.4	7.6	-6.3	.6	2.2	7.3	-6.7
	300	-.2	3.9	10.2	-12.6	-.4	4.4	13.3	-14.0	-.4	3.4	9.4	-12.0
	100	0	5.8	25.5	-14.1	-1.5	5.0	16.9	-15.1	-.5	4.0	10.3	-9.1
v component ($m\ s^{-1}$)	850	.1	2.7	9.2	-10.0	-.3	3.5	8.9	-17.4	-.3	2.4	8.4	-13.5
	700	0	3.3	8.7	-11.1	1.4	3.8	13.1	-13.7	.6	2.7	8.1	-9.5
	500	.7	3.0	8.9	-8.1	2.0	3.8	15.0	-10.1	1.7	2.8	9.5	-9.9
	300	.1	3.7	9.6	-12.3	.9	5.4	15.5	-16.0	1.3	4.2	17.4	-8.4
	100	-.5	2.7	6.2	-7.1	.1	2.9	10.7	-7.2	1.1	2.1	6.7	-4.1

Table 11. (continued)

Parameter	p (mb)	3 h Mean	3 h St. Dev.	3 h Max	3 h Min	6 h Mean	6 h St. Dev.	6 h Max	6 h Min	9 h Mean	9 h St. Dev.	9 h Max	9 h Min
Divergence ($10^{-5}s^{-1}$)	850	0	1.3	4.0	-5.5	0	1.4	5.4	-5.3	0	1.0	3.8	-3.5
	700	-.1	1.2	4.9	-3.1	-.1	1.6	4.3	-4.8	-.3	1.4	4.1	-4.4
	500	-.2	1.3	3.0	-4.3	-.2	1.4	3.7	-4.8	0	1.1	3.4	-3.4
	300	-.3	1.4	5.2	-4.0	-.1	1.6	5.4	-5.6	-.2	1.3	2.9	-4.5
Vertical Motion ($\mu b\ s^{-1}$)	850	-.1	1.2	3.9	-5.7	-.1	1.3	5.2	-5.2	-.2	.9	3.5	-2.3
	700	0	1.8	6.4	-8.2	-.1	2.1	8.7	-8.5	-.3	1.5	3.6	-5.2
	500	-.2	2.1	7.7	-7.3	0	2.6	10.5	-7.4	-.2	1.9	7.5	-5.6
	300	-.5	1.9	4.3	-7.0	-.3	2.3	5.4	-7.5	-.4	1.8	5.9	-5.6
Relative Vorticity ($10^{-5}s^{-1}$)	850	.1	1.1	3.9	-3.9	.4	1.5	3.9	-3.8	.2	1.1	3.1	-3.0
	700	.2	1.5	6.8	-2.8	.1	1.9	6.9	-4.3	.1	1.3	4.5	-2.9
	500	-.3	1.6	4.8	-4.9	-.2	2.0	6.9	-4.9	.1	1.4	5.7	-3.5
	300	-.3	1.8	4.5	-5.3	-.5	2.9	9.0	-8.6	-.5	2.1	7.5	-6.8
Advection of Vorticity ($10^{-9}s^{-2}$)	850	0	.5	2.3	-2.2	.1	.6	2.4	-2.0	0	.4	1.3	-2.1
	700	.1	.6	2.7	-3.6	.1	.9	5.1	-2.4	.1	.7	3.0	-3.1
	500	.1	1.2	3.9	-4.5	.1	1.4	7.4	-4.3	.1	.8	3.0	-2.5
	300	0	2.1	4.8	-6.5	.2	2.4	8.0	-7.2	.1	1.9	7.4	-6.8
Advection of Temperature (10^{-5}°C s^{-1})	850	-2.7	5.2	32.5	-19.0	.4	3.5	13.4	-11.4	-.2	4.6	8.5	-15.2
	700	-.1	3.3	9.7	-14.2	.6	3.4	13.7	-14.4	.2	5.4	27.2	-23.1
	500	.8	5.2	17.8	-11.5	.5	5.9	29.7	-16.4	.6	5.8	28.1	-18.9
	300	1.1	6.9	28.5	-24.8	1.0	7.3	17.6	-31.0	-.8	5.7	16.0	-18.2
Convective Instability (10^{-2}°C mb^{-1})	900-700	.9	1.9	6.1	-3.9	.3	2.1	5.5	-5.3	.3	2.0	7.1	-5.3
	700-500	.3	1.7	5.3	-4.3	.2	1.7	4.4	-3.4	.4	2.1	7.4	-7.0
	900-500	.3	.6	2.8	-2.0	.1	.7	2.6	-2.4	0	.7	1.9	-3.0

height differences were also largest at 6 h and increased with altitude at each time interval. This can be expected since averages of temperature differences were positive from 700 mb upward, and geopotential height is a function of the vertical integral of mean temperature.

Magnitudes of the average differences for wind direction were largest in the mid troposphere at 3 and 6 h and at 850 and 500 over 9 h. Magnitudes of 6-h means were greatest. Mean differences for the v-component of velocity were largest at the 500-mb level and at 6 h, while those for the u-component and wind speed were more variable both in time and in the vertical.

Mean values for differences in divergence, vertical motion, vorticity and vorticity advection were for the most part consistent in time and showed little variation in the vertical. Vorticity means changed sign at 500 mb or 300 mb for all time periods. Means for temperature advection and stability differences were more variable.

Standard deviations of the differences were very systematic in time and with altitude. Deviations for differences in temperature (below the tropopause), mixing ratio, and wind direction decreased with altitude, while deviations for geopotential height, wind speed, vorticity, and the advection of vorticity and temperature increased with altitude. Dispersions of vertical motion differences increased with altitude up to 500 mb and decreased near the tropopause, represented by the 300-mb surface, while those for divergence varied little with altitude.

Standard deviations were largest for 6-h differences for all variables with the exceptions of temperature (below the tropopause) and mixing ratio where the largest deviations were found after the first 3 h of the interpolation period. Near the tropopause, represented by the 300-mb surface, temperature difference variations (from the mean) increased in time, and peaked after 6 h for layers above the tropopause. Overall, standard deviations of the differences were larger than the means, especially for wind direction. Standard deviations for geopotential height differences, however, were less than the means.

Extreme values of the differences were, for the most part, three to four times as large as the standard deviations for most variables. Extremes of wind direction, however, were four to five times the standard deviation in the low to mid troposphere. Vertical variations of the maxima and minima values for most variables were analogous to that for the standard deviation.

d. Comparison of Differences in Convective and Nonconvective Areas

Statistical methods were used to compare differences between measured and interpolated values of synoptic variables in convective and nonconvective areas. In this study, convective areas were defined by grid points with MDR ≥ 4, which were areas of strong convection (thunderstorms) with maximum rainfall rates in excess of one inch per hour. The mean $(\bar{x})$, standard deviation (σ_x), and standard deviation of the mean $(\sigma_{\bar{x}})$ were computed for each variable for convective and nonconvective regions at each time interval, and results are presented in vertical profiles. Horizontal bands were constructed for $\pm 2\sigma_{\bar{x}}$ to show dispersion of the mean values. At levels where the band about the average contained zero, the differences may be due to random variation.

Fig. 28 shows the average and standard deviation for differences between observed and linearly interpolated values of temperature in convective and nonconvective areas. At most levels, averages were larger in magnitude in convective regions than nonconvective regions, especially for differences computed 3 and 6 h after the initial time of the interpolation period. General shapes of the profiles for both regions were quite similar with negative differences in the lower-most layers and positive differences above 800 mb. Average differences decreased and became negative above the tropopause (250 mb) in convective regions and increased again above 150 mb. Largest differences between profiles of average differences for each region were found in the lower-most layers. Standard deviation profiles were similar in shape in both areas. However, larger deviations of the mean values

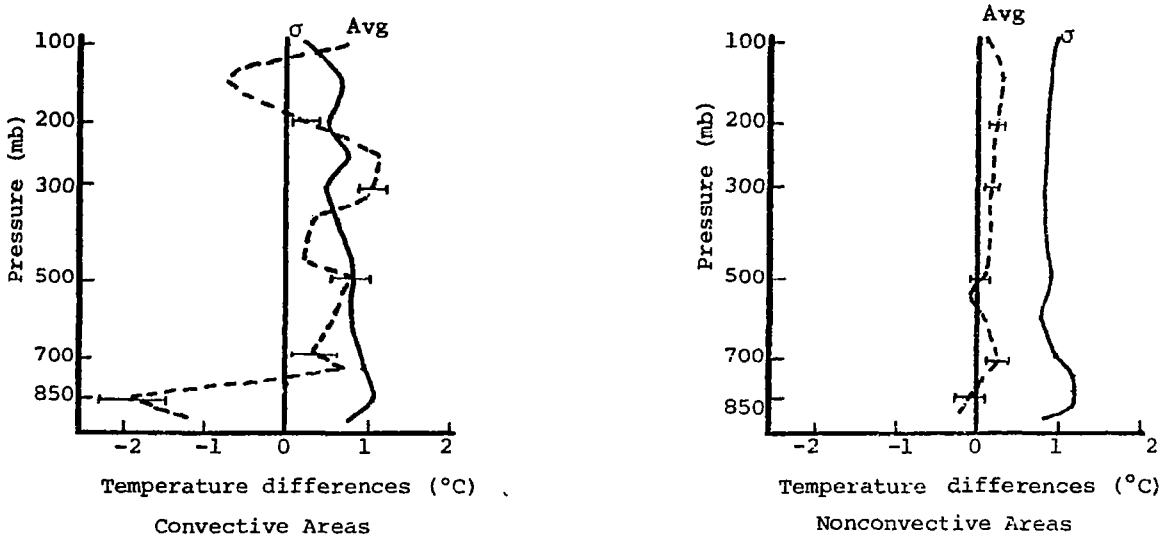

a. 3 h

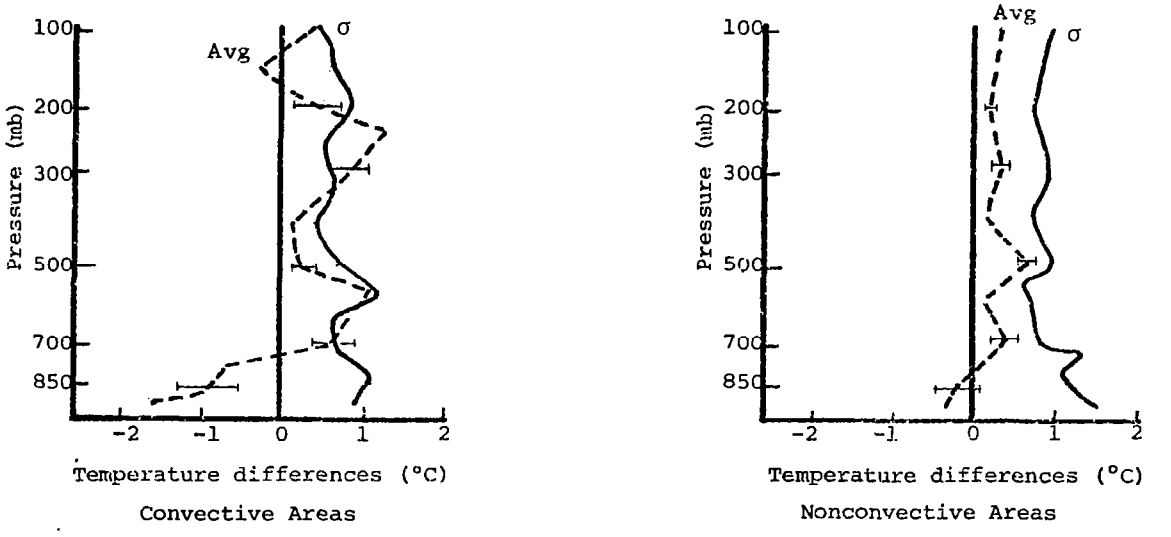

b. 6 h

Fig. 28. Profiles of the average and standard deviation of differences between observed and linearly interpolated values of temperature (°C) computed over 3-, 6-, and 9-h intervals for convective and nonconvective areas. Horizontal bands are drawn for $\pm 2\sigma_{\bar{x}}$.

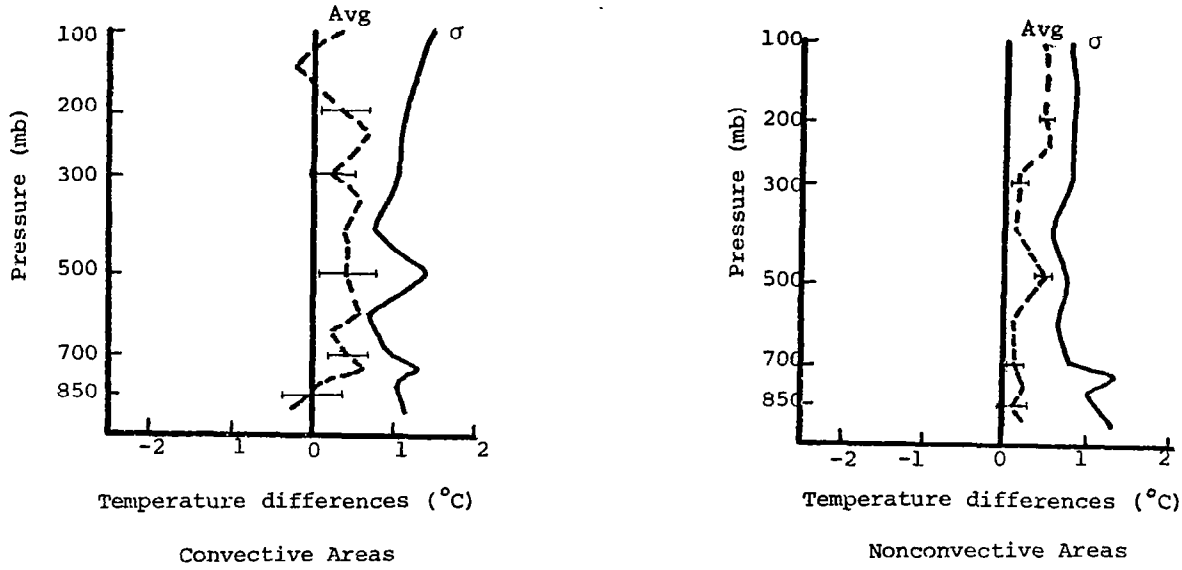

c. 9 h

Fig. 28. (Continued)

were found in areas of convective activity.

Profiles of the averages for differences in mixing ratio in convective and nonconvective regions are presented in Fig. 29. In areas of strong convection, average differences were negative in the lower layers with largest magnitudes around 750 mb, the approximate location of cloud bases. Values decreased in magnitude above the 750- to 700-mb layer and became positive above the 650-mb surface. Analysis of the moisture budget for AVE IV indicated moisture losses in the sub-cloud layers and moisture gain aloft in areas of strong convection (Scott and Scoggins, 1977). The resulting differences or nonlinear changes in mixing ratio in areas of strong convection could be an indication of such moisture losses in lower layers and moisture gain in the upper layers resulting from vertical transport of moisture upward by vertical motions. This also suggests that assuming linearity in the mixing ratio over a 12-h interval is inadequate to define such processes which can occur on a time scale much shorter than 12 h.

Magnitudes of average differences in areas free of convection were smaller than those in convective areas and were more variable with height. Standard deviations of individual values were larger for convective-free areas, especially in the lower-most layers, and decreased with height above about 800 mb. Standard deviations in convective regions were largest near 750 to 700 mb and decreased with altitude above this layer. Standard deviations of the means were smaller in areas free of convection, and Fig. 29 shows that on the average, differences in areas free of convection were not significantly different from zero.

Profiles of the average and standard deviations of differences in geopotential height (Fig. 30) show that average differences were smaller in convective areas than nonconvective areas in the lower layers and slightly larger in convective areas near the tropopause (300 to 200 mb). This can be expected since geopotential height is a function of the vertical integral of mean temperature, and temperature differences were more negative in lower layers and more positive in upper layers in convective regions than nonconvective regions.

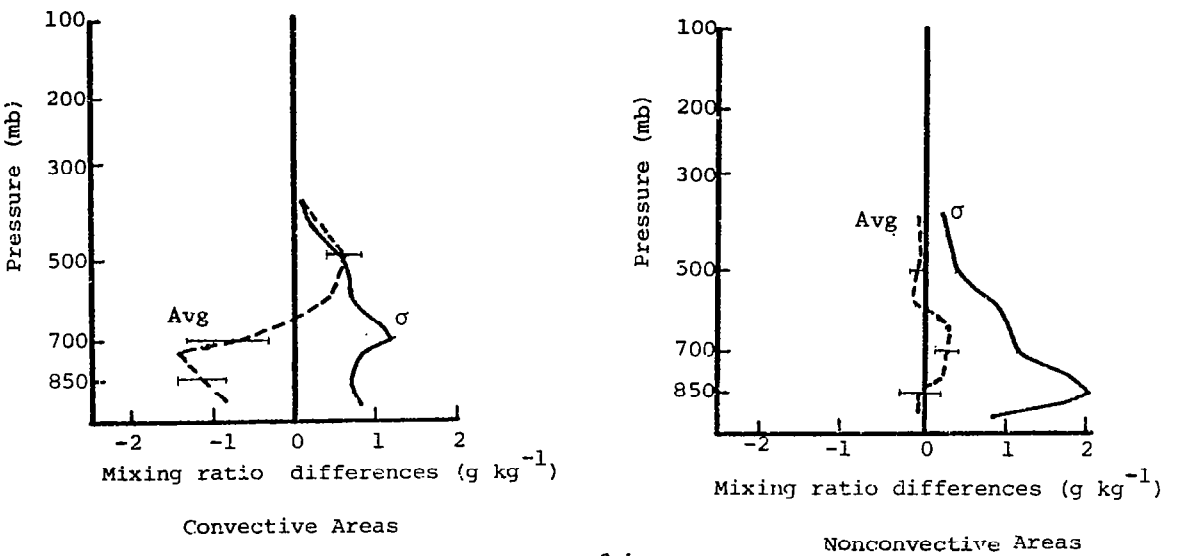

a. 3 h

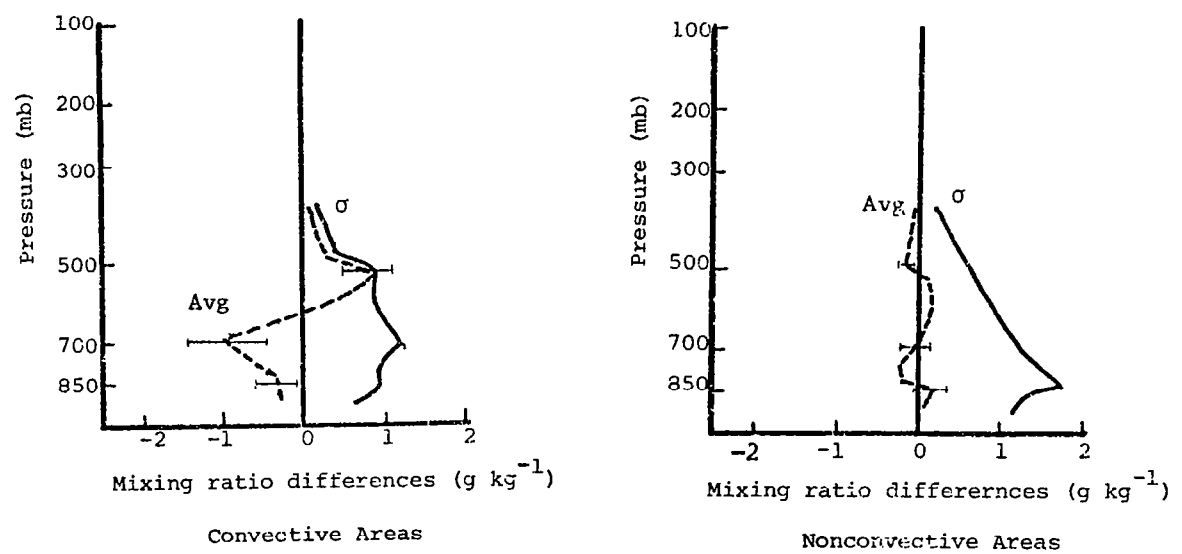

b. 6 h

Fig. 29. Profiles of the average and standard deviation of differences between observed and linearly interpolated values of mixing ratio (g kg^{-1}) computed over 3-, 6-, and 9-h intervals for convective and nonconvective areas. Horizontal bands are drawn for $\pm 2\sigma_{\bar{x}}$.

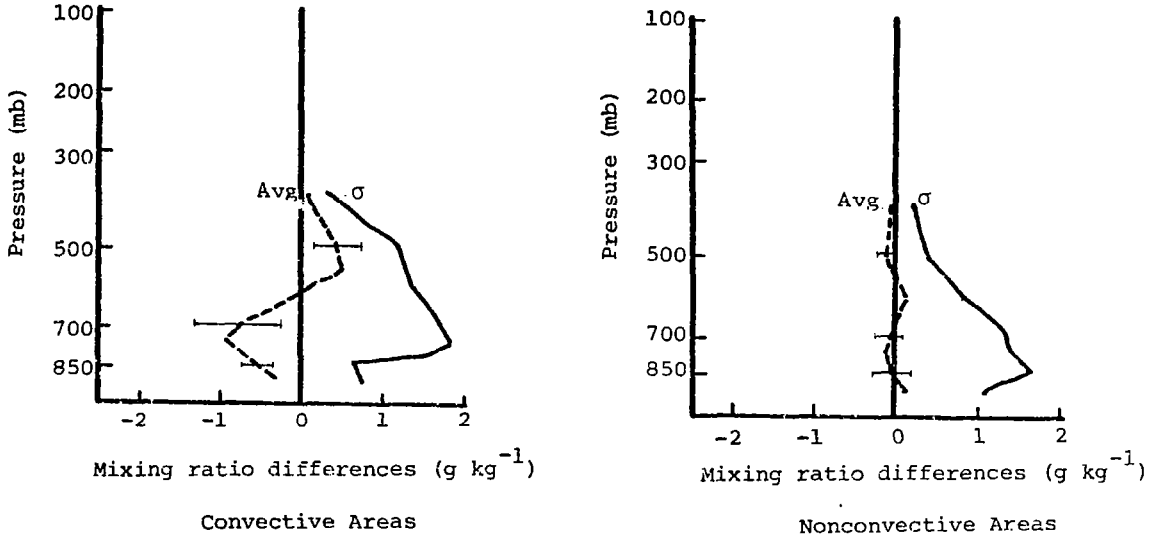

c. 9 h

Fig. 29. (Continued)

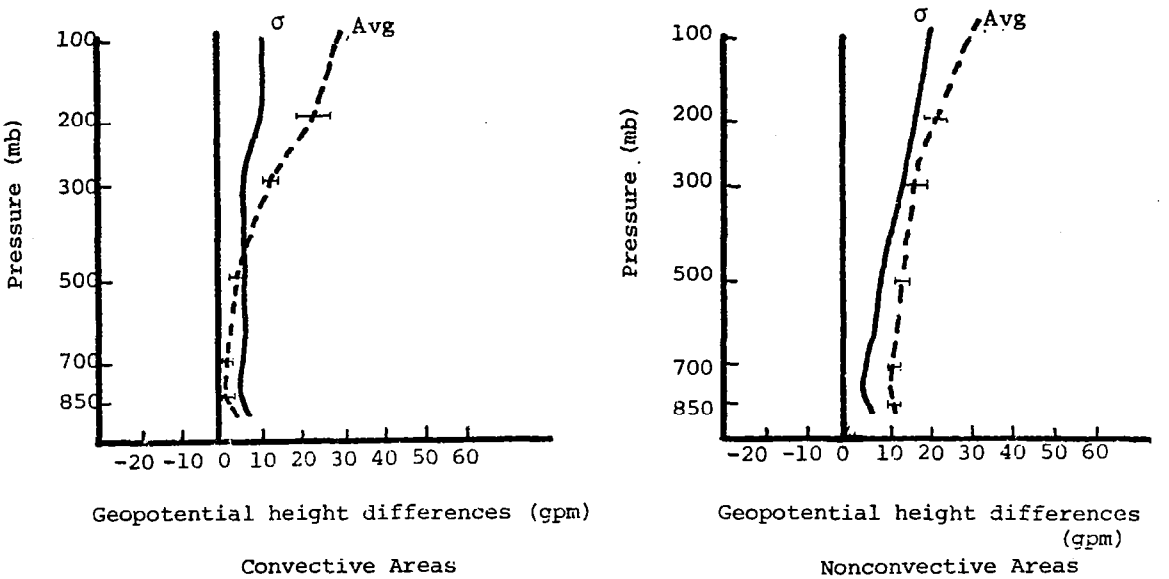

a. 3 h

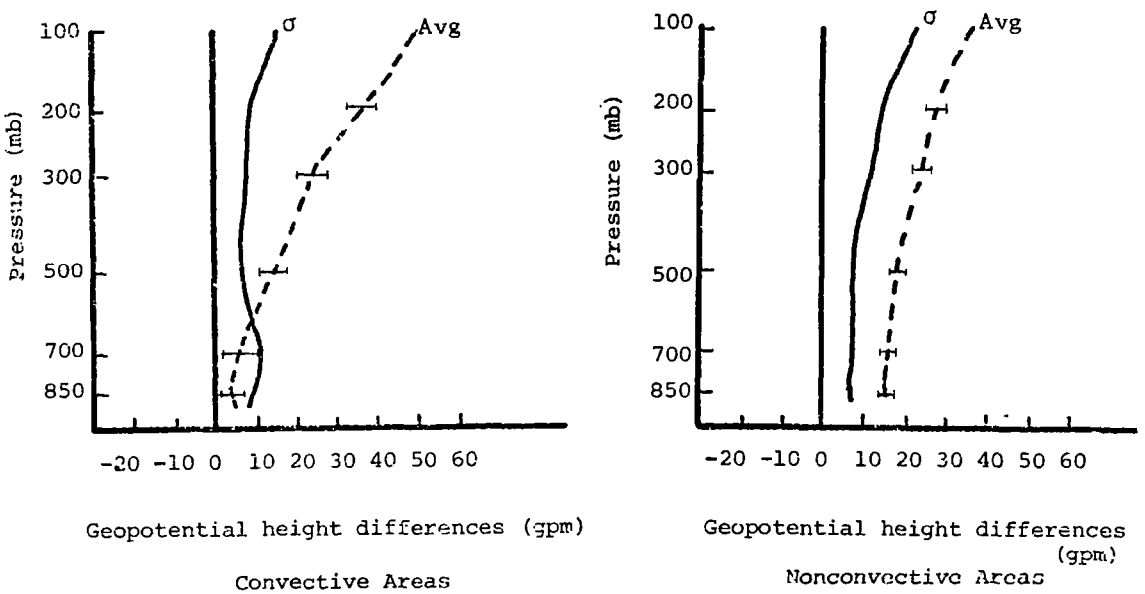

b. 6 h

Fig. 30. Profiles of the average and standard deviation of differences between observed and linearly interpolated values of geopotential height (gpm) computed over 3-, 6-, and 9-h intervals within the 12-h interpolation period for convective and nonconvective areas. Horizontal bands are drawn for $\pm 2\sigma_{\bar{x}}$.

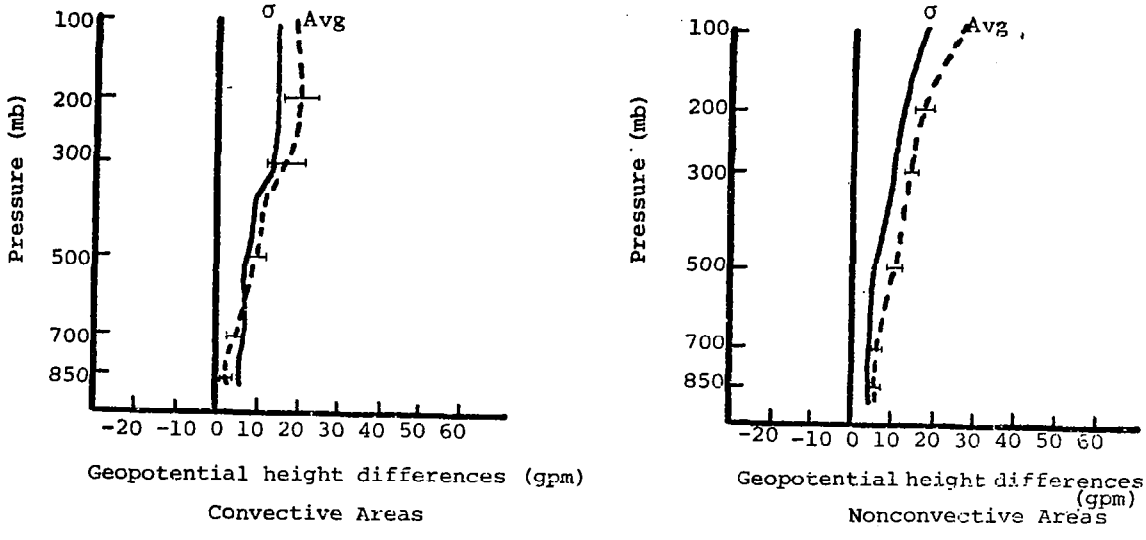

c. 9 h

Fig. 30. (continued)

Standard deviations of individual values in convective regions were larger than in nonconvective regions in lower layers and smaller than nonconvective areas aloft. Profile shapes were very similar in both areas with average and standard deviations increasing with altitude. Average values were larger than the standard deviation, except in lower layers in areas of strong convection.

Profiles of the average and standard deviation of differences in vertical motions computed from observed and interpolated winds are presented in Fig. 31. Magnitudes of average differences and standard deviations were larger for convective areas for 3- and 6-h differences, while profiles for convective and nonconvective areas were similar for 9-h differences. Average values in convective-free areas were negligible for all time periods.

While profiles for nonconvective regions were fairly consistent in time, those for convective areas differed over each time interval. Fig. 31 shows that differences were positive in areas of strong convection after 3 h into the interpolation interval and negative after 6 h. At 1500 GMT, 24 April (3 h), very strong convective activity was found over Arkansas (MDR=8) with moderate-to-strong convection in western Kentucky (MDR=4). The activity over Arkansas, however, had decreased over the 3 h interval and dissipated completely after 6 h. An intense center of positive vertical motion differences was centered over Arkansas (Fig. 19) and indicated decreases in the amount of upward motion that could not be measured by interpolation. Differences over the area of increasing intensity in Kentucky were smaller in magnitude. Thus, average values shown in Fig. 31 were positive after 3 h. Standard deviation profiles show large variation in the data, however, especially in the lower layers.

After 6 h, convection which was increasing in intensity was located mostly in the form of a squall line over central Kentucky and Tennessee, and along the warm front in eastern Kansas. Negative differences of as much as 3 $\mu b\ s^{-1}$, resulting from increases of upward motion not accounted for by interpolation, were associated with the squall line in Tennessee (Fig. 19), while smaller differences were

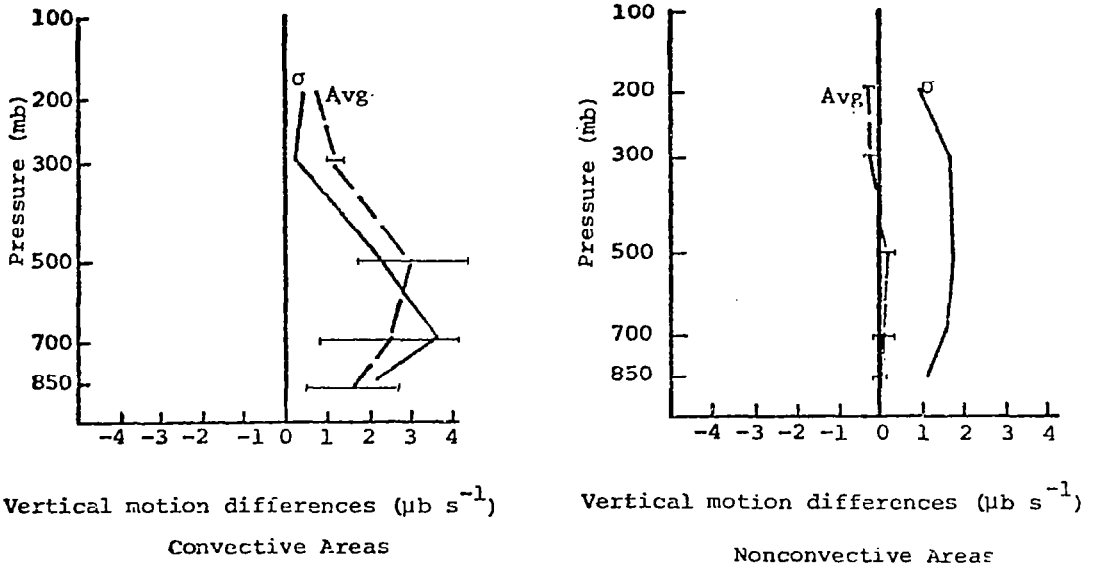

a. 3 h

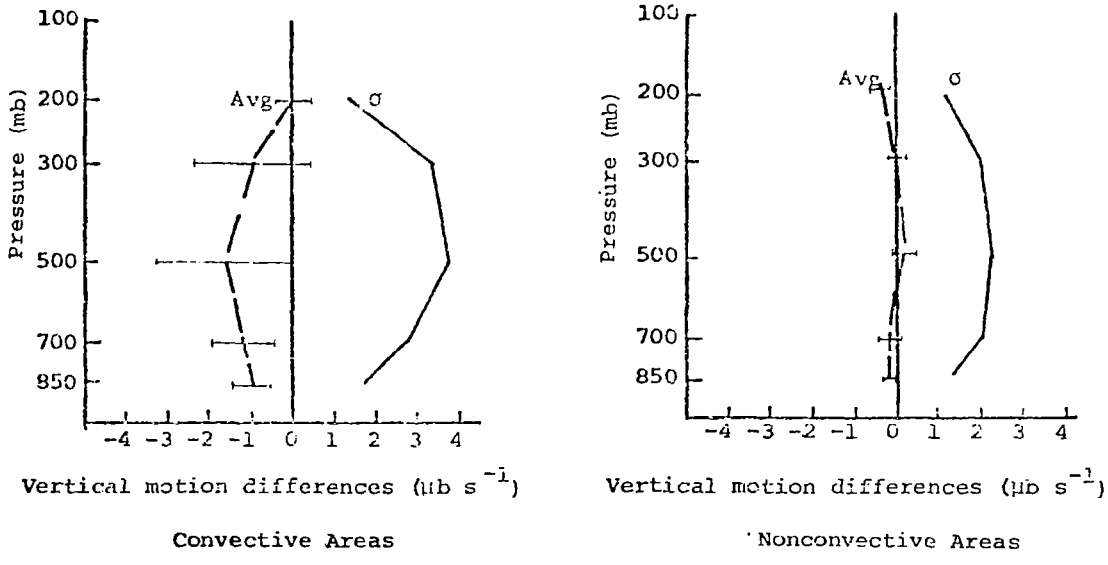

b. 6 h

Fig. 31. Profiles of the average and standard deviation of differences between values of vertical motion (μb s^{-1}) computed from observed and interpolated winds over 3-, 6-, and 9-h intervals within the 12-h interpolation period, for convective and nonconvective areas. Horizontal bands are drawn for $\pm 2\sigma_{\bar{x}}$.

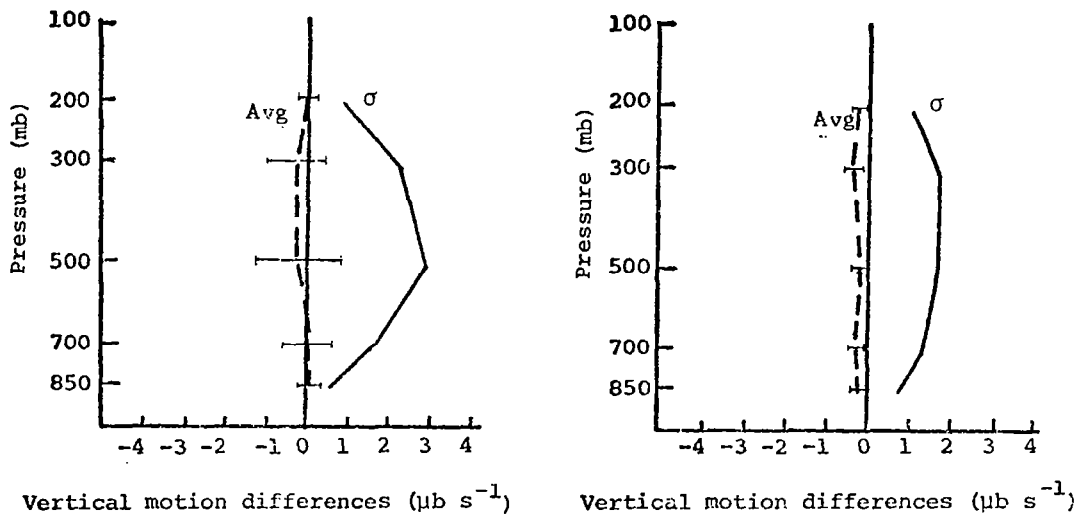

c. 9 h

Fig. 31. (Continued)

found in Kansas. Areal coverage of convective activity also was much larger in Tennessee than in Kansas, and the average negative values shown in Fig. 31 suggest the dominance of this area in the calculations. The large standard deviations reflect the large amount of variability in the data, particularly at the 500- and 300-mb levels.

After 9 h, convection was more widespread. Another squall line developed in eastern Kansas and Oklahoma, while the line in Tennessee moved slightly eastward. Strong convective activity also broke out in South Dakota and in the Ohio Valley. Fig. 31 shows that magnitudes of the vertical motion differences in convective areas were much smaller after 9 h than they were at previous time periods. In fact, the vertical profiles in convective and nonconvective regions were nearly identical, except for larger deviations in areas of convection. This can be explained first by the fact that centers of vertical motion differences were much less intense after 9 h, suggesting that perhaps interpolation is more accurate over larger intervals. Secondly, because convective activity was more widespread after 9 h, profiles were not as representative of one particular area, or were not dominated by one area, as were those for 3- and 6-h differences. This suggests that differences at each point throughout the interpolation interval also were dependent upon initial and final conditions at each particular point. In Oklahoma and Arkansas, for instance, heavy activity occurred at both endpoints of the interpolation period with large amounts of upward motion. Interpolation favored these conditions throughout the entire 12-h period. Therefore, although convective activity was increasing in intensity in this area at 9 h, differences were positive because interpolation indicated more upward motion than was actually found in association with convection because conditions at the initial and final times of the 12-h period were unfavorable for convection.

Fig. 32 shows that average differences for vorticity were larger in convective than nonconvective areas. Positive differences of 10^{-5} s^{-1} to $2x10^{-5}$ s^{-1} were found in the areas of strong convection at 3 and 6 h, particularly from the 700- to 300-mb levels, and indi-

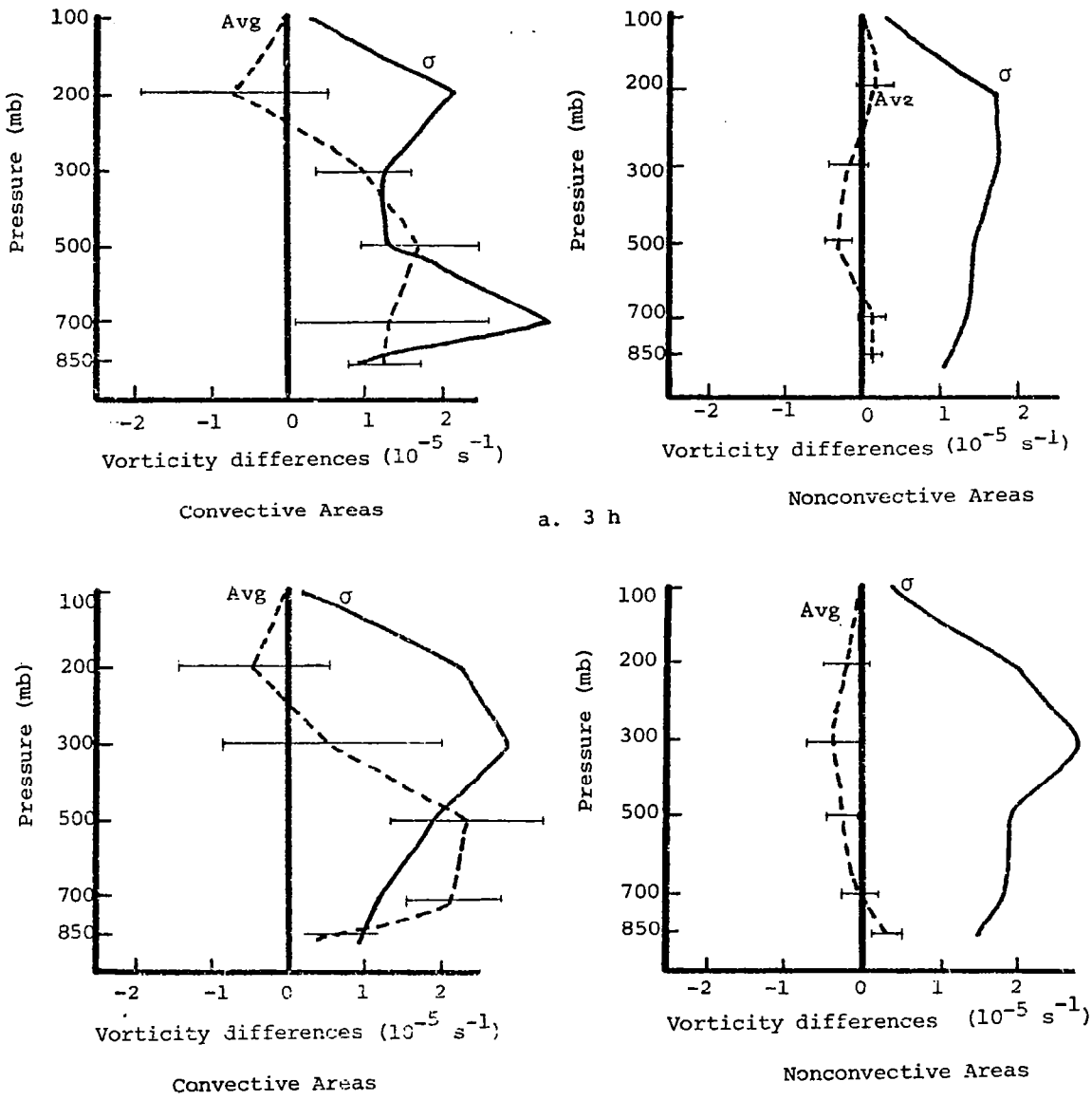

Fig. 32. Profiles of the average and standard deviation of differences between values of vorticity (10^{-5} s^{-1}) computed from observed and interpolated winds over 3-, 6-, and 9-h intervals within the 12-h interpolated period for convective and nonconvective areas. Horizontal bands are drawn for $\pm 2\sigma_{\bar{x}}$.

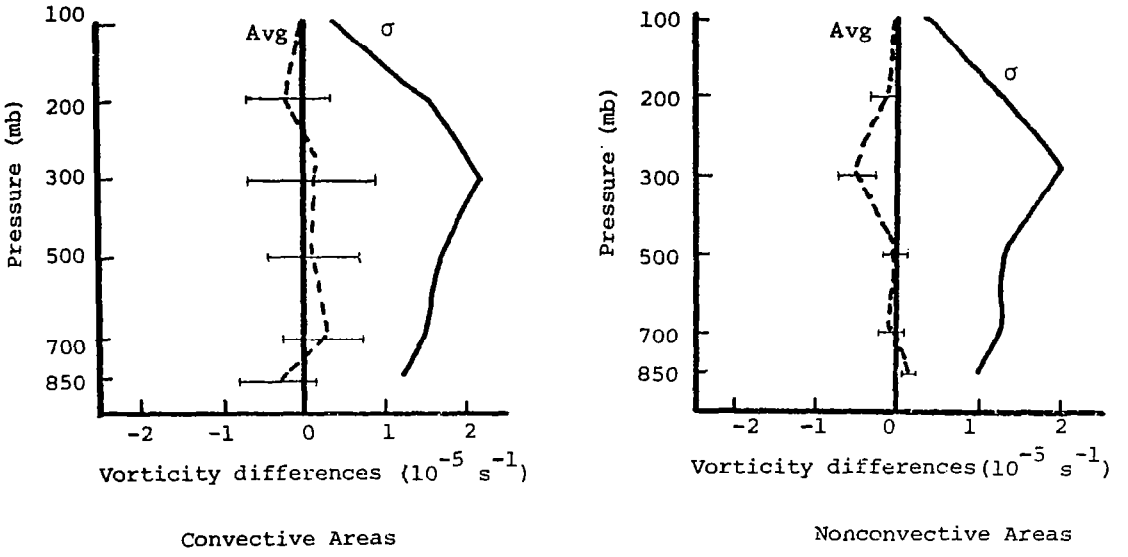

c. 9 h

Fig. 32. (continued)

cated increased cyclonic circulation that was not accounted for by linear interpolation. Average differences were mostly negative in nonconvective areas with largest magnitudes in the mid to upper troposphere. Nine-hour average differences were smaller in magnitude than previous time intervals and not significantly different from zero. In nonconvective areas, average differences were negligible at most levels of the atmosphere. Profiles were nearly identical over all time periods in nonconvective regions.

Standard deviation profiles were similar in both areas for 6- and 9-h differences and indicate a large amount of variability in the data. Largest deviations were found in the upper layers of the troposphere (near 300 mb) except after 3 h in areas of strong convection, where largest values were found near 700 mb.

Averages and standard deviations of differences in vorticity advection for convective and nonconvective areas are shown in Fig. 33. Once again, profiles show good consistency in time for nonconvective areas. Average differences were negligible, while standard deviations increased with height at all time periods.

In areas of convection, differences in the profiles over each period reflected the overall tendency of the intensity of convection over the period. At 6 and 9 h, convection was generally increasing in intensity. Positive average differences, which were largest in the mid to upper troposphere, indicate increases in positive vorticity advection (PVA) that were not accounted for by assuming linearity of the wind field over a 12-h period. After 3 h, however, convection was generally decreasing in intensity. An area of intense thunderstorms over Arkansas began to decrease in intensity over the period, and had completely dissipated by 6 h. Average differences were negative as a result of increasing amounts of negative advection that was not accounted for by interpolation. These results further suggest the importance of PVA in the mid to upper troposphere in the initiation, intensification, and maintenance of convective storms.

Standard deviations in areas of strong convection were generally larger than in nonconvective areas, and increased with altitude except

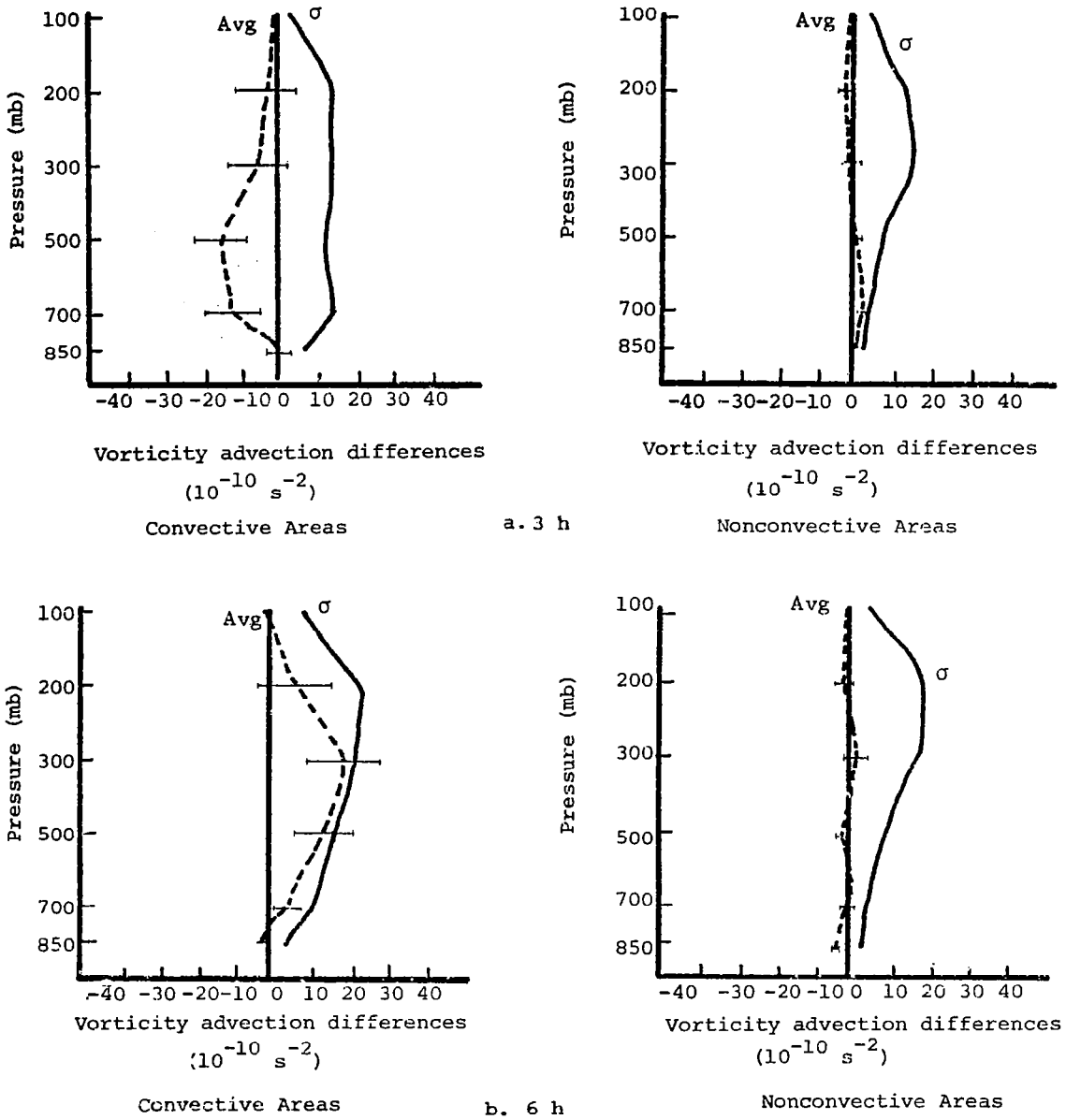

Fig. 33. Profiles of the average and standard deviation of differences between values of vorticity advection (10^{-10} s^{-2}) computed from observed and interpolated winds over 3-, 6-, and 9-h intervals within the 12-h interpolation period for convective and nonconvective areas. Horizontal bands are drawn for $\pm 2\sigma_{\bar{x}}$.

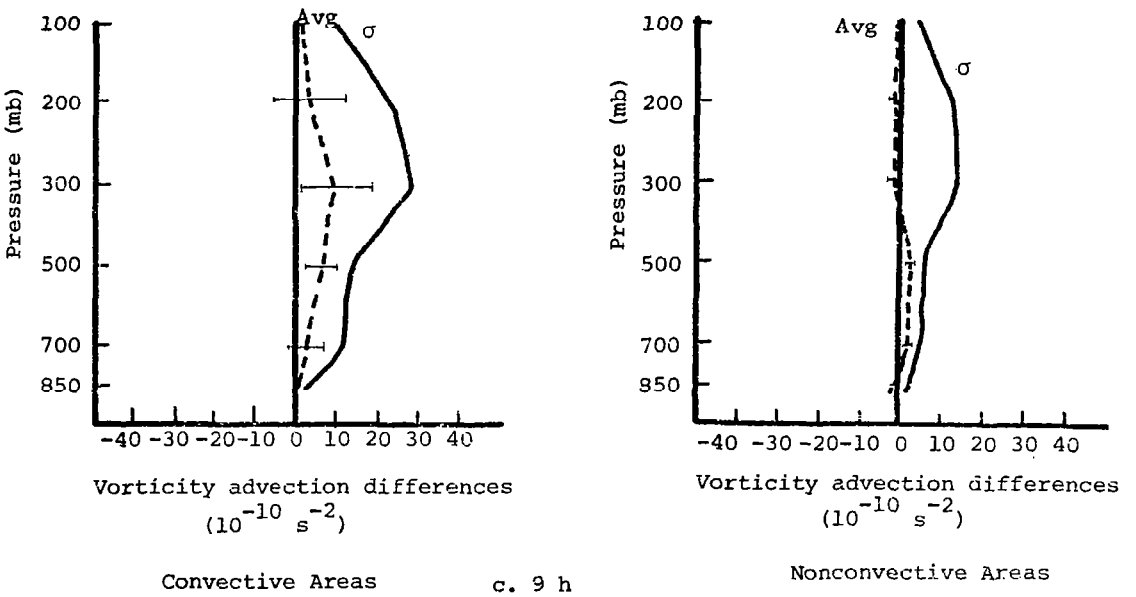

Fig. 33. (continued)

for 3-h differences when the largest deviations were found around 700 mb.

Statistics for differences between measured and interpolated values of temperature advection are presented in Fig. 34. Profiles show that average differences and standard deviations in areas free of convection were fairly systematic in time. Average differences were very small at all levels, and standard deviations increased with altitude except from 850 to 700 mb.

In areas of strong convection, differences were positive in the lower layers (above 850 mb) of the atmosphere and negative aloft after 3 and 6 h. This was the result of increasing amounts of warm air advection in lower layers and cold air advection (or sometimes less warm air advection) aloft that were not accounted for by linear interpolation. These effects suggest decreasing amounts of stability through a deep layer of the atmosphere in areas of strong convection. However, the larger differences at 700 mb as compared to 850 mb show more warm air advection at the 700-mb level and suggest a more stable layer from 850-700 mb, which may be the result of thunderstorms interacting with their environment. Profiles of standard deviation were fairly systematic in time in areas of strong convection and similar in shape to those for nonconvective areas. Standard deviations generally increased with altitude above 700 mb.

Statistics for differences in the convective instability index are shown in Fig. 35. Average values are indicated by bars and standard deviations appear in parentheses beneath each bar.

Fig. 35 shows that on the average nonlinear increases in stability occurred in convective-free areas while decreases in stability were found in areas of thunderstorms. The increasing stability found in areas of convection after 3 h, particularly in the lower layer (900-700 mb), could attribute to the overall dissipating activity over this time interval. This further indicates the importance of instability in the lower layers of the atmosphere in the maintenance of thunderstorms. Although the graphs indicate that thunderstorms generally occurred in an unstable environment, the large amounts of

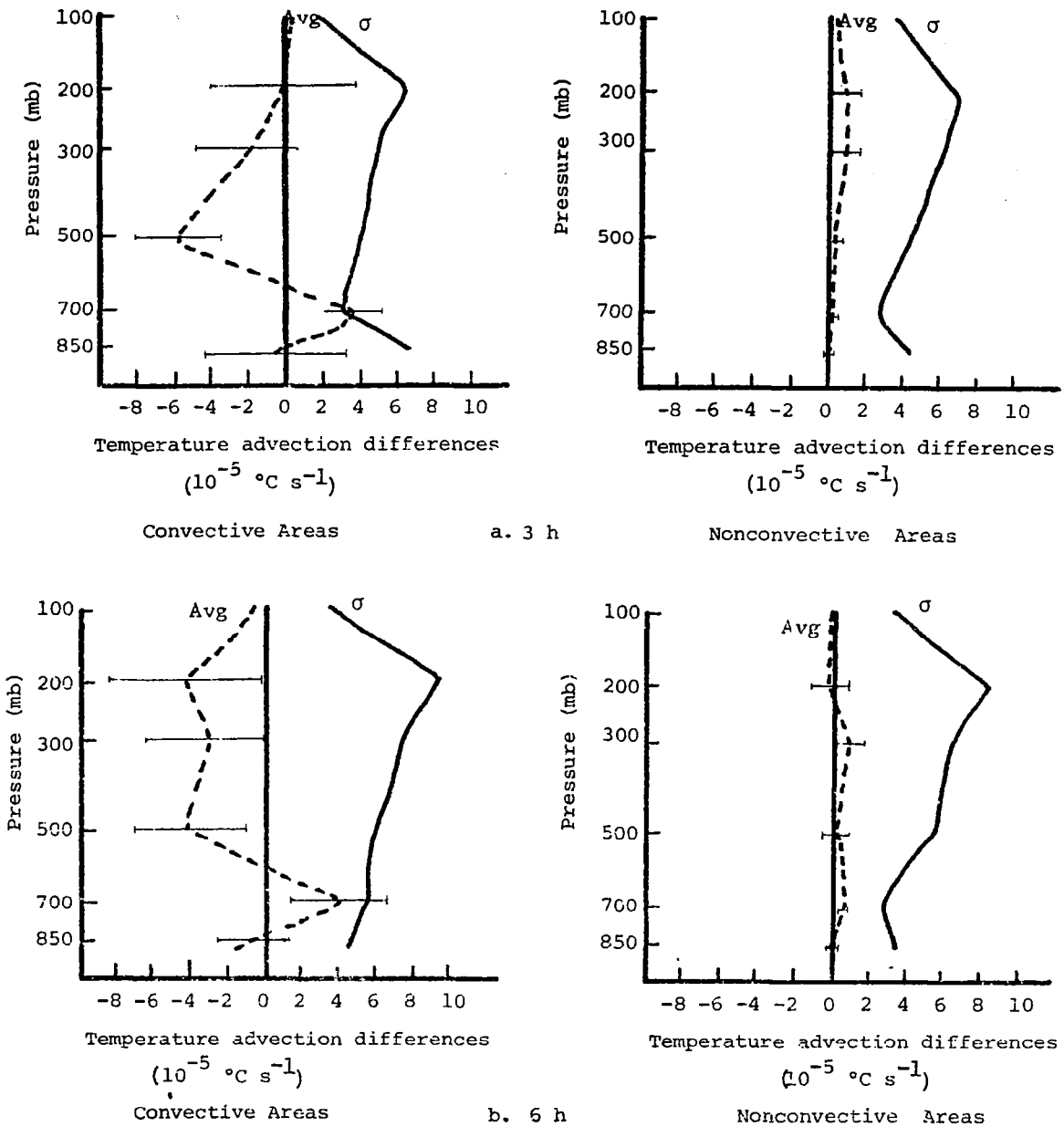

Fig. 34. Profiles of the average and standard deviation of differences between values of temperature advection (x 10^{-5} °C s^{-1}) computed from observed and interpolated winds over 3-, 6-, and 9-h intervals within the 12-h interpolation period for convective and nonconvective areas. Horizontal bands are drawn for $\pm 2\sigma_{\bar{x}}$.

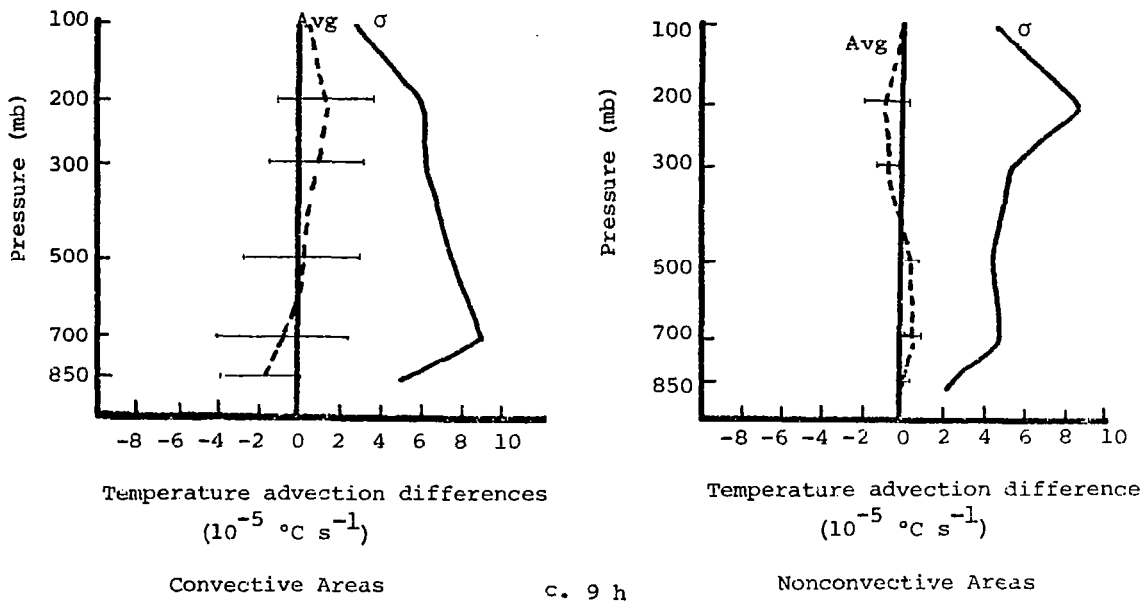

Fig. 34. (continued)

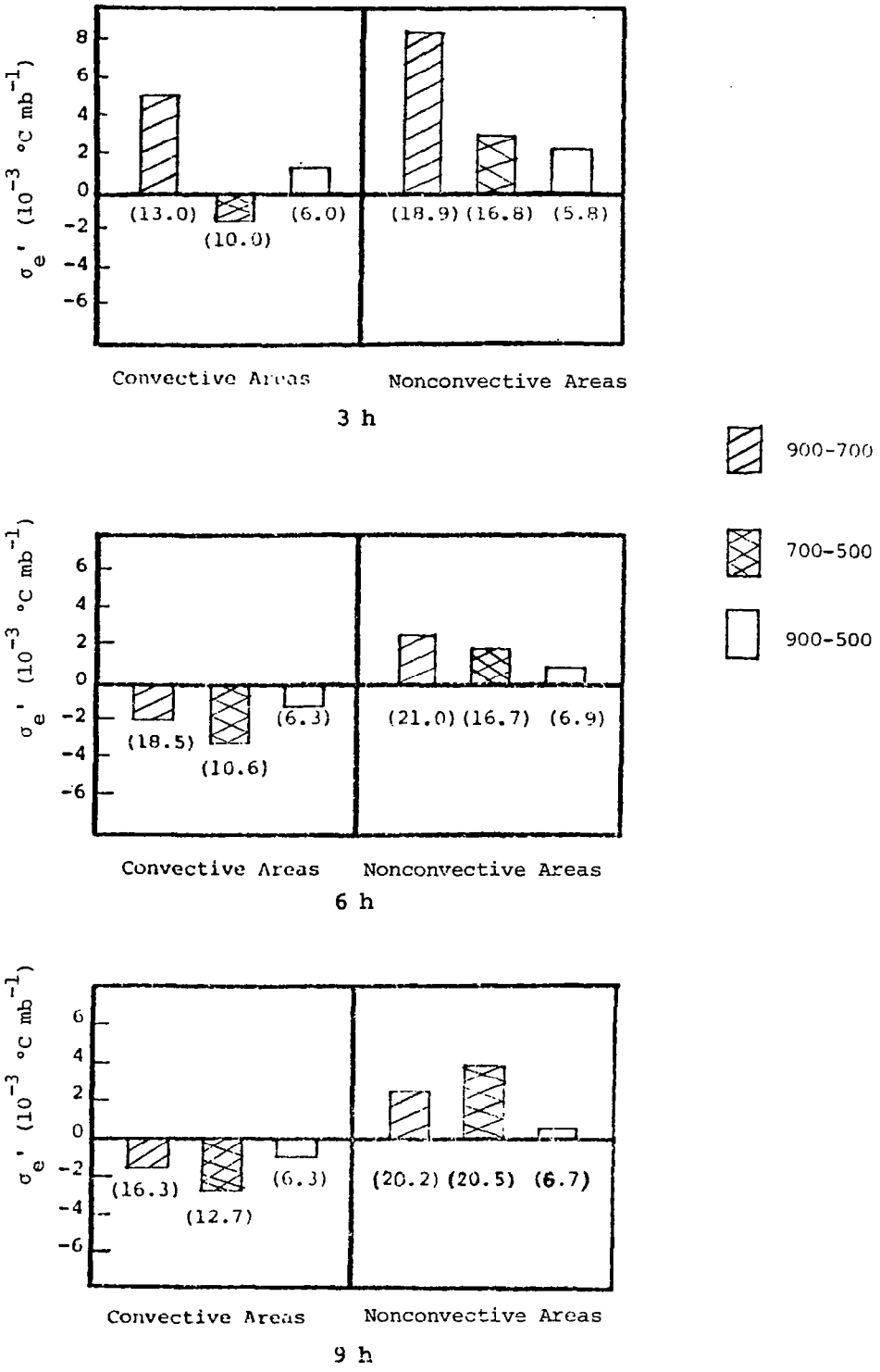

Fig. 35. Average and standard deviations (in parenthesis) for differences in convective instability (10^{-3} °C mb^{-1}) in convective and nonconvective areas.

instability found in convective-free regions (Fig. 24) suggest that the release of instability resulting in thunderstorms must be triggered by other processes such as kinematic features.

Average values of differences in convective instability were generally an order of magnitude smaller than typical observed values of convective instability. Standard deviations, however, were three to as much as ten times the mean values, indicating large variability in the data. Average values and standard deviations were larger in magnitude in nonconvective than in convective regions.

e. Interrelationships between Differences and Synoptic Conditions

Analysis has indicated that interrelationships between nonlinear changes in synoptic variables existed and that some relationships may be important in the development, maintenance, and dissipation of thunderstorms. During the 12-h interpolation interval chosen in this study, severe weather occurred mainly in the form of two active squall lines. While the first of these areas of thunderstorms dissipated over southern Missouri and Arkansas during the first 6 h of the period, the second line intensified rapidly between 1800 and 2100 GMT as it passed through central and eastern Kentucky and Tennessee.

Centers of nonlinear increases in low-level wind convergence and upper-level divergence were associated with the squall line in Tennessee, along with upward vertical motion. Decreases in stability not accounted for by interpolation also were found in this region. Instability also was found in convective-free regions which suggests that the release of instability, essential in the production and maintenance of thunderstorms, must be triggered by kinematic processes.

Figures 36 and 37 show time cross sections of differences between measured and linearly interpolated values of vertical motion and temperature computed for the center of four surrounding grid points in east-central Tennessee and in southern Missouri and northeast Arkansas. Maximum intensity of convection occurred at around 2100 GMT in eastern Tennessee (MDR=6). Fig. 36a shows that differences changed in sign from

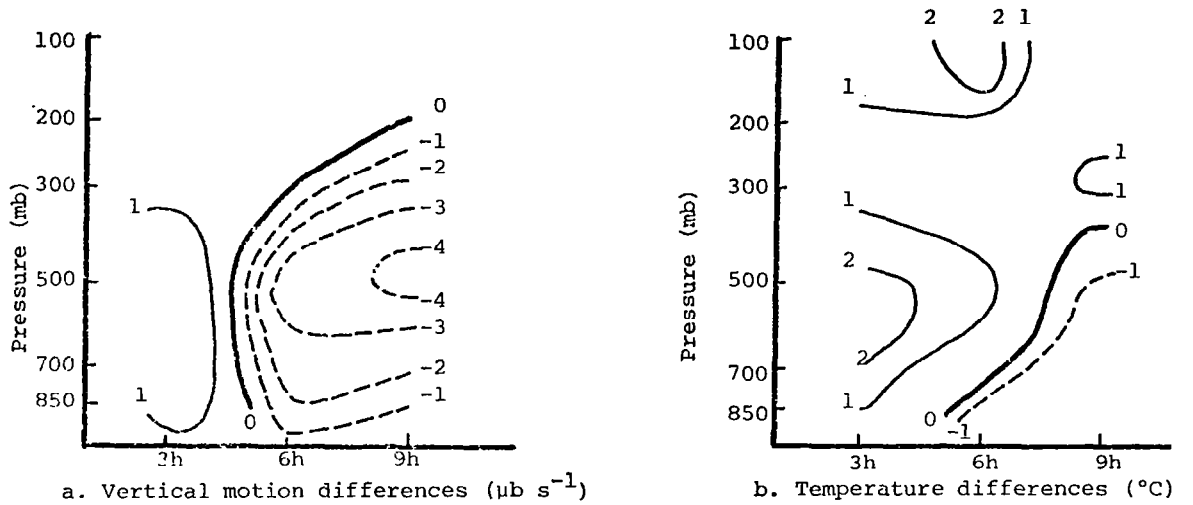

Fig. 36. Time cross sections of vertical motion and temperature differences in central and eastern Tennessee.

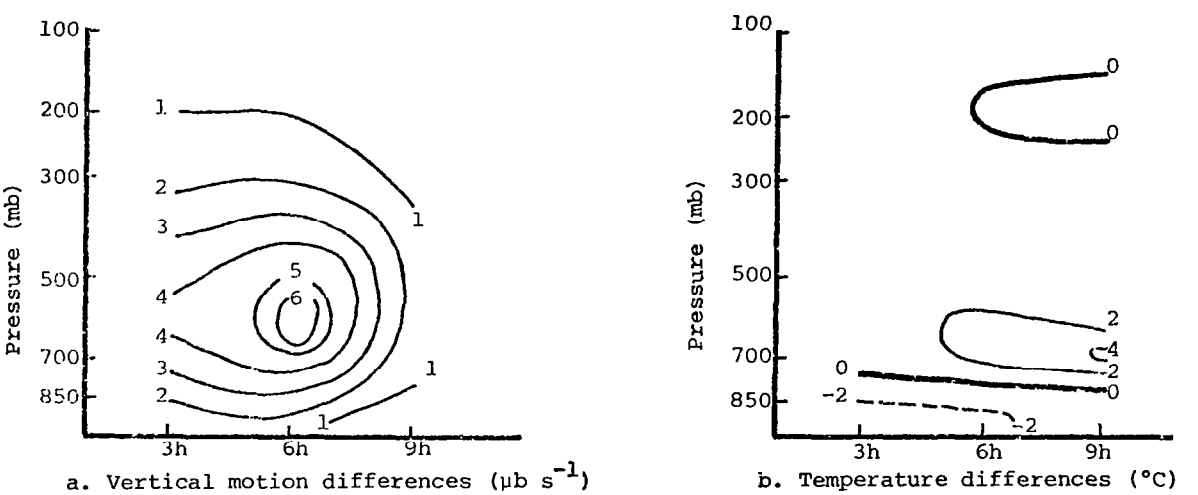

Fig. 37. Time cross sections of vertical motion and temperature differences in SE Missouri and NE Arkansas.

positive to negative in conjunction with the passage of an upper-level short wave around 1800 GMT. The rapid change in sign indicates large amounts of increases in upward motion that were not accounted for by linear interpolation occurred just prior to and during thunderstorm development. These nonlinear increases in low-level convergence and upward vertical motion could have been an important mechanism releasing the instability necessary for the maintenance and intensification of the thunderstorms associated with the squall line.

Results have also shown that nonlinear increases in vorticity, indicating increased circulation and lifting due to convergence, were found in these areas of strong convection. Large amounts of positive vorticity advection, unaccounted for by linear interpolation, also were found in the mid to upper troposphere prior to and during convective activity.

In convective-free areas and regions of thunderstorm dissipation, significant amounts of instability were present but there existed no mechanism to release the instability necessary for further development or maintenance of thunderstorms. Nonlinear increases in downward motion suppressed the release of instability, and increased divergence cut off the moisture supply into these convective systems. Fig. 37a shows large increases in downward motion in the Missouri-Arkansas area which may have been largely responsible for the suppression of the release of instability and the consequent dissipation of thunderstorm activity in this area over the first 6 h of the interpolation period. Large amounts of negative vorticity advection, not accounted for by linear interpolation, also were found in these areas, particularly in the mid to upper troposphere.

Figs. 36 and 37 suggest a relationship between differences (observed-interpolated) in vertical motion and temperature. At most times when nonlinear increases in upward vertical motion occurred, nonlinear decreases in temperature were observed, probably the result of cooling due to lifting. When greater amounts of downward motion than was measured by interpolation were observed, higher temperatures were generally observed than indicated by interpolation, except near

the surface in areas of cloudiness such as Missouri and Arkansas (Fig. 37). These nonlinear increases in temperature may have been, at least in part, the result of adiabatic warming due to subsidence.

Fig. 38 shows similar relationships between differences for vertical motion and temperature. Nonlinear decreases of temperature correlated fairly well in space with regions of nonlinear increases in vertical motion, while increases in temperature again were found in areas of subsiding air.

The fact that the intensity of vertical motion differences did not relate to the intensity of temperature differences suggest that nonlinear changes in temperature also were caused by other factors such as temperature advection. In central and eastern Tennessee, for example, cold air advection unaccounted for by linear interpolation, was found at most levels. In Missouri and Arkansas warm air advection may have been an important factor in increasing temperatures.

Differences between measured and linearly interpolated values of equivalent potential temperature were found to correlate well in space with differences in mixing ratio at all levels up to 500 mb. Nonlinear changes in mixing ratio were negligible above that level. Fields of equivalent potential temperature and mixing ratio differences are presented in Fig. 39 for the 900-mb level at 1800 GMT, 24 April. The good correlation in space between the two fields suggests that nonlinear changes in moisture were largely responsible for the variability in equivalent potential temperature and, therefore, the variability in stability. These relationships were well-established at all time periods within the 12-h interpolation interval.

In summary, nonlinear changes in synoptic variables were related, with spatial distributions correlating well with each other at all time periods. Such relationships between variables indicate processes occurring in the atmosphere that induce large variability that cannot be accurately resolved by use of 12-h data, and that this variability may be important in the development of severe weather and thunderstorms.

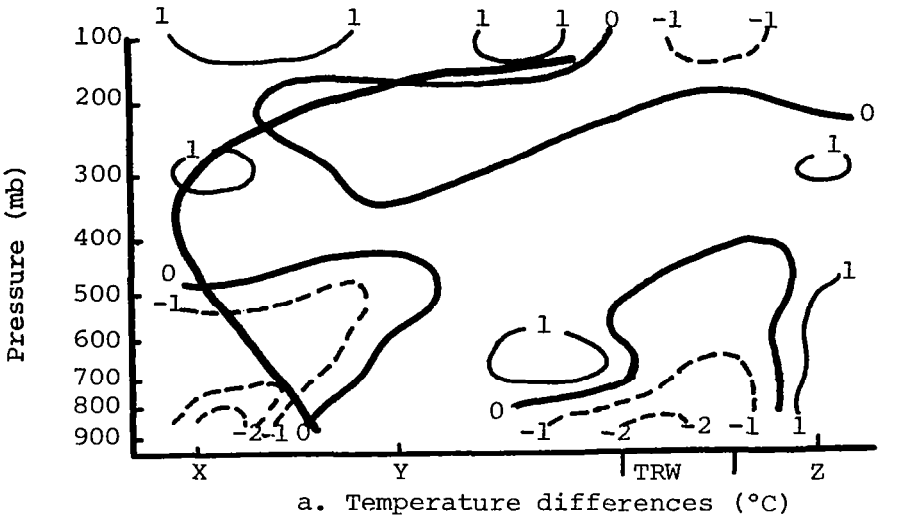

a. Temperature differences (°C)

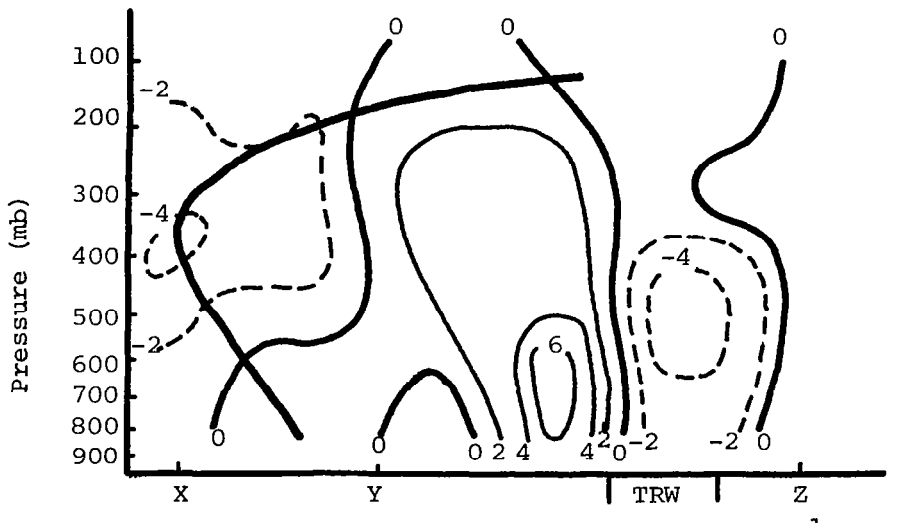

b. Vertical motion differences (μb s^{-1})

Fig. 38. Vertical cross section of differences between observed and interpolated values of temperatures and vertical motion along line XYZ in Fig. 6 computed 6 h after the initial time of the interpolation period.

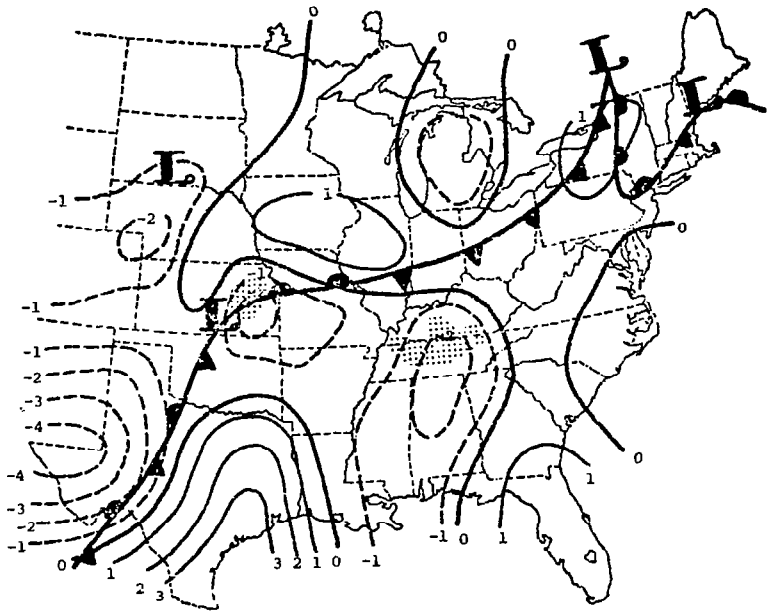

a. Mixing Ratio (g kg^{-1})

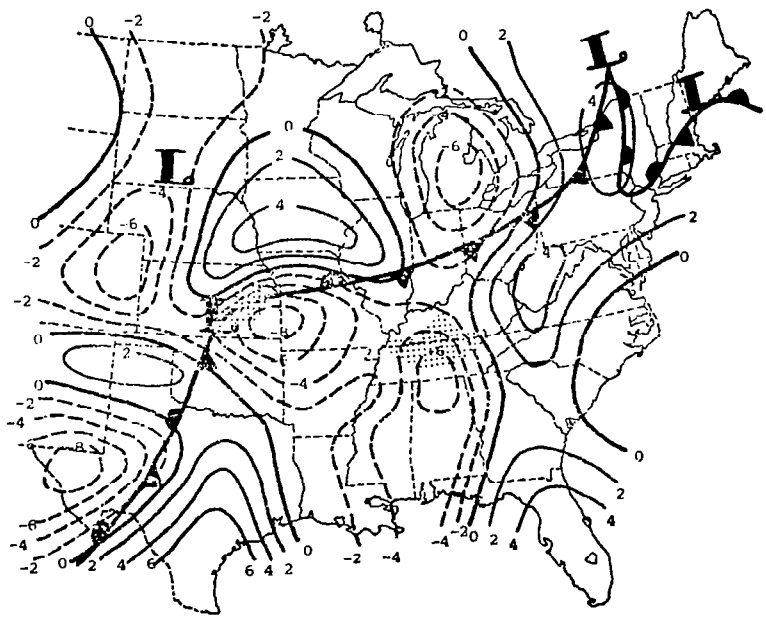

b. Equivalent Potential Temperature (°C)

Fig. 39. Differences between measured and interpolated values of equivalent potential temperature and mixing ratio computed 6 h into the interpolation period for the 900-mb level.

f. Significance of Differences: The Nonlinear Coefficient

As shown in Fig. 10, differences between observed and linearly interpolated values of synoptic variables over time intervals within the 12-h interpolation period also represent the amount of change in a variable over the interval that is not accounted for by an assumed linear change. This unaccounted for change was defined as the nonlinear change of the variable over the particular time interval.

A coefficient of nonlinearity was computed from Eq. (4) in order to determine the significance of nonlinear changes over 3-, 6-, and 9-h intervals, within a 12-h period between regular synoptic observations, relative to an observed change over the same intervals. Average coefficients for selected variables at each pressure level were computed, and results are presented in Fig. 40.

Profiles show that on the average nearly 80 to 100% of an observed change in temperature, mixing ratio, geopotential height, and vertical motion over a 3-h interval was unaccounted for by an assumed linear change based upon 12-h sounding information. Coefficients decreased slightly after 6 h and more rapidly at 9 h at most levels for all variables except temperature. Variations in time of the nonlinear coefficient for temperature were more variable with altitude. The largest decreases were found between 3 and 6 h in the lower and upper troposphere, while decreases between 6 and 9 h were greatest in the middle levels. Above the tropopause, temperature coefficients increased slightly from 3 to 6 h. Coefficients for mixing ratio were largest of all variables for each time period indicating that linear changes in mixing ratio were more inadequate in approximating actual changes than for any other variable.

Although the nonlinear coefficient decreased in time, magnitudes were still quite large after 9 h. Profiles indicate that 38 to as much as 75% error was possible in the low and mid troposphere by assuming linear changes in synoptic variables with even larger errors (95%) possible above the tropopause.

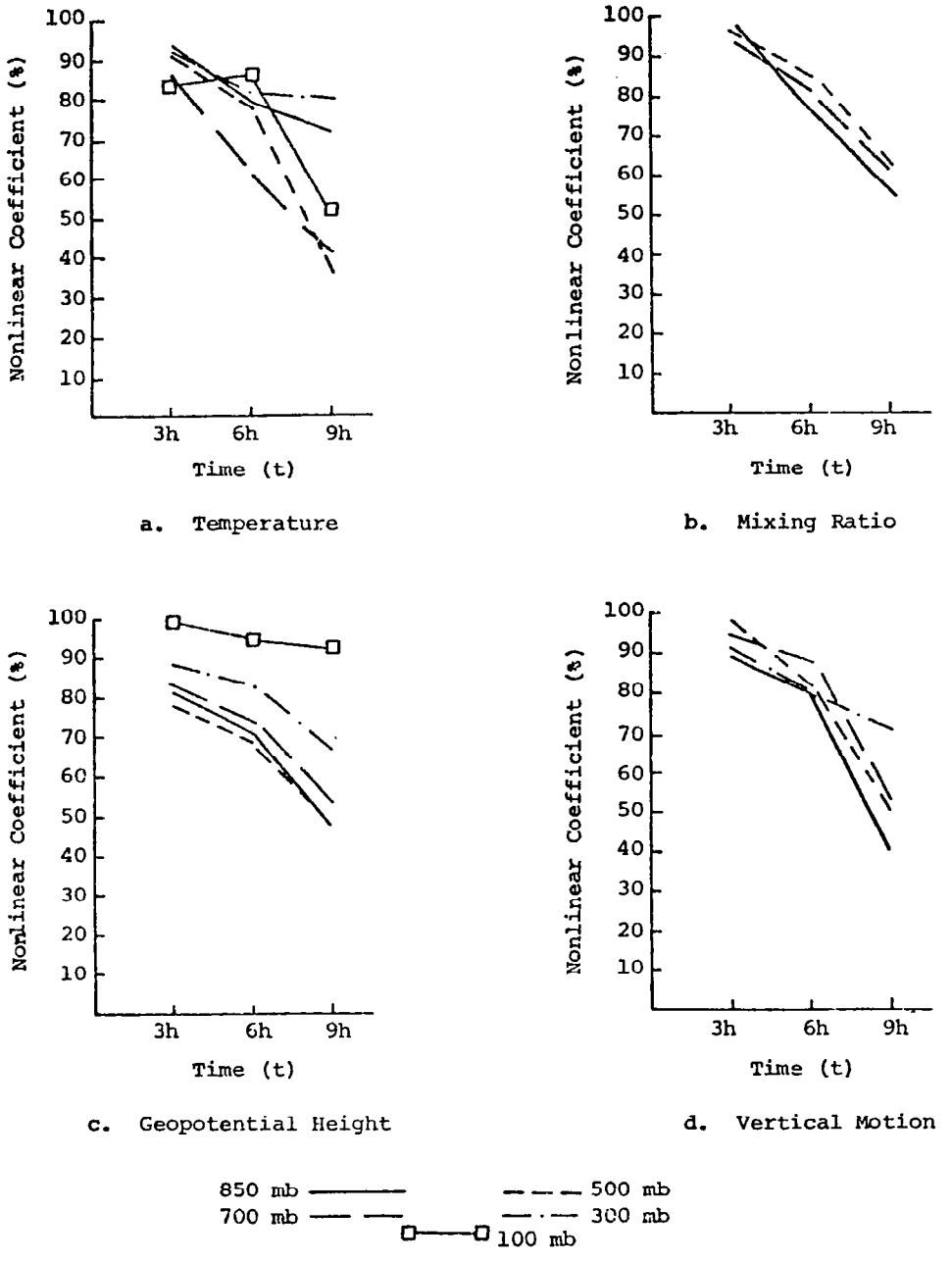

Fig. 40. Average nonlinear coefficient computed over 3-, 6-, and 9-h intervals at selected pressure levels for various synoptic variables.

The overall decrease in the nonlinear coefficient as the time interval increases suggests that, on the average, the change in t was the dominating factor determining the value of the coefficient in Eq. 4, and indicates that as the time interval increases, a linear change accounts for an increased amount of the observed change over the same time interval.

The results here may relate to other methods utilized in many meteorological studies that are similar in principle to linear temporal interpolation, such as linear extrapolation of systems in space over a 12-h period. Although extrapolation involves the movement of spatial trends of variable changes, rapid development of these systems and changes in their structure over short time periods are often unresolved. Many of the sub-synoptic processes or systems that are important in the development of convective activity have a time scale shorter than 12 h, and their effects on the variability of atmospheric structure over such short intervals cannot be defined by methods of interpolation and extrapolation based upon 12-h data. The increasing ability over larger time intervals of linear changes in approximating actual changes over the same intervals, however, may explain why extrapolation techniques are more successful in forecasting for periods of 12 h than for short time periods, such as a 3 or 6 h. Nevertheless, the use of 3-h rawinsonde data obviously allows a better understanding of the variability of atmospheric variables over short time periods, and thereby allows better resolution of convective and subsynoptic systems than is obtained with 12-h data.

6. SUMMARY AND CONCLUSIONS

a. Summary

An examination of nonlinear changes in synoptic variables over 3-, 6-, and 9-h intervals within 12-h sounding observations has been carried out using the unique rawinsonde data from NASA's fourth Atmospheric Variability Experiment (AVE IV). A linear change was assumed in variables over the 12-h period and differences between values computed from 3-h sounding data and values interpolated linearly were evaluated. Analyzed fields of differences were examined to investigate relationships to synoptic features, and Manually Digitized Radar (MDR) were utilized to establish relationships between nonlinear changes and thunderstorms. Systematic patterns of these differences in time and space were examined as well as their vertical continuity. The relative importance of nonlinear changes with respect to observed changes in synoptic variables also was determined by use of a nonlinear coefficient which represented the amount of observed change that was not accounted for by a linear change over a time interval within the interpolation period.

b. Conclusions

The following conclusions were reached from this study:

1) Nonlinear changes in synoptic variables formed centers or systems which appear to be mesosynoptic in nature. These changes represented resolution that was lost by assuming variables to change linearly through a 12-h period betwee sounding obsérvations.
2) Centers of nonlinear changes were very systematic in time and space. Many of the centers extended to the upper atmosphere; some sloped with altitude (such as temperature) while others stacked vertically in the atmosphere (vertical motion, geopotential height). Vertical relations of fields of non-

linear changes were verified by inter-level correlations.

3) The vertical continuity of many of these systems show that nonlinear changes are related to synoptic features such as frontal zones, short waves, and other sub-synoptic scale systems. Analysis of constant pressure charts further documents these relationships. Nonlinear changes correlated well in space with upper-level troughs and ridges, frontal zones, and areas of thunderstorms at all time periods. Largest magnitudes of nonlinear changes occurred in these regions.
4) Statistical profiles of differences between measured and linearly interpolated values of synoptic variables in convective and nonconvective areas showed that, on the average, differences or nonlinear changes were larger in magnitude in areas of strong convection than in regions free of thunderstorms. Standard deviations for most variables were larger than mean values in both regions and suggested variation in the data sets.
5) Error analysis showed that the nonlinear changes in most variables were larger in magnitude than the computed errors of the changes. This implies that these changes can be attributed to the nonlinearity of synoptic variables and that the RMS errors in the original data did not have a significant effect on the computations of the changes. Nonlinear changes in vertical motions, however, did exceed computed errors at and above 500 mb.
6) Nonlinear changes were associated with areas of convective activity. Nonlinear increases in instability were found in areas of thunderstorms, and nonlinear increases in low-level convergence and upward motion were important in the release of instability. In unstable regions free of thunderstorms, nonlinear increases in downward motion suppressed this release.
7) Linear interpolation was inadequate in defining variability in atmospheric variables over short time intervals, and could

not resolve some sub-synoptic scale systems which had life cycles less than 12 h. As the time interval increased from 3 to 6 to 9 h within the interpolation period, however, linear changes accounted for more and more of the observed change over the 12-h interval. Since linear extrapolation of systems in space over a 12-h period is based upon the same principle, these results may explain why extrapolation techniques, used in forecasting, are more successful over larger time periods than over short time periods, such as 3 or 6 h.

REFERENCES

Barnes, S. L., 1964: A technique for maximizing detail in numerical weather map analysis. J. Appl. Meteorol., 3, 396-409.

Barr, S., W. K. Widger, Jr., I. A. Miller, and R. Stanton, 1971: Objective subsynoptic upper level analysis. J. Appl. Meteorol., 10, 410-417.

Endlich, R. M., and R. L. Mancuso, 1968: Objective analysis of environmental conditions associated with severe thunderstorms and tornadoes. Mon. Wea. Rev., 96, 342-350.

Fankhauser, J. C., 1969: Convective processes resolved by a mesoscale rawinsonde network. J. Appl. Meteorol., 8, 778-798.

Foster, D. S., and R. M. Reap, 1973: Archiving of manually-digitized radar data, Techniques Development Laboratory Office Note 73-6, National Weather Service, Silver Springs, Md., 12 pp.

Fucik, N. F. and R. E. Turner, 1975: Data for NASA's AVE IV experiment: 25-mb sounding data and synoptic charts, NASA TM X-64952, Marshall Space Flight Center, Alabama, 458 pp.

Fuelberg, H. E., 1974: Reduction and error analysis of the AVE II pilot experiment data. NASA CR-120496, NASA Marshall Space Flight Center, Huntsville, Alabama, 131 pp.

Fujita, T. and H. A. Brown, 1960: Design of a 3-dimensional mesometeorological network. Quart. Rept. No. 4, Contract DA-36-039 SC 78901, Univ. of Chicago, 63 pp.

Horn, L. H., R. A. Petersen, and T. M. Whittaker, 1976: Intercomparisons of data derived from Nimbus 5 temperature profiles, rawinsonde observations, and initialized LFM model fields. Mon. Wea. Rev., 104, 1363-1371.

House, D. C., 1960: Remarks on the optimum spacing of upper-air observations. Mon. Wea. Rev., 88, 97-100.

Kreitzberg, C. W., and H. A. Brown, 1970: Mesoscale weather systems within an occlusion. J. Appl. Meteorol., 9, 417-432.

McCown, M. S., and J. R. Scoggins, 1977: Gradients of meteorological parameters in convective and nonconvective areas. NASA CR-2818,

NASA Marshall Space Flight Center, Huntsville, Alabama, 86 pp.

Miller, R. C., 1967: Notes on analysis and severe storm forecasting procedures of the Military Weather Warning Center. AWS Tech. Report 200, 94 pp.

_____, 1969: Forecasting the degree of intensity of severe thunderstorms. Preprints 6th Conf. Severe Local Storms, Chicago, Amer. Meteor. Soc., 197-201.

Moyer, V., J. R. Scoggins, N. Chou, and G. S. Wilson, 1978: Atmospheric structure deduced from routine Nimbus 6 satellite data. Mon. Wea. Rev., 106, 1340-1352.

Ninomiya, K., 1971: Mesoscale modification of synoptic situations from thunderstorm development as revealed by ATS III and aerological data. J. Appl. Meteorol., 10, 1103-1121.

O'Brien, J. J., 1970: Alternate solutions to the classical vertical velocity problem. J. Appl. Meteorol., 9, 197-203.

Overall, J. W. and J. R. Scoggins, 1975: Relationships between motion on isentropic surfaces from 3-h rawinsonde data and radar echoes. NASA CR-2558, NASA Marshall Space Flight Center, Huntsville, Alabama, 59 pp.

Petterssen, S., 1956: Weather Analysis and Forecasting Vol. II, 2nd ed. McGraw-Hill, 266 pp. (see p. 193).

Read, W. L. and J. R. Scoggins, 1977: Vorticity imbalance and stability in relation to convection. NASA CR-2819, NASA Marshall Space Flight Center, Huntsville, Alabama, 111 pp.

Reap, R. M., and M. A. Alaka, 1969: An objective quasi-Lagrangian index for predicting convective weather outbreaks. Preprints 6th Conf. Severe Local Storms, Chicago, Amer. Meteor. Soc., 119-124.

Scott, R. W. and J. R. Scoggins, 1977: The moisture budget in relation to convection. NASA CR-2817, NASA Marshall Space Flight Center, Huntsville, Alabama, 88 pp.

Shuman, F. G., 1957: Numerical methods in weather prediction: II Smoothing and Filtering. Mon. Wea. Rev., 357-361.

Vincent, D. G. and L. N. Chang, 1975: Kinetic energy budgets of moving systems: Case studies for an extratropical cyclone and hurricane Celia, 1970. Tellus, 27, 224-235.

Wilson, G. S. and J. R. Scoggins, 1976: Atmospheric structure and variability in areas of convective storms determined from 3-h rawinsonde data. NASA CR-2678, NASA Marshall Space Flight Center, Huntsville, Alabama, 118 pp.

Wine, R. L., 1964: Statistics for Scientists and Engineers. Prentice-Hall, Inc., Englewood Cliffs, New Jersey, 671 pp. (see p. 658).

Young, H. D., 1962: Statistical Treatment of Experimental Data. New York, McGraw-Hill, 172 pp.

APPENDIX I

RAWINSONDE STATIONS PARTICIPATING IN AVE IV EXPERIMENT

Station Number	Location
208 (CHS)	Charleston, South Carolina
211 (TPA)	Tampa, Florida
213 (AYS)	Waycross, Georgia
220 (VPS)	Apalachicola, Florida
226 (CEN)	Centerville, Alabama
232 (BVE)	Boothville, Louisiana
235 (JAN)	Jackson, Mississippi
240 (LCH)	Lake Charles, Louisiana
248 (SHV)	Shreveport, Louisiana
255 (VCT)	Victoria, Texas
260 (SEP)	Stephenville, Texas
261 (DRT)	Del Rio, Texas
265 (MAF)	Midland, Texas
304 (HAT)	Hatteras, North Carolina
311 (AHN)	Athens, Georgia
317 (GSO)	Greensboro, North Carolina
327 (BNA)	Nashville, Tennessee
340 (LIT)	Little Rock, Arkansas
349 (UMN)	Monette, Missouri
363 (AMA)	Amarillo, Texas
402 (WAL)	Wallops Island, Virginia
405 (IAD)	Sterling, Virginia (Dulles Airport)
425 (HTS)	Huntington, West Virginia
429 (DAY)	Dayton,Ohio
433 (SLO)	Salem, Illinois
451 (DDC)	Dodge City, Kansas
456 (TOP)	Topeka, Kansas
486 (JFK)	Fort Totten, New York (Kennedy Airport)
518 (ALB)	Albany, New York
520 (PIT)	Pittsburgh, Pennsylvania
528 (BUF)	Buffalo, New York
532 (PIA)	Peoria, Illinois
553 (OMA)	Omaha, Nebraska
562 (LBF)	North Platte, Nebraska
606 (PWM)	Portland, Maine
637 (FNT)	Flint, Michigan
645 (GRB)	Green Bay, Wisconsin
654 (HUR)	Huron, South Dakota
655 (STC)	St. Cloud, Minnesota
662 (RAP)	Rapid City, South Dakota
11001 (MFS)	Marshall Space Flight Center, Alabama
22002 (FSI)	Fort Sill, Oklahoma

1. REPORT NO.	2. GOVERNMENT ACCESSION NO.	3. RECIPIENT'S CATALOG NO.
NASA CR-3150		

4. TITLE AND SUBTITLE	5. REPORT DATE
Differences between Measured and Linearly Interpolated Synoptic Variables over a 12-h Period during AVE IV	June 1979
	6. PERFORMING ORGANIZATION CODE
7. AUTHOR(S)	8. PERFORMING ORGANIZATION REPORT #
Leonard R. Dupuis and James R. Scoggins	
9. PERFORMING ORGANIZATION NAME AND ADDRESS	10. WORK UNIT NO.
	M-284
Department of Meteorology	11. CONTRACT OR GRANT NO.
Texas A&M University	NAS8-31773
College Station, Texas 77843	13. TYPE OF REPORT & PERIOD COVERED
12. SPONSORING AGENCY NAME AND ADDRESS	Contractor
National Aeronautics and Space Administration	
Washington, D. C. 20546	14. SPONSORING AGENCY CODE

15. SUPPLEMENTARY NOTES

Prepared under the technical monitorship of the Atmospheric Sciences Division, Space Sciences Laboratory, NASA/Marshall Space Flight Center

16. ABSTRACT

Differences between measured values of synoptic variables and like variables interpolated linearly from 12-h data were computed over 3-, 6-, and 9-h intervals within bracketing 12-h rawinsonde soundings by using the unique 3-h rawinsonde data from NASA's fourth Atmospheric Variability Experiment (AVE IV) conducted on 24 and 25 April 1975. These differences represented the nonlinear change in the variables or the amount of change over a time interval (3, 6, or 9 h) that was not accounted for by assuming a linear change through a 12-h period.

Results of analyses revealed that nonlinear changes or differences formed centers or systems that were mesosynoptic in nature. These systems correlated well in space with upper-level short waves, frontal zones, and radar-observed convection, and were very systematic in time and space. Many of the centers of differences were well established in the vertical, extending up to the tropopause.

Statistical analysis showed that on the average nonlinear changes were larger in convective areas than nonconvective regions. Errors often exceeding 100 percent were made by assuming variables to change linearly through a 12-h period in areas of thunderstorms, indicating that these nonlinear changes are important in the development of severe weather. Linear changes, however, accounted for more and more of an observed change as the time interval (within the 12-h interpolation period) increased, implying that the accuracy of linear interpolation increased over larger time intervals.

17. KEY WORDS	18. DISTRIBUTION STATEMENT
Atmospheric variability Variability versus convective activity Observed versus interpolated atmospheric variables Kinematic variables over periods < 12 h Nonlinear changes versus convective activity Sub-synoptic scale systems	Category 47

19. SECURITY CLASSIF. (of this report)	20. SECURITY CLASSIF. (of this page)	21. NO. OF PAGES	22. PRICE
Unclassified	Unclassified	135	$7.25

* For sale by the National Technical Information Service, Springfield, Virginia 22161

NASA-Langley, 1979